**FUEL COMPOSITION ANALYSIS OF ENDOTHERMICALLY HEATED JP-8
FUEL FOR USE IN A PULSE DETONATION ENGINE**

THESIS

Eric A. Nagley, Lieutenant, USN

AFIT/GAE/ENY/08-J08

The views expressed in this thesis are those of the author and do not reflect the official policy or position of the United States Air Force, Department of Defense, or the U.S. Government.

FUEL COMPOSITION ANALYSIS OF ENDOTHERMICALLY HEATED JP-8 FUEL FOR USE IN A PULSE DETONATION ENGINE

THESIS

Presented to the Faculty

Department of Aeronautics and Astronautics

Graduate School of Engineering and Management

Air Force Institute of Technology

Air University

Air Education and Training Command

In Partial Fulfillment of the Requirements for the

Degree of Master of Science in Aeronautical Engineering

Eric A. Nagley, BSET

Lieutenant, USN

June 2008

AFIT/GAE/ENY/08-J08

**FUEL COMPOSITION ANALYSIS OF ENDOTHERMICALLY HEATED JP-8
FUEL FOR USE IN A PULSE DETONATION ENGINE**

Eric A. Nagley, BSET

Lieutenant, USN

Approved:

_____/SIGNED/_____	2 June 2008
Paul I. King (Chairman)	Date
_____/SIGNED/_____	2 June 2008
Richard D. Branam, Maj, USAF (Member)	Date
_____/SIGNED/_____	2 June 2008
Mark F. Reeder (Member)	Date

AFIT/GAE/ENY/08-J08

Abstract

Waste heat from a pulse detonation engine (PDE) was extracted via zeolite catalyst coated concentric tube-counter flow heat exchangers to produce supercritical pyrolytic conditions for JP-8 fuel. A sampling system and method were developed that enabled samples of reacted fuel to be extracted during steady state operation. Samples were taken over a range of heat exchanger exit temperatures from 820 K (1016 ^{o}F) to 940 K (1232 ^{o}F). Offline analysis of liquid and vapor fuel samples indicated fuel decomposition via typical pyrolytic reaction pathways. The liquid analysis showed conversion of parent fuel components with formation of unsaturates (aromatics and alkenes) and smaller alkanes. The gaseous products consisted of predominantly C_1-C_3 alkanes and alkenes (> 75% of total vapor yield) with moderate amounts of hydrogen and C_4-C_6 alkanes and alkenes. The components that were present in the stressed fuel samples were more detonable and could be linked to improved PDE performance. The ignition time decreased by over 20% as temperature increased from 820 K (1016 ^{o}F) to 935 K (1224 ^{o}F) and by more than 30% when compared to unreacted (flash vaporized) JP-8.

Table of Contents

List of Figures

ix

x

List of Tables

List of Symbols

<u>Acronyms</u>
AFRL   = Air Force Research Laboratory
FF   = Fill fraction
FHS   = Fuel heating system
FID   = Flame ionization detector
FN   = Flow number
GC   = Gas chromatograph
GC-MS = Gas chromatography/mass spectrometry
HPLC = High performance liquid chromatography
NPT   = National Pipe Thread
PAH   = Polycyclic aromatic hydrocarbon
PDE   = Pulse detonation engine
PF   = Purge fraction
SI   = International standard of units
TCD   = Thermal conductivity detector

<u>Symbols</u> – All units shown with [ ] are SI, and all units shown with { } are English

A = area $[m^2]$ $\{ft^2\}$
B = bias limit
$\bar{c}_p$ = average specific heat at a constant pressure $[J/(kg*K)]$ $\{BTU/(lb*{}^oF\}$
C_p = specific heat at a constant pressure $[J/(kg*K)]$ $\{BTU/(lb*{}^oF\}$
D = diameter $[m]$ $\{in\}$
$E_{initiation}$ = initiation energy $[J]$ $\{BTU\}$
freq   = frequency $[Hz]$
h = heat transfer coefficient $[W/(m^2*k)]$ $\{BTU/(ft^2*hr*{}^oF)\}$
H = enthalpy $[J/g]$ $\{BTU/lbm\}$
k = thermal conductivity $[W/(m^2*k)]$ $\{BTU/(ft^2*hr*{}^oF)\}$
L = length $[m]$ $[in]$
M = Mach number
m = mass $[g]$ $\{lbm\}$
$\dot{m}$ = mass flow rate $[kg/sec]$ $\{lbm/s\}$
MW = molecular weight $[g/mol]$ $\{amu\}$
n = moles
N = number of individual readings
n_C = number of carbon atoms
Nu = Nusselt number
P = pressure $[Pa\ or\ atm]$ $\{psi\}$
P_x = precision limit
Pr   = Prandtl number

<u>Symbols (continued)</u> – All units shown with [ ] are SI, and all units shown with { } are English

q	=	heat of combustion [J/kg] {BTU/lbm}
$\dot{Q}$	=	rate of heat transfer [W] {BTU/s}
R	=	universal gas constant [J/(mol*K)] {(ft^3*psi*lb)/mol*$^{\circ}$F}
Ra	=	Rayleigh number
S_X	=	sample standard deviation
T	=	temperature [K] {$^{\circ}$F}
t	=	time [s]
u	=	velocity [m/s] {ft/s}
U	=	uncertainty
V	=	volume [ml] {ft^3}
X	=	measured variable of interest
$\bar{X}$	=	sample mean
Y	=	mass fraction
#	=	number of

<u>Greek Symbols</u> – All units shown with [ ] are SI, and all units shown with { } are English

χ	=	mole fraction
λ	=	cell size [mm] {in}
ρ	=	density [g/ml] {lbm/ft^3}

<u>Subscripts</u>

a	=	annulus
air	=	air
conv	=	convection
ex	=	exit
f	=	film
$fuel$	=	fuel
i	=	individual
in	=	inlet
L-G	=	liquid-to-gas
liq	=	liquid
s	=	surface
sam	=	sample
tube	=	tube
vap	=	vapor

FUEL COMPOSITION ANALYSIS OF ENDOTHERMICALLY HEATED JP-8 FUEL FOR USE IN A PULSE DETONATION ENGINE

I.   Introduction

Motivation

JP-8 is the predominant kerosene fuel currently used in the United States Air Force (USAF) and is of particular interest concerning military operation of a pulse detonation engine (PDE). A large challenge in using the PDE as a source of propulsion is the ignition and detonation of higher molecular weight straight-chain hydrocarbons. Ignition time is nearly an order of magnitude higher for complex liquid hydrocarbon fuels than it is for simpler gaseous fuels. This adverse characteristic leads to an overall increase in PDE cycle time thereby limiting thrust output. It is well known that if a hydrocarbon fuel can be decomposed outside of the combustion chamber, combustion efficiency can be improved (Edwards, 2003:1098-1104). Recent work showed that waste heat from a PDE can elevate JP-8 to endothermic temperatures with a subsequent beneficial influence on ignition time (Helfrich, 2007:6-8). Ignition time is defined as the time elapsed between ignition of the fuel at the closed end of a PDE tube and the commencement of deflagration. Helfrich et al. showed that the elevated fuel temperatures were directly related to a decrease in ignition time but could not link this to change in composition. The chemical make-up of the heated fuel was not known.

Problem Statement

When JP-8 is heated to a sufficient temperature (>811 K or 1000 ^{o}F), endothermic reactions known as thermal cracking occur (Helfrich, 2007:3), (Huang, 2002:2). During this process, thermal decomposition of high molecular weight hydrocarbons results in lower molecular weight aromatics, alkenes and alkanes (Edwards, 2006:4, 5). As these lower molecular weight hydrocarbons are formed, initiation energy decreases and substantial benefits are seen in PDE performance (Schauer, 2005:2).

The current research will extend the investigation further into the oxygen-free thermal decomposition of JP-8 induced by PDE waste heat. An apparatus will be developed that allows in-line sampling of stressed fuel during steady state PDE operation. This investigation will produce quantitative evidence of thermal cracking in the fuel after passing through thrust tube heat exchangers and examine the composition of both liquid and gaseous products present prior to combustion.

Research Objectives

It is the primary objective of this research to produce samples of fuel that have been reacted by thrust tube waste heat and examine the relationship between stressed fuel composition and PDE performance. The analysis on the collected samples will explore extent of thermal cracking, chemical composition, chemical reaction pathways, and effect of composition on PDE ignition time. Multiple intermediate goals must be met to accomplish the primary research objective. The following list includes the goals that will be met in order to accomplish the primary objective.

1. Develop a method to extract a portion of fuel after it has been heated and cracked while the PDE is operating at steady state and cool it to atmospheric temperature for ease of handling.

2. Develop a sample collection system that allows collection of the liquid and gaseous portions of the extracted and cooled fuel. Sample collection system must allow the volume measurement of both the liquid and gaseous samples.

3. Utilize gas chromatography for chemical composition analysis of the liquid and gas samples.

4. Examine the relationship between the change in fuel composition and PDE operation.

Units

Both English and international standard of units (S.I.) are used throughout the PDE community. For this work, both are presented where practical. If it is not practical to present both systems, only the S.I. is used.

Layout

Chapter I introduces the research focus of this work. Included was the motivation and problem statement defining this research, as well as the intermediate goals which met the main research objective. Chapter II gives the background and theory needed to

explore this facet of PDE experimentation. It includes PDE theory and background on pyrolytic reaction chemistry. In Chapter III, the PDE research facility, engine and methodology are discussed. Chapter IV explains the methods used to collect and analyze PDE data as well as fuel samples. Results and discussion about findings are included in Chapter V. Chapter VI discusses conclusions from this research and provides recommendations for future work.

II.   Background and Theory

Overview

      The study on how endothermically reacted JP-8 fuel affects the operation of a pulse detonation engine requires an understanding of detonation theory. Of equal importance is the impact that fuel composition has on a detonation. In this chapter, the background is presented that will help explain the development of a detonation and its structure from both a theoretical and experimental vantage point. Knowing that fuel type impacts the cell size within a detonation structure, a correlation can be made between fuel and the amount of energy required to directly initiate a detonation. If initiation energy can be decreased, PDE performance can be improved by achieving better ignition times and higher thrust output.

      A desirable scenario would be to have a readily available practical hydrocarbon, such as JP-8, that has initiation energy characteristic of lighter strained hydrocarbons to support increased PDE performance. Altering the chemical composition of JP-8 by thermal decomposition gives elements of this desirable scenario. A discussion of the chemical reaction pathways that the fuel follows during decomposition gives a better understanding of what types of compounds can be expected from supercritical pyrolysis of JP-8. Finally, a survey of previous research lends further information to what is expected in both thermal and catalytic cracking and introduces a gap in the community that will be filled with this work.

Detonation Wave Development

As suggested by the name, detonation waves are the means of thrust production in a PDE. A detonation is defined as a shock wave that receives its energy from combustion (Turns, 2000:598). Therefore, a detonation wave is a supersonic flame front consisting of a shock wave and trailing reaction zone. Detonation in a PDE begins with ignition of a combustible fuel at the closed end of a thrust tube. After the fuel is ignited, a deflagration wave is formed. A deflagration wave is a subsonic wave front that propagates by heat transfer. The deflagration wave propagates downstream as a result of the burned gas expanding against the closed end of the thrust tube. As the deflagration wave propagates through the thrust tube, a Shchelkin-type spiral (discussed in Chap. III) is utilized to help initiate detonation. After detonation occurs, energy is released very rapidly as the wave propagates downstream. Thrust is then produced from the trailing mass that is ejected from the tube after the detonation exits the thrust tube.

One-Dimensional Detonation Analysis

There are distinct differences that characterize detonation and deflagration wave fronts. To gain a quantitative understanding of the differences between the two waves, the changes in density (ρ), pressure (p), temperature (T), and velocity (u) are examined. The subscript one (1) denotes conditions upstream of the flame front while the subscript two (2) refers to conditions downstream of the flame front. Figure 1 shows a generic diagram of a stationary flame front. Table 1 shows Mach number as well as the ratios of upstream-to-downstream properties across a stationary flame front (Kuo, 2005:357).

6

Note that detonation Mach numbers are several orders of magnitude higher when comparing a detonation to a deflagration. Furthermore, detonation pressure ratio is an order of magnitude higher than the deflagration pressure ratio.

Stationary Flame Front

Premixed Reactants | Products

ρ_1, T_1, p_1, u_1 | ρ_2, T_2, p_2, u_2
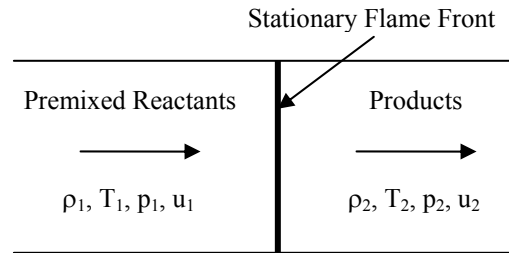
Figure 1. Generic diagram of a stationary flame front (Slack, 2006:10)

Table 1. Typical detonation and deflagration Mach numbers and ratios across a stationary flame front (Kuo, 2005:357)

	Detonation	Deflagration
u_1/a_1	5-10	0.0001-0.03
u_2/u_1	0.4-0.7 (Deceleration)	4-6 (Acceleration)
p_2/p_1	13-55 (Compression)	≈ 0.98 (Slight Expansion)
T_2/T_1	8-21 (Heat Addition)	4-16 (Heat Addition)
ρ_2/ρ_1	1.7-2.6	0.006-0.25

Realistically, the true structure of a detonation is highly complex and three-dimensional (Turns, 2000:600). However, there is a significant amount of information that can be learned from a one-dimensional analysis. The same assumptions that are typically applied to one-dimensional normal shock analysis are invoked as follows (Turns, 2000:600-601):

1. One-dimensional, steady flow.

2. Constant area.

3. Ideal gas behavior.

4. Constant and equal specific heats.

5. Negligible body forces.

6. Adiabatic conditions.

Consider the stationary flame front represented in Fig. 1. Here the velocities are with respect to the flame front and it is traveling from left to right through a channel. The one-dimensional steady conservation of mass, momentum, and energy as well as the equation of state can be applied and are given in Equations 1, 2, 3, and 4 respectively.

$$\rho_1 u_1 = \rho_2 u_2 \tag{1}$$

$$P_1 + \rho_1 u_1^2 = P_2 + \rho_2 u_2^2 \tag{2}$$

$$C_p T_1 + \frac{u_1^2}{2} + q = C_p T_2 + \frac{u_2^2}{2} \tag{3}$$

$$P = \rho R T \tag{4}$$

In Equations 1 through 4, ρ is the density, u is the velocity, P is the pressure, C_p is the specific heat at a constant pressure, T is the temperature, q is the heat of combustion, and R is the universal gas constant (Kuo, 2005:358). The speed of sound, a can be determined by Eq. 5:

$$a = \sqrt{\gamma R T} = \sqrt{\frac{\gamma P}{\rho}} \tag{5}$$

where γ is the ratio of specific heats, R is the specific gas constant, P is the static pressure, ρ is the static density, and T is the static temperature. If Eq. 5 is combined with the continuity equation (Eq. 1) and the momentum equation (Eq. 2), the Rayleigh-line relation is formed, given in Eq. 6 (Kuo, 2005:359).

$$\gamma M_1^2 = \frac{\dfrac{P_2}{P_1} - 1}{1 - \dfrac{\rho_1}{\rho_2}} \tag{6}$$

In Eq. 6, M is the Mach number and is defined as $M = u/a$. This relationship represents lines that obey both laws of continuity and momentum, where the slope magnitude measures the mass flux. The Rankine-Hugoniot relation is developed when the energy equation (Eq. 3) is satisfied in addition to the continuity and momentum equations, Eqs. 1 and 2 respectively. The Rankine-Hugoniot relation is given in Eq. 7 (Kuo, 2005:360).

$$\frac{\gamma}{\gamma-1}\left(\frac{p_2}{\rho_2} - \frac{p_1}{\rho_1}\right) - \frac{1}{2}(p_2 - p_1)\left(\frac{1}{\rho_1} + \frac{1}{\rho_2}\right) = q \tag{7}$$

If values of P_1, $1/\rho_1$, and q are given, all possible values of P_2 and $1/\rho_2$ can be solved for and plotted utilizing Eq. 7. The plot that is produced is a Hugoniot curve. Figure 2 is a representative Hugoniot curve with Rayleigh lines plotted.
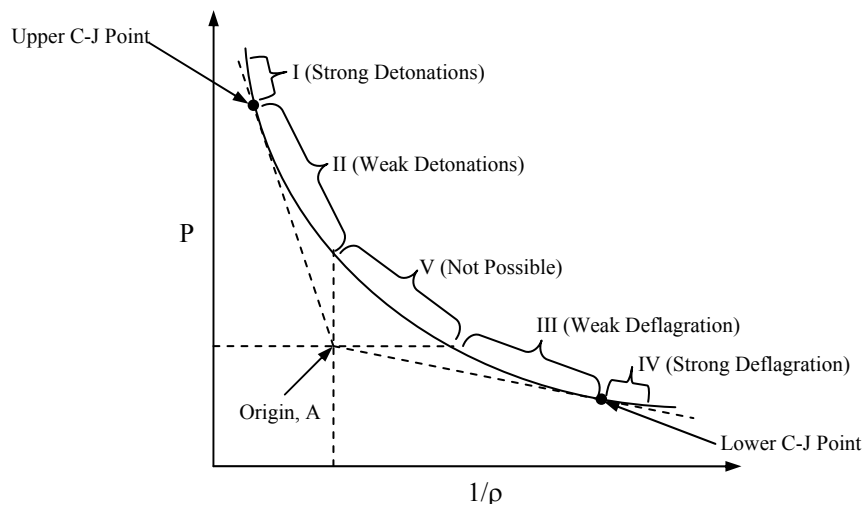
Figure 2. Representative Hugoniot curve with Rayleigh lines plotted (Kuo, 2005)

In Fig. 2, two tangent and two intersecting Rayleigh lines form four points on the

Hugoniot curve. The four points segment the curve into five regions. Two critical points

that correspond to the tangent of the upper and lower Rayleigh lines with the Hugoniot

curve are termed the upper and lower Chapman-Jouguet (C-J) points, respectively. The

other two points are intersections of the vertical and horizontal Rayleigh lines with the

Hugoniot curve. The vertical and horizontal Rayleigh lines represent the limit of infinite

mass flux and zero mass flux, respectively (Turns, 2000:603). Continuity must be

observed and therefore these two points form a region that is not possible, region V.

Strong deflagrations represented in region IV have never been experimentally observed.

For a strong deflagration to occur, the gas velocity relative to the flame front must be

accelerated from subsonic to supersonic (Kuo, 2005:364). Weak detonations occur in

region II and are not possible for liquid hydrocarbons. In this region, the pressure of the

products is less than that of the pressure of the upper C-J point. In order for this to

transpire, the chemical kinetics must be much faster than are possible with liquid

hydrocarbons (Helfrich, 2006:11). This leaves two regions of interest in PDE research.

Region I, where strong detonations occur, is of obvious importance to this work.

This region is bounded only by the upper C-J point. A strong detonation that occurs in

region I is in a transient state that will always go back to the upper C-J point (Slack,

2006:14). Region III is also of particular interest to PDE research because, as mentioned

earlier, a detonation wave occurs only after a deflagration wave forms (Turns, 2000:598).

In this research, the gaseous wavespeed of the upper and lower C-J point is the principal

measure that is used to designate whether it is a detonation or deflagration. For PDE

experiments that utilized liquid hydrocarbon fuels, the upper and lower C-J speed was

determined to be approximately 1800 m/s (5906 ft/s) and 500 m/s (1640 ft/s),

respectively (Slack, 2006:13), (Helfrich, 2006:12).

Detonation Wave Structure and Initiation Energy

The one-dimensional model described above gives considerable insight and the

tools needed to distinguish detonations from deflagrations. It is of equal importance to

understand the structure of a detonation and how it is affected by fuel type. The

detonation wave structure is a bit more intricate. The one-dimensional Zeldovich, von

Neumann, and Döring model (also know as ZND model) introduces the concept of a

three zone detonation wave. Figure 3 shows temperature, pressure, and density as a

function of distance for the ZND model. The shock wave resides in the first zone and a

large spike in temperature, pressure, and density occurs. Little or no reaction takes place

within this zone as the width of a shock wave is on the order of a few molecular mean free paths (Turns, 2000:613). The induction zone follows where little change is seen in thermodynamic properties and ideal gas shock relations can be used for analysis. The final zone is the reaction zone where there is a sharp rise in reaction rate. The reaction zone is finalized when the thermodynamic properties reach equilibrium (Kuo, 2005: 381-382). The one-dimensional ZND model gives a better understanding of detonation wave structure, but is not sufficient to help understand why particular fuels are better for PDE operation.
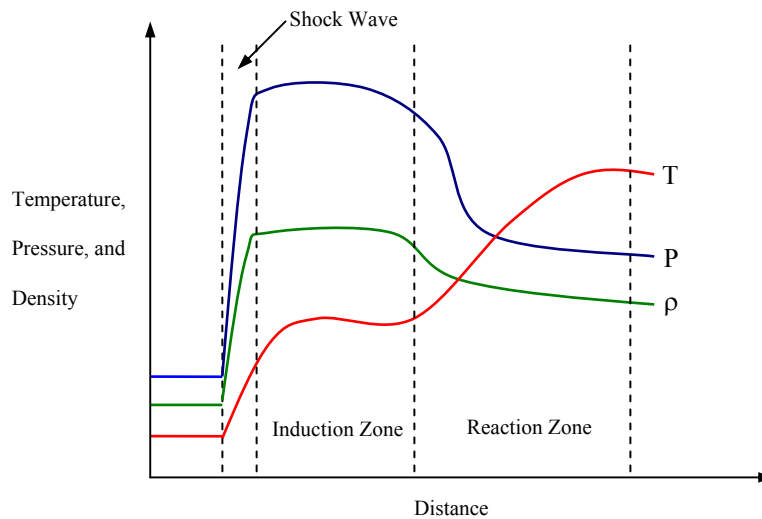
Figure 3. Temperature (T), pressure (P), and density (ρ) as a function of distance for a generic ZND model (Slack, 2006:17)

The relationship between detonation structure and fuel choice can be made by utilizing a two dimensional model. Detonations that occur in long narrow channels, like those used in a PDE, can be characterized by two-dimensional effects (Fickett,

1979:998). Figure 4 shows the structure of a fully developed two-dimensional detonation wave that is propagating from left to right and confined in a long narrow channel. Laboratory research shows that there are several shock fronts interacting in the traversing detonation wave (Turns, 2000:617). The triple point, shown in Fig. 4, indicates the intersection of the Mach stem, incident shock, and reflected shock. As the detonation propagates downstream, a fish scale-like pattern is formed by the triple shock interaction. This pattern has been experimentally captured via smoke foil tracings.
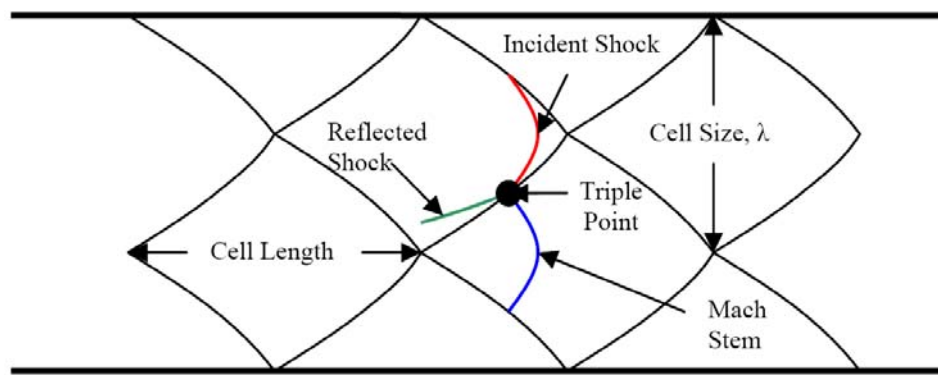
Figure 4. Drawing of two-dimensional detonation wave confined in a long narrow tube (Helfrich, 2006:15)

The parameter shown in Fig. 4, that is particularly important to this work is the cell size, λ. Previous research has shown a direct relationship between the amount of energy required to directly initiate a detonation ($E_{initiation}$) and cell size (Tucker, 2005:25). Figure 5 shows cell sizes of various fuel oxidizer mixtures as a function of initiation energy for an equivalence ratio of unity. In Fig. 5, other "practical hydrocarbons" refers to practical liquid hydrocarbons that are currently in use, such as JP-8, JP-5, or JP-10.

The best fit line represented in red produces a simple relationship between cell size and initiation energy (shown in Fig. 5 as E_{crit}), given in Eq. 8.

$$E_{initiation} = 3.375\lambda^3 \tag{8}$$

Because this fit was done on fuel oxidizer mixtures with an equivalence ratio of unity, Eq. 8 only applies to this condition. The key relation is that initiation energy is directly related to the cube of the cell size. This relationship was validated by experimental research that showed strained hydrocarbons such as acetylene and ethylene were more detonable than high molecular weight hydrocarbons typically found in JP-8 and JP-10 (Kaneshige, 1997) (Knystautas, 1984:23-37). The cracking of the JP-8 is hoped to produce these strained hydrocarbons with a subsequent positive influence on PDE operation.
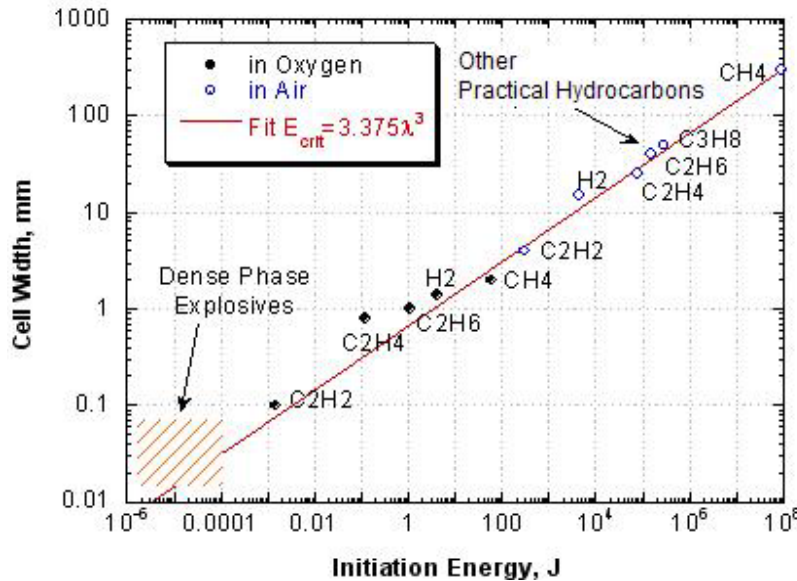
Figure 5. Cell size of various stoichiometric fuel-oxidizer mixtures as a function of initiation energy (Kaneshige, 1997), (Schauer, 2005:2)

14

Pulse Detonation Engine Operation Cycle

The correlation between fuel and initiation energy can be applied to PDE operation. It is necessary to examine the PDE operating cycle to understand why initiation energy is important to its performance. The PDE cycle, shown in Fig. 6, is segmented into three equally timed phases: fill, fire, and purge. The times shown in Fig. 6 are discussed later. A short description of each phase is discussed below with particular focus given to the fire phase. The time required to complete the fire phase is directly affected by the type of fuel used. It is important to define and understand each portion of this phase.
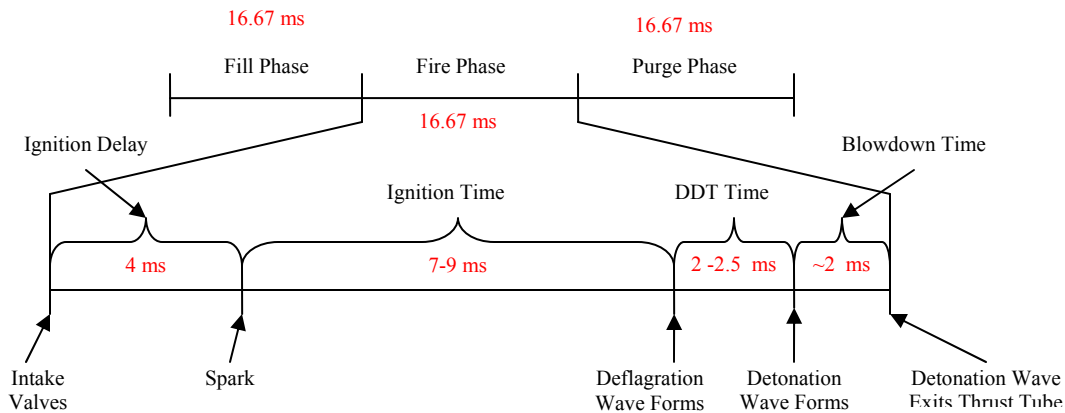
Figure 6. PDE cycle schematic with fire phase described in detail. Cycle phase times are shown for an engine operation frequency of 20 Hz. Time periods in fire phase are typical of JP-8

The PDE cycle is initiated by the fill phase. During fill, premixed fuel and air enter through intake valves to fill the tube volume to a pre-designated fraction (fill fraction). For most experiments, the tube volume was completely filled (unity fill

15

fraction). During select experiments, the fill fraction was adjusted higher or lower as an additional means of controlling equivalence ratio.

As shown in Fig. 6, there are four distinct time periods included in the fire phase. The first time period, ignition delay, is the time between the closing of the intake valves and the instant that a spark is deposited in the closed end of the tube. For this work, ignition delays ranging from 2 to 6 ms were used. The next time period, ignition time, was defined in Chapter I as the time elapsed between ignition of the fuel at the closed end of a PDE tube and the commencement of deflagration. Because the ignition time is such a large portion of the fire phase, considerable impact to overall cycle time can be made by reducing ignition time (more discussion later). DDT time is the duration needed for the deflagration to transition to a detonation. And finally, the length of time that is needed for the detonation to exit the thrust tube is termed blowdown time.

The cycle terminates with the purge phase. Purge is initiated by the opening of the purge valves. A volume of air is injected into the thrust tubes. The volume of air that is injected is determined by the purge fraction (PF). The PF is a ratio defined as the purge air volume at ambient conditions normalized by the tube volume. For this work, the PF was utilized to help control the thrust tube heat exchanger temperature.

The frequency that the PDE cycle is able to be performed has a direct impact on the amount of thrust that can be produced. Previous work has shown that there is a linear increase in thrust as the frequency of the PDE goes higher (Schauer, 2001:6). The amount of thrust produced was not quantified for this work. However, the relationship

between thrust and frequency give more understanding to why this research is being performed.

The frequency that the PDE can be operated at is limited by the amount of time it takes to complete the fire phase of the operating cycle. As the frequency of the PDE is increased, the time allotted for each phase of operation is decreased. Figure 6 shows an example of a PDE that operates at a frequency of 20 Hz. Each cycle is equally timed and allotted 16.67 ms. The completion of the fill and purge cycles are of little concern at this frequency. For this configuration, a commonly used ignition delay time is 4 ms and blowdown time is approximately 2 ms. For JP-8, the ignition time and DDT time are 7-9 ms and 2-2.5 ms, respectively. This approximately fills the total allotted time of a 20 Hz fire phase, thereby limiting the amount of thrust that can be produced. This is one of the representative challenges that is inherent to using liquid hydrocarbons to fuel a PDE. For this reason it is more advantageous to exploit a fuel that requires lower initiation energy to minimize time ignition time and overall time to detonation so that the PDE may be operated at a higher frequency.

Altering JP-8 by Pyrolytic Thermal Decomposition

The fuel of choice for this research is JP-8 for many practical reasons. JP-8 is the predominant kerosene fuel currently used in the United States Air Force and is of particular interest concerning military operation of a PDE. Even though gaseous fuels such as hydrogen, acetylene, and ethylene possess lower initiation energies than JP-8, they introduce explosion hazards and large-scale storability challenges (Galligan,

2005:7). Pyrolysis introduces an avenue that may allow the use of a practical high

molecular weight fuel, such as JP-8, while maintaining the benefits to detonation seen

from using hydrogen, ethylene, and other gaseous fuels. Previous research (Helfrich,

2007:2) shows that PDE thrust tube waste heat can be used to produce temperatures that

induce thermal cracking via zeolite catalyst coated heat exchangers.

Pyrolysis can be defined as chemical decomposition of organic materials by

heating in absence of oxygen. This endothermic process requires significant heat input

and proceeds via free radical reaction chemistry (Ford, 1986:240). At temperatures

above approximately 811 K (1000 ^{o}F) the fuel will undergo thermal, and in this research,

catalytic cracking reactions (Huang, 2002:2). The end result is a change in fuel

composition and significant shift in the molecular weight distribution. These reactions

follow the free radical chain mechanism that can be summarized in three different types

of reactions: initiation, propagation, and termination.

Initiation

The mechanism is started by an initiation reaction where a molecule undergoes

bond fission and produces free radicals (molecular species with unpaired electrons). The

heat that needs to be added to break the bond is dependent upon the bond dissociation

energy. Because the carbon-carbon single bond is the weakest and alkanes make up the

majority fuel composition, the long straight chain alkanes or alkylbenzenes are generally

among the first to react (Edwards, 2003:1104). A generic free radical initiation reaction

is represented in Eq. 9:

$$R_i\text{—}R_j \quad \rightarrow \quad R_i\text{—}CH_2\text{—}CH_2\bullet + \bullet R_k \qquad (9)$$

18
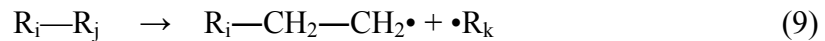
where the "•"denotes a free radical and R with subscripts i, ,j, or k represent a

hydrocarbon molecule. The free radicals that are formed in the initiation reaction drive

the reactions that follow.

Propagation

Immediately following the initiation step are a variety of propagation reaction

possibilities. The propagation reactions can be categorized into four types: hydrogen

abstraction, β-scission, intramolecular hydrogen shift, and molecular addition (Rice,

1933:3035-3040), (Kossiakoff, 1943:590-595). The hydrogen abstraction reaction occurs

when a free radical removes a hydrogen atom from another molecule. The molecule that

loses the hydrogen atom becomes a free radical and subsequent reactions will follow.

Equation 10 is an example of a hydrogen abstraction reaction.

$$R_i\bullet + R_i\text{---}CH_2\text{---}CH_2\text{---}R_j \quad \rightarrow \quad R_iH + R_i\text{---}\overset{\bullet}{C}H\text{---}CH_2\text{---}R_j \qquad (10)$$

A β-scission reaction takes place when a scission occurs at the bond located in the

β position (Galligan, 2005:16). Figure 7 shows the location of bond (α ,β ,or γ)

relative to the free radical. The resultant molecule is generally an α-olefin (alkene with

double bond in alpha or terminal position) or ethylene. Equation 11 shows an example of

a β-scission reaction.

$$R_i\text{---}\overset{\bullet}{C}H\text{---}CH_2\text{---}R_j \quad \rightarrow \quad R_i\text{---}CH\text{==}CH_2 + \bullet R_j \qquad (11)$$

Bond Location

$$R_i \text{—} \overset{\bullet}{C}H \text{—} CH_2 \text{—} CH_2 \text{—} R_j$$
$$\quad\quad\quad \alpha \quad\quad \beta \quad\quad \gamma$$
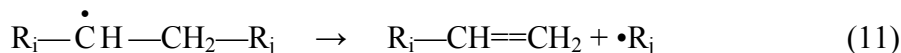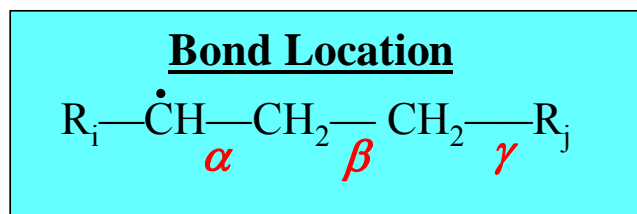
Figure 7. Location of bond (α, β, or γ) relative to free radical (DeWitt, 2007:15)

The next type of propagation reaction is the intramolecular hydrogen shift. As the name suggests, the radical shifts position within a molecule, given in Eq. 12.

$$R_i\bullet \quad \rightarrow \quad CH_3\text{—}CH_2\text{—}CH_2\text{—}CH_2\text{—}\overset{\bullet}{C}H\text{—}R_j \tag{12}$$
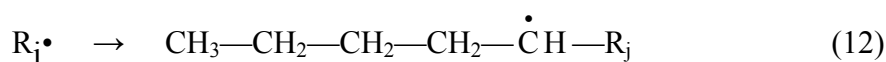
Figure 8 depicts a reaction where an intramolecular hydrogen shift occurs. The shift typically occurs from position one to five or six (numbered with top center position being number one going clockwise to six).
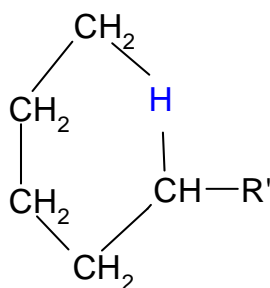
Figure 8. Intramolecular hydrogen transfer propagation reaction (DeWitt, 2007:16)

The final type, molecular addition, becomes important at further extents of reaction. Molecular addition occurs when two or more molecules form bonds that reduce overall bond multiplicity. The result at higher extents of cracking is polycyclic aromatic hydrocarbon (PAH) formation, which is a known precursor to coke deposition (talked about later).

Termination

The reaction chain can terminate in two different ways. One of the mechanisms is called coupling or recombination, example reaction given in Eq. 13.

$$R_i\bullet + \bullet R_j \quad \rightarrow \quad R_i\text{—}R_k \tag{13}$$

This is simply two free radicals combining to form a larger molecule. Disproportionation, the other means of termination, occurs when the hydrogen is abstracted from one free radical leaving an alkene and attaches to another free radical yielding a stable species. Equation 14 shows a generic reaction that represents disproportionation.

$$R_i\bullet + \bullet R_k \quad \rightarrow \quad R_i\text{—}CH\text{==}CH_2 + H\text{—}R_k \tag{14}$$
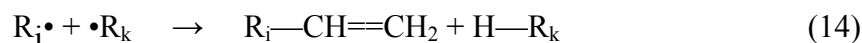
In both of these situations the free radical chain mechanism is terminated with the formation of stable species.

Catalysts can be introduced to the reactor that will alter the decomposition pathways during pyrolysis. For this work, the fuel heating system (described in Chapter III) employs heat exchangers that have been coated with a zeolite catalyst in a ceramic-like binder (sol-gel). It is known that the zeolite structure is made from a silica-alumina; however, the catalytic agent is proprietary information (Helfrich, 2007:5). The motivation for using a catalyst like this includes the possibility of: improvement in selective production of desired species that may have faster ignition times; enhancement of the endothermic reaction rate; mitigation in coke formation; and lower initiation energy (initiation reactions occur at lower temperature) (Huang, 2004:285).

Based on the free radical reactions discussed earlier, the pathways for decomposition can be outlined to indicate some mechanisms that the JP-8 fuel will follow during pyrolysis. These mechanisms can be used to give insight into the potential changes in reacted fuel composition, thereby indicating the prospective production of fuel compounds that would support improved PDE performance. The pathways that are followed during thermal hydrocarbon decomposition are outlined in Fig. 9.

f.r.r = free radical reactions; surface carbon can grow by addition of fluid phase radicals
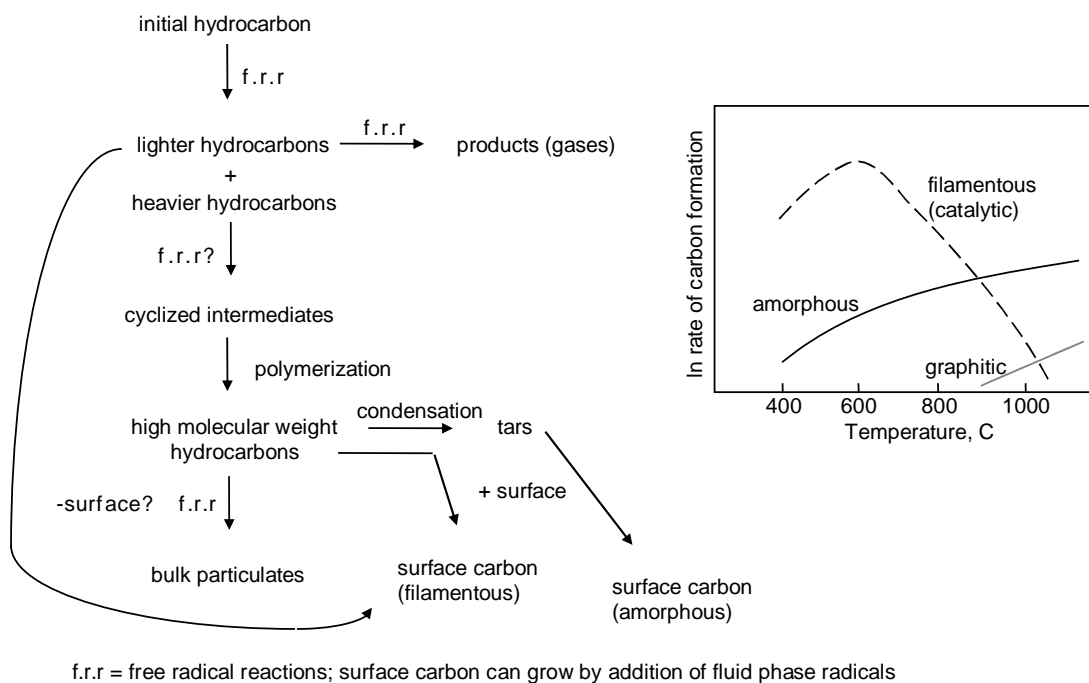
Figure 9. Reaction pathways that are followed during pyrolysis (Edwards, 2003:1103)

The pathways shown in Fig. 9 can be applied to any hydrocarbon. However, the final fuel composition after it is cracked is going to rely on the components that were present in the parent fuel, the conditions, and to what extent the fuel is reacted. The

extent of thermal cracking is dependent upon the amount of energy that is transferred to the fuel which is a function of both temperature and residence time. Figure 9 shows that initial free radical reactions produce lighter hydrocarbons and potentially some gaseous products. These pathways suggest initial reactions would cause longer straight chain alkanes to be broken down into lower molecular weight alkanes and alkenes, including some in vapor form. As pyrolysis continues with increased energy input, the lighter and heavier hydrocarbons can react to form cyclized intermediates like cycloalkanes and aromatics. Further conversion leads to the formation of multi-ring aromatics called polycyclic aromatic hydrocarbons (PAH) and eventually carbon deposition. As more PAH forms at higher extents of reaction, coke production increases.

Properties of JP-8

The reactions that will occur via oxygen free thermal decomposition will vary depending on the original fuel composition. For this study, JP-8 is the exclusive fuel used during testing. Table 2 shows properties that are helpful in characterizing JP-8 and giving insight into what free radical reaction pathways may be followed. Alkanes make up the majority composition followed by cycloalkanes, aromatics, and alkenes.

Table 2. Characteristics and properties of JP-8 (Edwards, 2003:1095)

Property	JP-8 Characteristics
Approximate formula	$C_{11}H_{21}$
H/C ratio	1.91
Critical Temperature K (^{o}F)	683.2 (770)
Critical Pressure atm (psia)	23 (340)

Specific Gravity @ 288.7K (60 ^{o}F)	0.81
Average Composition (vol %)	
Paraffins (Alkanes)	45
Napthenes (Cycloalkanes)	35
Aromatics	18
Olefins (Alkenes)	2

Coke Formation

The adverse result in any system that involves pyrolysis of hydrocarbon fuel is coke deposition. This poses challenges in experimentation and more importantly is a major safety concern for airborne systems. There are two principle sources of the solid formation and each occurs in a different temperature regime. At around 436 K (325 ^{o}F), dissolved oxygen begins to react with hydrocarbons to produce carbon deposits (Edwards, 2003:1098). This process, known as auto-oxidative coke deposition, is the primary cause of coking up to approximately 644 K (700 ^{o}F) and continues until all dissolved oxygen has been consumed (Huang, 2004:285), (Edwards, 2003:1098). This type of carbon formation can be mitigated by removing dissolved oxygen in the fuel via nitrogen sparging, discussed in Chapter III.

As temperature is increased through the regime that promotes pyrolysis, carbon formation is again initiated. The coke deposition in this case can be explained by the hydrocarbon cracking process. Figure 9 shows a schematic of the reactions that occur through the thermal cracking process. As mentioned earlier, the pyrolysis proceeds via free radical reactions (represented as f.r.r in Fig. 9). The mechanisms in Fig. 9 show that carbon deposition of some kind is eventually formed during the thermal cracking process

(Edwards, 2003:1103). As mentioned earlier, carbon deposition increases at higher extents of reaction. Ideally, for use in a PDE, it is desired to minimize coke formation while maximizing production of lower molecular weight species.

Experiments in Thermal and Catalytic Cracking

Considering the reaction pathways discussed earlier and the composition of JP-8, a large shift in overall fuel composition would be expected as a result of pyrolysis. The unknowns for this experimental setup that remain are extent of reaction and identification of compounds that will make up the final composition. Previous experiments that considered thermal and catalytic cracking were examined to gain more information about the results that may be expected in this work. Previous work in pyrolytic decomposition of fuels explore either effects on PDE performance or fuel composition, but not both. There is no study known that employs waste heat from a steady state operating engine to react the fuel and simultaneously extract cracked fuel for analysis. This leaves a void when considering operational performance of a PDE with thermally cracked fuels.

The first study that was found explored catalytic cracking of JP-8 +100 (Huang, 2004). The JP-8 +100 differs from conventional JP-8 by additives that are incorporated to suppress the auto-oxidative mechanism discussed earlier (Heneghan, 1996:171). The reactor used during experimentation was coated with a zeolite catalyst that is similar to what is used for the heat exchanger coating in this work. Figure 10 shows the weight percent of different carbon numbers for JP8 +100. Note the dramatic shift from heavier hydrocarbons (high carbon number) in the unreacted fuel to lighter hydrocarbons in the

25

reacted fuels. This shift indicates that decomposition is following the pyrolytic reaction

pathways discussed earlier. Figure 10 also shows the selective formation of lower

molecular weight species; the weight percent of C_{10} and above hydrocarbons consistently

decrease while C_8 and below hydrocarbons consistently increase.
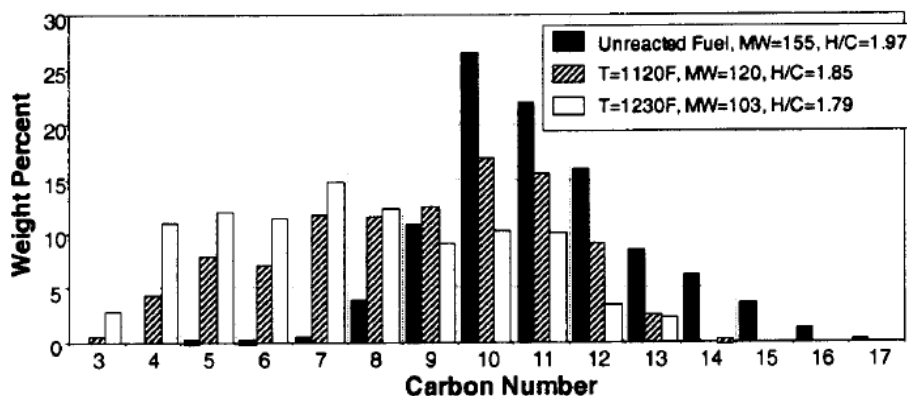
Figure 10. Molecular weight distribution of JP-8+100 as well as liquid products after thermal and catalytic cracking (Huang, 2004:290)

Figure 11 shows the gaseous products that were formed as a result of JP-8 + 100

catalytic cracking. The majority composition is C_1-C_3 alkanes and alkenes as well as

hydrogen. Also note the trend that is shown here toward lower molecular weight species

as the reaction temperature increases. This is consistent with what would be expected of

larger hydrocarbons breaking down and selectively forming smaller species.
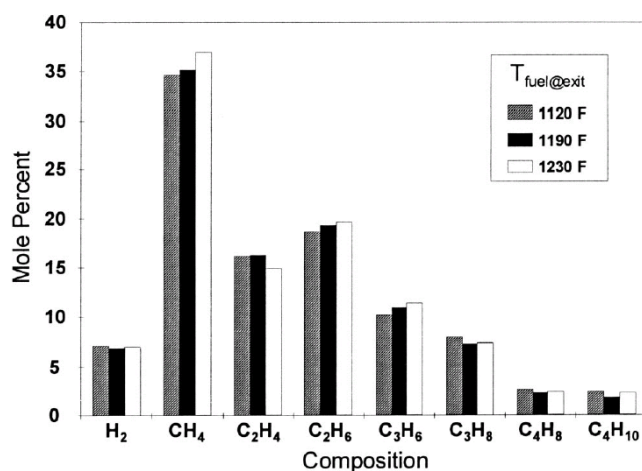
Figure 11. JP-8 + 100 gaseous product composition at various temperatures (Huang, 2004:289)

Figure 12 shows the volumetric liquid-to-gas conversion percentage for various reaction temperatures of a synthetic Fisher-Tropsch (F-T) fuel and Jet A-1 (Edwards, 2006:6). Pyrolysis was performed in a type 316 stainless reactor at a pressure of 47.6 atm (700 psig). The Jet A-1 is similar in composition to JP-8 while the F-T fuel is solely comprised of straight chain and branched alkanes. Figure 12 shows that the Jet A-1 is more pyrolytically stable (less prone to thermal decomposition) than the F-T fuel at given temperatures (Edwards, 2006:5). This stability characteristic is consistent with the earlier discussion about termination of the free radical chain mechanism and is expected given the Jet A-1 parent fuel composition. Jet A-1 has over 15% (by volume) cycloalkane composition, whereas cycloalkanes are not contained in the F-T fuel. Cycloalkanes can act as hydrogen donors to terminate the free radical chain mechanism (Song, 1994:548). Because H-donors are not readily available in the F-T fuel, decomposition is more likely to persist via the free radical reaction mechanism.

27
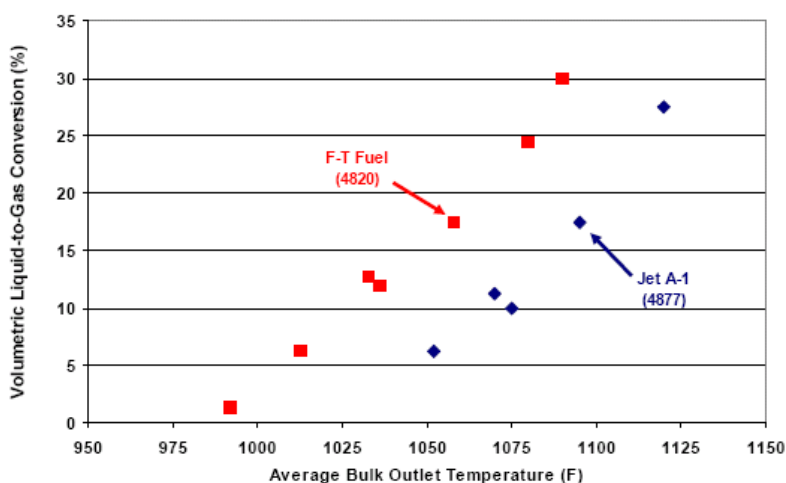
Figure 12. Volumetric liquid-to-gas conversion as a function of average bulk outlet temperature (Edwards, 2006:6)

Recent work (Helfrich, 2007) conducted on a PDE with JP-8 preheated and cracked by detonation tube waste heat demonstrated performance benefits. As the injection temperature is increased from 800 K (980 °F) to 900 K (1160 °F), the ignition time decreased by nearly 20 percent; however, this study did not report the composition change that resulted from thermal cracking.

In both of the studies examined that explored cracked fuel composition, the common thread was that they followed the free radical reaction pathways that are expected in pyrolysis. The fuel used in this work is of a different composition. Additionally, conditions (catalyst, temperature, pressure, residence time, etc.) are also different; however it is expected that reactions will follow similar decomposition pathways. The current research examines the vital link between extents of pyrolytic reaction and PDE performance. Understanding how JP-8 fuel decomposes and what types of product yields are seen is important if an operational PDE using cracked fuel is

to be achieved. This work is the first known to use waste heat from a steady state

operating engine to react JP-8 while simultaneously extracting cracked fuel for analysis.

III.   Experimental Setup and Instrumentation

Pulse Detonation Research Facility

Experimental research for this work was accomplished at the Pulse Detonation

Research Facility located at Building 71A, Wright-Patterson Air Force Base, Ohio (D-

Bay). While everyday operations and testing are contractor managed, D-Bay is an

element of the Air Force Research Laboratory Propulsion Directorate, Turbine Engine

Division, Combustion Sciences Branch (AFRL/RZTC).

D-Bay consists of four main areas: test cell, control room, fuel room and

compressor room. The original purpose for the facility was the testing of conventional

turbine engines. Consequently, the 21,200 m^3 (748,670 ft^3) explosion proof test cell is

surrounded by a minimum 0.61 m (2 ft) of reinforced concrete to protect personnel

during periods of testing (Schauer, 2001:3). The turbine engine test stand, located inside

the test cell, enables the support of 267,000 N (60,024 lbf) thrust experiments. In order to

accommodate the accurate measurement of the pulsed thrust produced by a PDE, a

damped test stand has been mounted on top of the turbine engine test stand. (The focus

of this work was not on thrust produced by the PDE and therefore the thrust measurement

mechanism was disabled.) The PDE research engine is mounted to the damped test

stand. An exhaust tunnel is located directly downstream of the PDE research engine that

allows post combustion products to vent to the atmosphere during experiments.

The control room, located adjacent to the test cell, is utilized to remotely control

and monitor all experimentation. Visual observation of the fuel room as well as multiple

test cell locations is enabled with the use of closed circuit cameras. Three main

components are utilized in the control room to manage and monitor experiments: control panel, control computer, and data collection computer. The control panel contains multiple solid state switches and controls that supply power to various facility operations. The control computer is outfitted with *LabVIEW*® control software that handles various fuel and air control inputs. The control computer also allows multiple engine operating parameters to be analyzed and controlled in real-time. Additionally, the *LabVIEW*® control software can be utilized for low speed (Hz and KHz) data acquisition. The data collection computer contains a *LabVIEW*® program that permits high speed (up to 5 MHz) data acquisition for post-run analysis.

Air Supply System

The air required for the fill and purge cycles of the PDE is supplied by an Ingersoll-Rand Pac Air Compressor (Model# PA 300V), located in the compressor room. The compressor is rated to 6.8 atm (100 psi) with the capability of producing 40 m^3/min (1412 ft^3/min). Storage of the compressed air is achieved in a 4.5m^3 (159 ft^3) receiver tank (Serial# 10894, Buckeye Fabrication Co.). From the receiver tank, the air exits the compressor room and enters the test cell. The air is routed underneath the turbine engine test stand and separated by plumbing that accommodates two individual airstreams: fill and purge. Major components of the air supply system are shown in Fig. 13. Pressure regulators (Tescom Electro-pneumatic PID Controller, Model # ER 1200) are used to manage pressure in the fill and purge lines. Pressures and temperatures downstream of the pressure regulators are monitored by transducers and T-type thermocouples,

31

respectively. In-line fill and purge critical flow nozzles are employed in the airstreams to identify mass flow rates for known pressures. A 12.55 mm (0.494 in) nozzle was used in the fill supply line, while a 10.03 mm (0.395 in) nozzle was used in the purge supply line for this work.
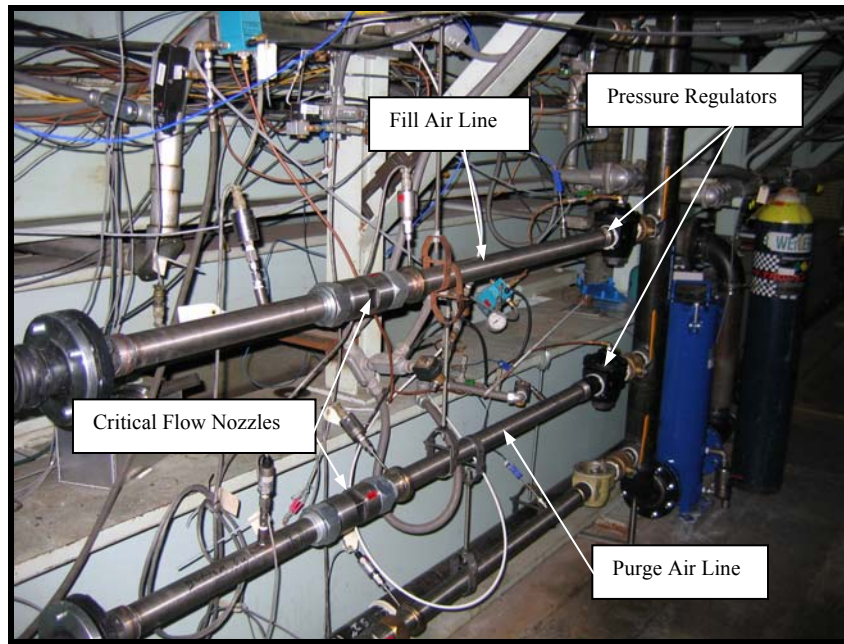
Figure 13. Air supply lines and major components (air flow direction is right to left)

The fill air is directed to the damped thrust stand where the PDE research engine is mounted. Before entering the fill manifold to be mixed with fuel, the air is heated via Chromalox Circulation heater (P/N 053-500870-187). The temperature of the air is controlled and monitored from the control room by the *LabVIEW*® program. An upper temperature limit is entered into the computer as an amperage and sent to the Chromalox

temperature controller (Model #2104) on the control panel. The purge air enters the

purge manifold and is routed to the PDE head.

Air Mass Flow Control

Mass flow control for the fill and purge air is enabled by the *LabVIEW*® program.

Equation 15 is utilized by *LabVIEW*® to calculate the required mass flow rate ($\dot{m}$):

$$\dot{m} = \frac{(\#_{tubes})(freq)(V_{tube})(FF)(P)}{R_{air}T} \tag{15}$$

where $\#_{tubes}$ is the number of tubes used for the experiment, *freq* is the motor frequency,

V_{tube} is the volume of one tube, *FF* is the fill fraction (portion of tube volume to be filled

with air), *P* is the air pressure, R_{air} is the specific gas constant for air (287.1 J/kg*K or

1716 ft^2/s^2*°R), and *T* is the air temperature. Fill fraction, tube volume, and frequency

are *LabVIEW*® user inputs. The computer obtains required equation inputs from the user

as well as measurement instrumentation (described earlier), then sends an electronic

signal to the Tescom pressure regulator. The Tescom manages the pressure to produce

the required pressure differential across the fill or purge critical flow nozzles. A closed

control loop is formed with input from pressure transducers, ensuring that the required air

mass flow rate is maintained.

Fuel Deoxygenating System

As fuel temperatures increase beyond 436 K (325 °F), the auto-oxidative chain

mechanism, discussed in Chapter II, causes rapid consumption of dissolved oxygen and

formation of carbonaceous deposits (Edwards, 2003:1099). While the auto-oxidative process does not alter fuel composition and affect PDE ignition time, it does form coke deposits that hinder fuel flow. Previous research (Panzenhagen, 2004:3.13) had shown that removing dissolved oxygen in the fuel leads to increased thermal stability, thereby decreasing the amount of coking. For this research, nitrogen sparging is used to reduce the amount of oxygen dissolved in the fuel to less than 1 ppm. In the sparging process, oxygen-free nitrogen is bubbled through the JP-8 fuel to displace the dissolved oxygen. Figure 14 shows the fuel deoxygenating system used to reduce dissolved oxygen.
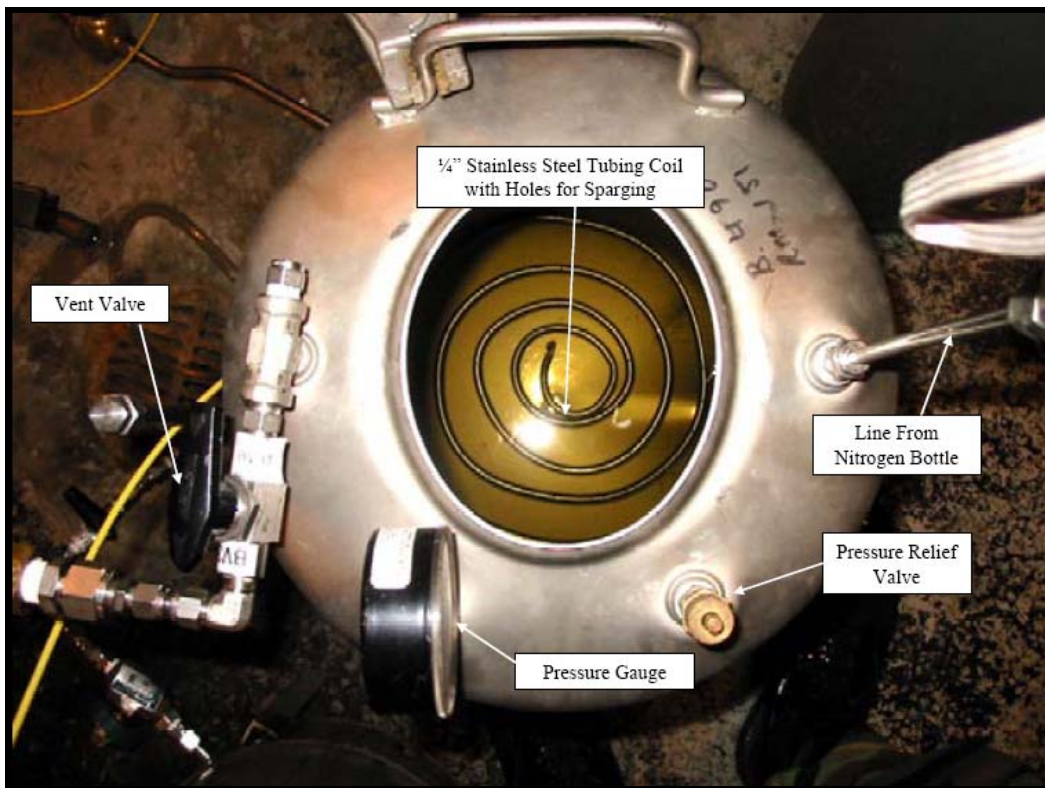
Figure 14. Fuel deoxygenating system showing JP-8 storage tank with nitrogen sparging coiled tube at the tank bottom

To initiate the fuel preparation process, the JP-8 fuel is transferred into the 41.6 L (11 gal) stainless steel fuel tank (S/N 28108-007), shown in Fig. 14. After the tank is filled, it is sealed and the vent valve is opened. The vent valve allows dissolved oxygen and excess nitrogen to exit to the facility's ventilation system. Nitrogen is introduced to fuel through a perforated stainless steel tube that receives regulated nitrogen from a standard nitrogen bottle. The manually operated pressure regulator is adjusted to allow enough nitrogen to enter the system (enough to make the nitrogen bubbling through the fuel audibly detected). After nitrogen was bubbled through the fuel for at least four hours, the vent valve was closed and the fuel tank was pressurized (Helfrich 2006:48-49).

Liquid Fuel Feed System

Liquid fuel is managed by the *LabVIEW*® control software and delivered via feed system that utilizes nitrogen as a pressure source. After the fuel has been deoxygenated using the nitrogen sparging process explained earlier, it is transferred into two 9.5 L (2.5 gal) Greer hydraulic accumulators (Model #30A-2½A) capable of handling pressures up to 204.14 atm (3,000 psi), shown in Fig. 15. Valving is closed to the fuel reservoir making the accumulators the sole fuel supply source during PDE operation. Two high-pressure nitrogen bottles supply pressure to the accumulators and are regulated by a Tescom dome loader type regulator. Each accumulator contains a rubber bladder that separates the liquid fuel from the nitrogen. During testing, ball valves are opened that allow the fuel to travel to the test cell. The accumulator filling and fuel feed to PDE processes are represented in the schematic diagram shown in Fig. 16.

35
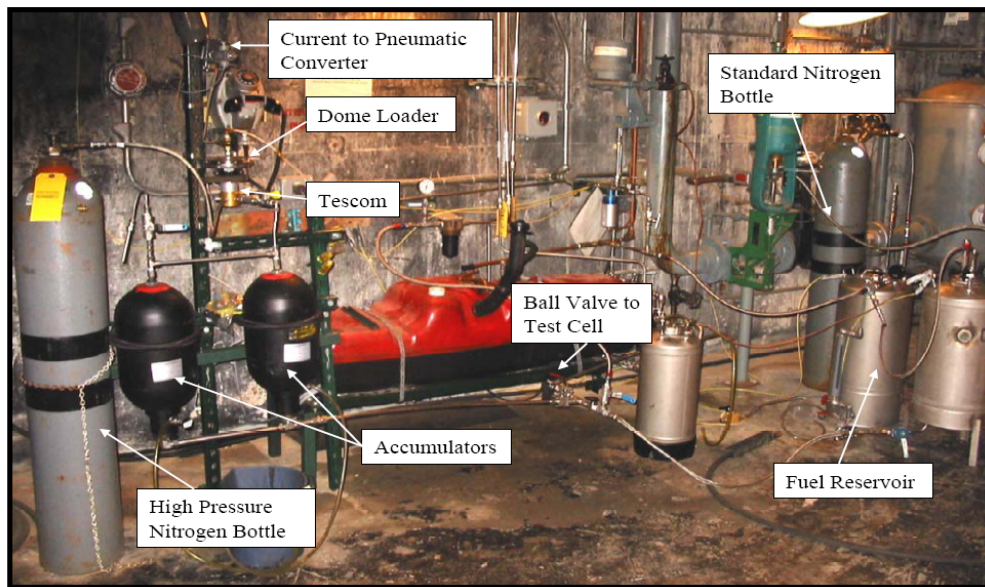
Figure 15. Photograph of liquid fuel supply system located in the fuel room
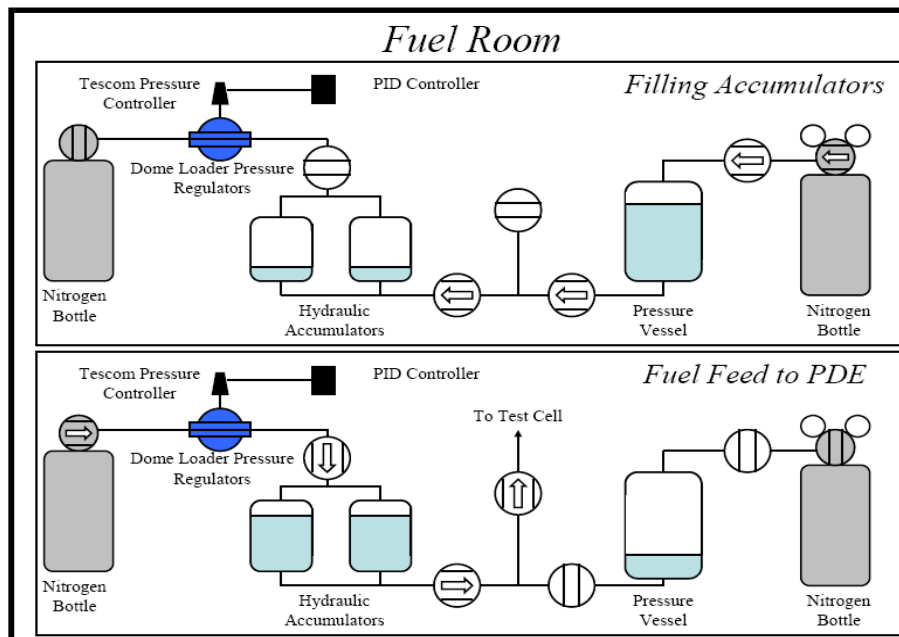
Figure 16. Schematic diagram showing valve settings during accumulator filling and fuel feed to PDE processes

When the fuel reaches the test cell, fuel lines direct it to a Flow Technologies

(Model #FT4-8AEU2-LEAT5) turbine volumetric flow meter. During initial

pressurization the flow meter can be damaged by air pockets in the feed line. For this

reason, a bypass is built into the line that routes fuel around the flow meter for initial

pressurization. After the line has been pressurized, the bypass is closed and the fuel is

routed to flow through the flow meter and continue downstream to the last chance valve.

Variations in temperature are measured by a thermocouple located directly downstream

of the flow meter. The measured temperature is used in the *LabVIEW*[®] control program

to compensate for fuel density changes when calculating fuel mass flow. The last chance

valve is the last valve that is controlled by the *LabVIEW*[®] program prior to reaching the

PDE test stand. This valve is utilized to start fuel delivery at the beginning of an

experiment and terminate fuel delivery at experiment end. During testing the fuel flows

from the last chance valve to the PDE test stand. The JP-8 then flows through the fuel

heating system (discussed later). At this juncture the heated fuel is split into two paths.

One path leads to the sample collection system (discussed later). The other flow path

directs the fuel to be mixed with air in the manifold by way of Delevan flow nozzles,

shown in Fig. 17. The nozzles are screwed into two hollow bars that are welded to the

manifold (both combined are referred to as the spray bar). The nozzles are

interchangeable allowing the operator to specify a mass flow of a fuel for given operating

pressures and temperatures.
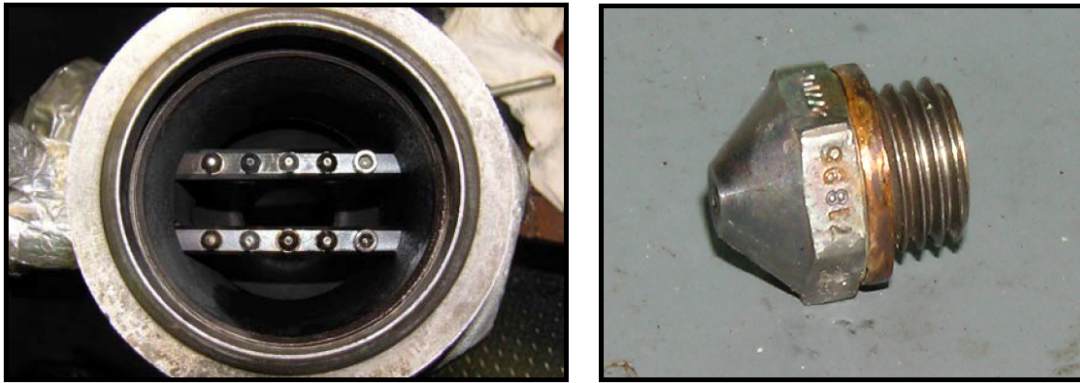
Figure 17. Photographs of air manifold with spray bar (left) and a Delevan flow nozzle (right)

Ignition System

Management of PDE ignition is achieved remotely by the control computer via the *LabVIEW*® control program. A 12 VDC MSD Digital DIS-4 ignition system supplies the ignition energy needed by the PDE. Camshaft position is measured by a BEI optical encoder (Model #H25) and sent to the control computer. The *LabVIEW*® control program translates the signal to a valve position. By using operator inputted ignition delay (mitigates chances of backfiring), valve position, and engine frequency, the control program determines the ignition timing. The timing signal is transmitted to the MSD ignition system by way of an ignition relay box. Each ignition event consists of four 105-115 mJ sparks totaling 420-460 mJ of ignition energy per tube. A modified automotive spark plug is used to deposit the spark.

Pulse Detonation Research Engine

The head and valve train from a General Motors Quad Four engine provides the fuel and air delivery. The dual overhead cams are motivated by a variable speed Baldor electric motor (Model #M4102T). Motor frequency and control is achieved through the control computer. Automotive motor oil is pumped through the engine by a Viking electric oil pump (Model #FH432) and engine cooling is provided by a 1.5 hp Teel electric water pump (Model #9HN01). The four valve design allows for two intake ports and two exhaust ports per thrust tube. During the fill cycle, only the two intake valves open to allow injection of the heated fuel air mixture. Likewise, only the two exhaust valves are open during the purge cycle, allowing purge air to flow through the tubes. Figure 18 shows a photograph of the head without thrust tubes attached.
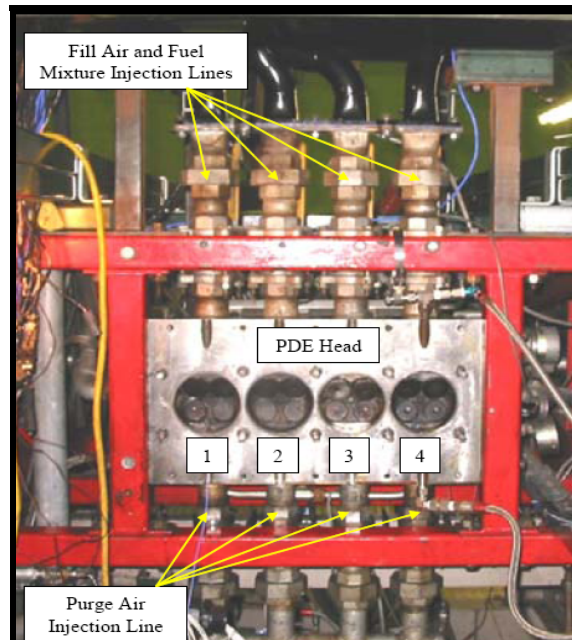
Figure 18. Photograph PDE head with intake and exhaust lines

Two detonation tubes of length 1.91 m were employed, each having a 1.22 m long structurally reinforced Shchelkin-type spiral to facilitate DDT (Shchelkin, 1940:823-827). Mounted on each tube was a concentric-tube counter flow heat exchanger to pre-heat the fuel (further fuel heating details discussed later). The heat exchanger/detonation tube assembly is attached to the head using mounting plates. The order of installation is as follows. First the detonation tube is assembled using the heat exchangers and 2" NPT threaded pipe. Next the tube assembly is screwed onto the mounting plates. The Shchelkin-type spiral was inserted into the tube assembly. An automotive head gasket was used as a seal between the mounting plates and the head. Finally the tube and spiral were mounted to the head with nuts and washers. Figure 19 shows the tube assembly attached to the PDE head. For this work, tubes were attached to positions one and four of the PDE head (numbered one through four, counting from left to right).
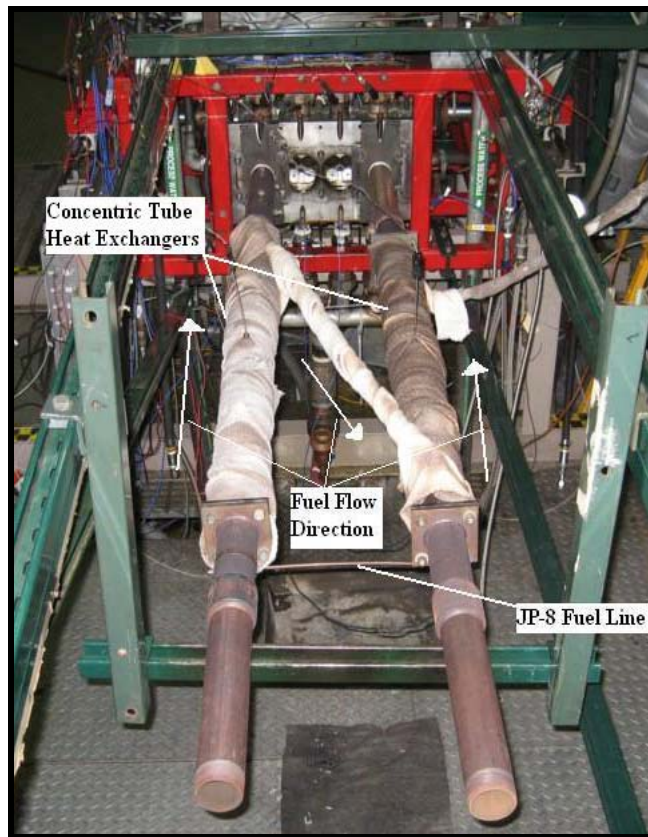
Figure 19. Photograph of PDE thrust tubes with heat exchangers attached and fuel flow direction indicated

Fuel Heating System

The fuel heating system (FHS) was developed and used in other work (Helfrich, 2006:54-57), (Helfrich, 2007:5). The FHS consisted of two concentric tube heat exchangers fabricated from inconel, a single seven-micron particulate filter, and instrumentation. In both heat exchangers, all parts that come in contact with the fuel have been coated with a zeolite catalyst in a ceramic-like binder (sol-gel). The zeolite structure is made from a silica-alumina, however the catalytic agent is proprietary information (Helfrich, 2007:5). Each inconel heat exchanger was constructed of an inner

2 in. alloy 625 schedule 10 pipe and an outer 2 ½ in. alloy 600 schedule 40 pipe, 0.91 m

(36 in.) in length. Both pipes were welded concentrically onto two square 10.16 cm (4

in.) mounting plates, one on each end. Numerous ports for thermocouples and ion probes

were added for instrumentation. Figure 20 shows a heat exchanger like those used during

this study. As shown in Fig. 8, the fuel entered the heat exchanger attached to thrust tube

number one, flowing counter to the direction of detonation flow. Fuel was subsequently

transferred to the second heat exchanger attached to thrust tube number four maintaining

a counter flow orientation. To prevent clogging of the fuel injection nozzles, a seven-

micron filter was inserted in the flow path to collect carbonaceous deposits formed during

fuel stressing.
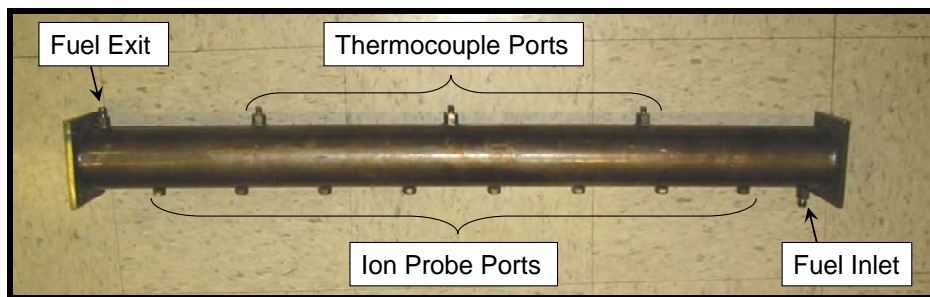
Figure 20. Example of the type of heat exchanger used in the FHS

Sample Collection System

A large obstacle that was overcome in this work was the creation of a reliable

apparatus and method to enable sample collection of reacted fuel during steady state PDE

operation. A sample fuel flow was extracted from engine feed fuel flow through a nozzle

inserted downstream of a seven-micron filter. In this manner, the fuel flow rate was split

and regulated by nozzle selection. The relationship for flow number (*FN*) is given by Eq. 16 (Bartok, 1991:552-553).

$$FN = \frac{\dot{m}_{fuel}}{\sqrt{\Delta p_{fuel}}}\sqrt{\frac{\rho_{cal}}{\rho_{fuel}}} \qquad (16)$$

From this relationship, fuel mass flow ($\dot{m}_{fuel}$) is a function of nozzle flow number, square root of pressure drop (Δp_{fuel}) across nozzle, and square root of fuel density (ρ_{fuel}). Density of the fluid used to calibrate the nozzle (ρ_{cal}) must also be included. The density of the fuel was the same for both the peanut nozzles used for fuel injection and for the nozzle used for sample extraction. The pressure drop across the sample and fuel injection nozzles was equal (verified by use of transducer measurement), and therefore selection of nozzle flow number determined the fraction of mass flow extracted for sampling (approximately 10 percent). Early experiments found that nozzle flow number was greatly affected by coking, making sample mass flow determination by flow number impossible. For more discussion on coking affects on flow number, see Appendix C. Sample mass flow was needed for calculation of percent volumetric liquid-to-gas conversion, discussed in Chapter IV. It was therefore necessary use a linear bag that allowed quantification of the entire sample collected.

Upon expanding the sampled fuel through its nozzle, it was cooled to room temperature by flowing through 3.66 m (12 ft) of coiled $^3/_8$-inch type 316 stainless steel tube immersed in chilled water as shown in Fig. 21. During normal operation (no sample storage) the cooled sample flow was redirected back into the main manifold through a remotely operated three-way valve. This occurred while the PDE was allowed to run up

to a steady state operating temperature. When the system temperature stabilized, the

three-way valve was actuated to redirect the sample flow to the liquid and gas sample

collection apparatus for a specified period of time (time needed to find sample mass flow

rate).
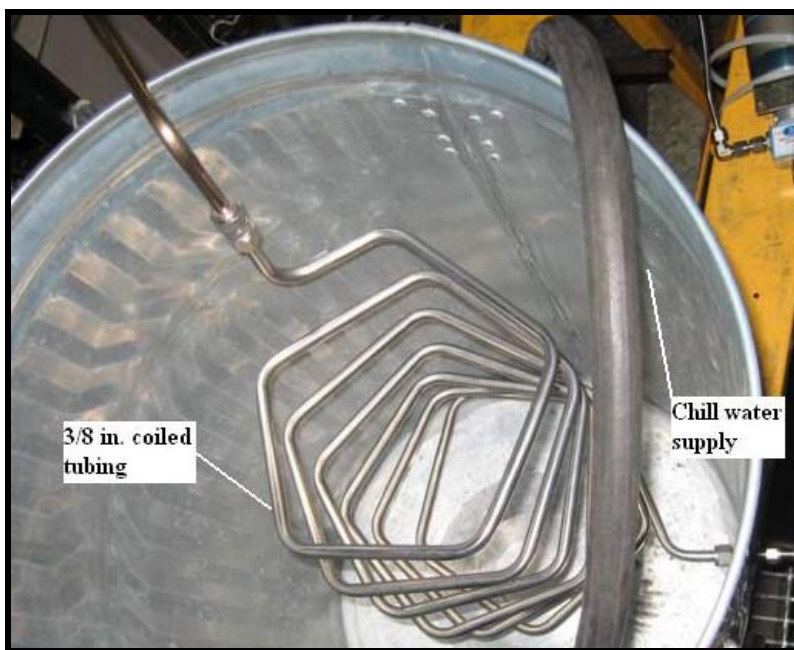
Figure 21. Photograph of coiled stainless steel tubing immersed in chilled water, used to cool fuel sample

Upon thermal cracking, the fuel decomposed into lower molecular weight

products, including liquid and other components that were in gaseous phase at ambient

conditions. The liquid portion was collected in a 500 ml (30.51 in^3) Erlenmeyer flask

while the gaseous portion was collected in a 1000 ml (61.02 in^3) Swagelok stainless steel

sample vessel. The trap shown in Fig. 22a directed both portions into the flask through

an inner tube. The outer tube enabled the gaseous products to flow further downstream to

be collected in the stainless steel sample vessel shown in Fig. 22b. After exiting the

vessel, the vapor was collected in a linear bag, shown in Fig. 22c.
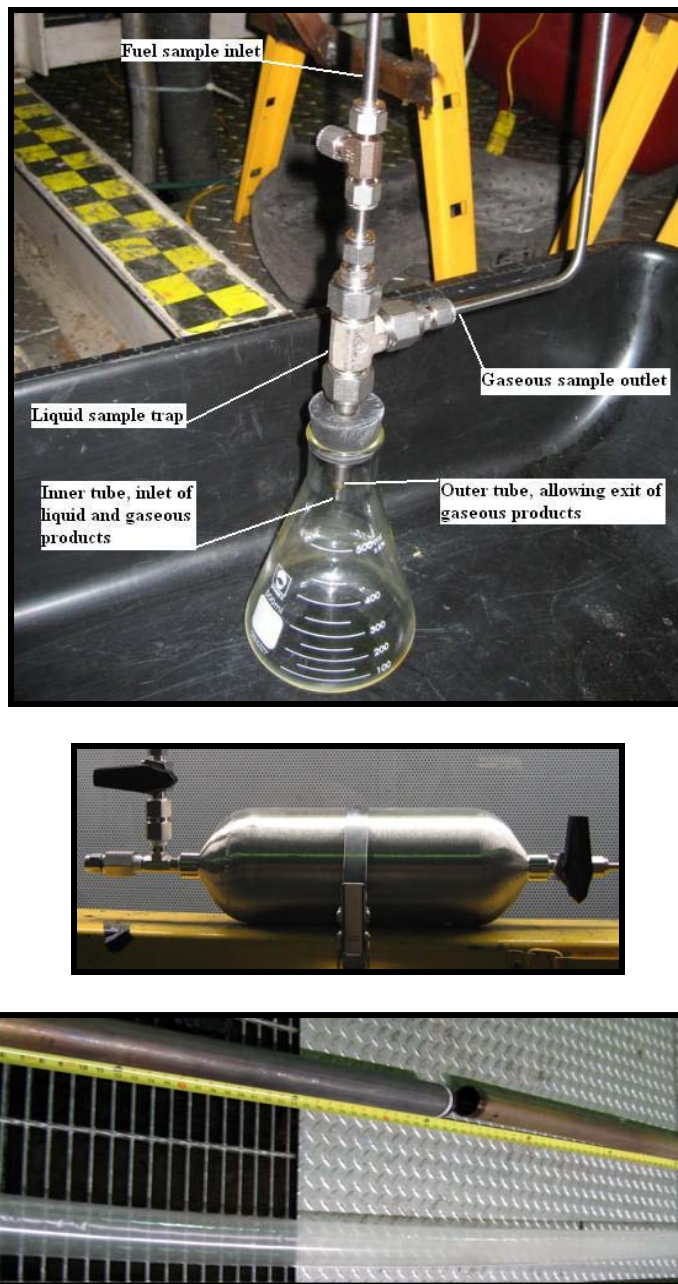
Figure 22. Photograph of a) liquid sample collection trap (top), b) stainless steel vapor sample vessel (middle), and c) linear bag used to quantify vapor sample (bottom)

The vapor produced during sampling was accumulated in an 8.6 cm (3.4 in.) diameter linear plastic bag, shown in Fig. 22c. This allowed the volume of the gas that was formed to be quantified with measurement of bag length. This quantity was necessary to calculate the amount of liquid that was converted to gas during experiments (discussed in Chapter IV). Figure 23 shows a schematic drawing of the PDE with the FHS and sample collection system connected.
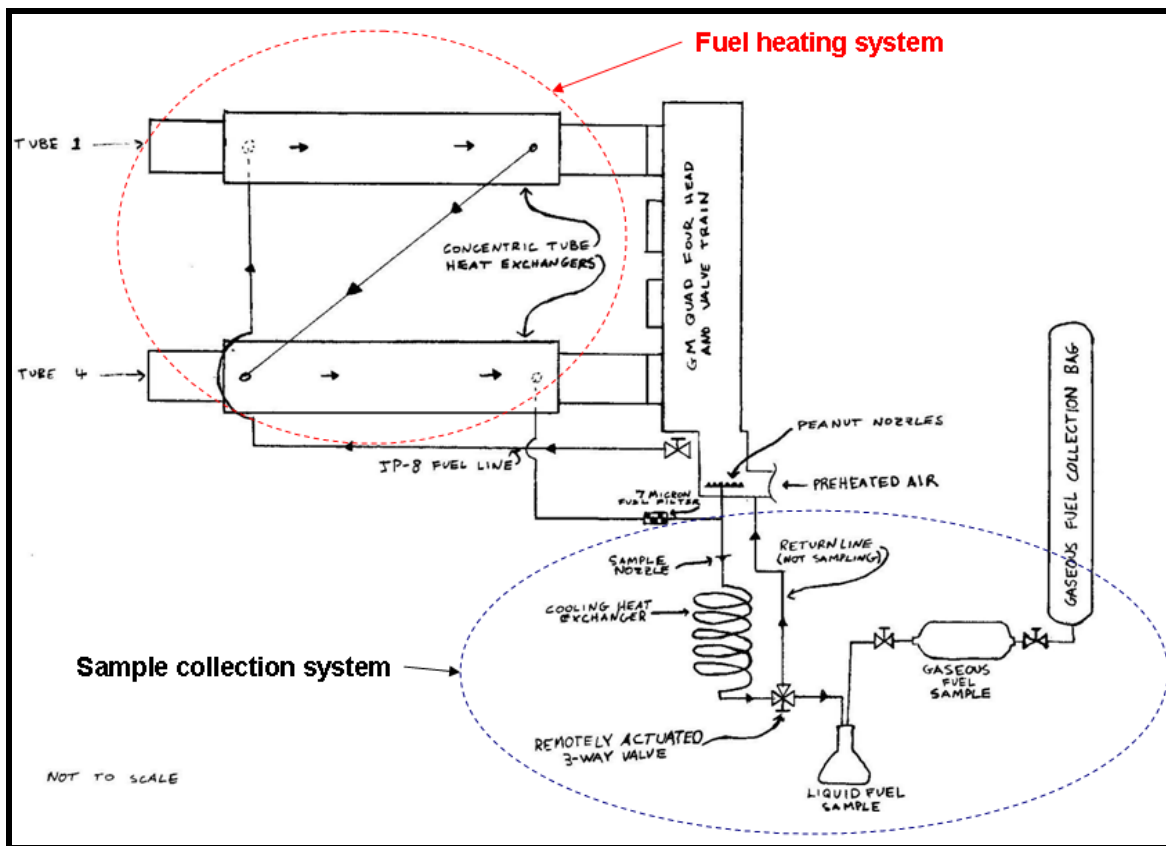
Figure 23. Schematic drawing of FHS and sample collection system connected to PDE

PDE Instrumentation

The same instrument configuration was used for the duration of this work. Two ion probes were installed in both detonation tubes one and four, axial distances measured from the head are shown in Table 3. Pressure transducers were employed to determine the head pressure in tubes one and four. Five $^1/_{16}$ in. J-type thermocouples were inserted into the fuel flow path to monitor temperatures. Two were placed at the center of each heat exchanger and one at the exit. During all experiments the exit temperature was taken to be the maximum value reached. The injection temperature was measured directly upstream of the spray bar and the last thermocouple was inserted at the end of the coiled stainless steel tubing to monitor the cooled fuel temperature.

Table 3. Location of ion probes in detonation tubes for experimentation

Ion Probe Number	Tube Number	Axial Location (cm)	Axial Location (in.)
1	1	140.97	55.5
2	1	162.56	64
3	4	144.78	57
4	4	165.10	65

Test Procedure

Each of the multiple tests that were run followed the same procedures. Prior to testing the JP-8, fuel was sufficiently sparged and transferred to the bladder accumulators. Any residual fuels other than JP-8 were purged from the fuel lines. The JP-8 was allowed to fill the lines through the last chance valve. The air compressor was energized and air was blown through the main air pipes with the vent open to flush out

any settled rust or water. Electric power was supplied to the oil pump, water pump, and electric PDE drive motor, allowing operation if commanded from the control room. The engine frequency, ignition delay, fill fraction, purge fraction, tube volume, number of tubes, and critical flow air nozzle size were entered into the *LabVIEW*® control program. After the oil and water pumps were turned on, the engine was brought to operation frequency and air without fuel flowed through the engine. The air heater was set to the desired temperature. When the temperature was reached, the engine was ready to run and low speed data collection was initiated on the control computer.

To begin engine operation, the igniters were turned on and the last chance valve was opened. The engine operator manually adjusted the injection pressure of the fuel to give the desired fuel mass flow (equivalence ratio). After fuel flow stabilized, combustion began in the detonation tubes. Data collection on the high speed computer was completed at various times throughout each test. As the fuel temperature began to rise, the operator had to increase pressure to compensate for the changing density. Special attention was given to keep the pressure above the critical point (app. 24.14 atm or 340 psi) to prevent boiling. When the fuel temperature reached the desired level, the three-way valve was actuated and a sample was collected simultaneously with PDE performance data. When sample and data collection were completed, the three-way valve was turned to cut fuel off from the sample collection path. The test was ended by turning fuel off at the last chance valve and turning the igniters off.

Immediately following each test, the valves attached to the stainless steel sample vessel were closed. The liquid sample was transferred to an appropriately sized

graduated cylinder and the volume was recorded. Two 30 ml (1.01 oz.) capped sample vials were filled with the stressed fuel. Finally the length of linear bag filled with vapor was measured, thereby completing each experiment.

IV.   Data Analysis

Overview

Analysis performed on each experiment was twofold. The goal was to examine how stressed fuel chemical composition related to PDE performance. It was therefore necessary to collect data that would allow examination of ignition time. It was equally important to characterize the fuel as it underwent different levels of pyrolytic decomposition. The analysis of PDE performance required data collection on both the high speed computer and the control computer. This data was then converted to a useable form using a C++ data reduction program. To characterize fuel properties, off-line chemical composition analysis was performed on both liquid and vapor samples for each experiment at the Air Force Research Laboratory, fuels branch (AFRL/RZTG).

Data Acquisition

The *LabVIEW*® control software on the control computer was utilized to collect low speed (Hz and KHZ) data. This included all thermocouple temperature readings, mass flow measurements, air flow measurements, and various pressure transducer readings. These data were compiled and outputted as an *Excel*®-formatted document. The high speed computer was used to collect all combustion data. A *LabVIEW*® program named *OnLineWavespeed* was employed to collect eight channels of raw data in 0.5 second intervals; channel and data signal information shown in Table 4. The data master scan rate was set at 1,000,000 scans per second. With 0.5 second intervals 500,000 data

points were produced for each data collection point. Each data collection point was

outputted as approximately 20 megabits of binary data including a curve fit that enabled

conversion of binary values to floating point values. These data had to be interpreted and

changed into a useful form.

Table 4. Data collection channels

Channel Number	Data Trace
1	Tube one ignition
2	Tube four ignition
3	Tube one head pressure
4	Tube four head pressure
5	Ion probe #1
6	Ion probe #2
7	Ion probe #3
8	Ion probe #4

Data Reduction and Ignition Time

The tool that was utilized to transform the raw binary output data from

OnLineWavespeed to floating point values was a *C++*®program named *PTFinder*. The

program separated the data into combustion events, using each spark trace to signal a new

event. Each event was then analyzed to determine ignition time. Ignition time is defined

as the time period between ignition of the fuel at the closed end of a PDE tube and the

commencement of deflagration. For these experiments, rates of pressure increase greater

than 340.2 atm/sec (5,000 psi/sec) define initiation of deflagration. The ignition times

were found by using the spark trace and the slope of the pressure trace. Because there

was a substantial amount of high frequency noise, the signal was passed through the

Savitzky-Golay digital finite response filter (Parker, 2003:1). The fourth order, 401 point

filter translates the high frequency noise into a smooth signal while retaining the original form of the pressure trace. *OnLineWavespeed* then found the slope of the pressure trace by way of linear regression. Sections of 1,000 points were examined to establish the average pressure rise. The program started at the beginning of the pressure trace and continued forward in time until the average pressure rise was equal to 340.2 atm/sec (5,000 psi/sec). The time at the center of the 1,000 point section that met the pressure threshold value was taken to be the ignition time.

Gaseous Sample Analysis

Analyses of liquid and gas samples were performed post running (off-line). Liquid samples were volumetrically quantified using a 250 ml graduated cylinder. Sample analysis was performed at Air Force Research Laboratory, fuels branch (AFRL/RZTG). Quantitative analysis of the gaseous samples was performed using an Agilent model 6890 gas chromatograph (GC) equipped with both flame ionization detector (GC/FID) and thermal conductivity detector (GC/TCD). Gaseous hydrocarbon products were quantified via GC/FID while the hydrogen was quantified using GC/TCD. In either case, a sample is injected into a column that retains the different compounds in the fuel by their respective volatility. Since each compound has a characteristic volatility, they became separated at different times. The time that a compound is retained in the GC column is referred to as a retention time.

Quantitation of the hydrogen was performed first with a 0.1 ml injection of the gaseous sample. As mentioned earlier, the TCD was utilized to detect the concentration

52

of hydrogen in the sample. The TCD works by comparing the thermal conductivity of the sample to the known thermal conductivity of the gas in which it was carried. During analysis, argon was employed as a carrier gas. The difference in conductivity was outputted as a signal and integrated to find an area. This area was translated to hydrogen concentration through a calibration curve. The calibration curve was formulated by injecting calibration gas with known concentrations of hydrogen and recording response areas for each.

Quantitation of the hydrocarbons followed via FID. The gaseous sample was injected into the GC in the amount of $10\,\mu l$. Following separation by the column, the sample was eluted and then passed through the FID. A hydrogen/air gas mixture ignited the sample and electrons were formed as a result of ionization (Littlewood, 1970). The resistance in the gap between two electrodes was reduced allowing a current to flow. The FID signal was outputted and integrated to show quantities of the different compounds in the fuel.

Unlike the method used to quantify hydrogen, the amount of hydrocarbons were not determined by utilizing a calibration standard for each compound. Instead the FID response for each compound was compared on the basis of carbon number. The signal coming from the FID was proportional to the number of carbon atoms that were eluted at a specific time (Cooper, 2003:4). The GC/FID signal resembles a multitude of peaks that occur over a variety of retention times, each peak representing a compound. The area under each peak ($Area_i$) was proportional to the amount and number of carbon atoms ($n_{C,i}$) in that region, shown in Eq. 17 (Cooper, 2003:4).

$$Area_i \propto n_{C,i} \tag{17}$$

The entire signal was integrated and individual areas were summed. The fraction of each individual area to the sum of areas was equated to the mole fraction χ_i of each individual compound, given in Eq. 18 (Cooper, 2003:4).

$$\frac{Area_i}{\sum_i Area_i} \propto \frac{n_{C,i}}{\sum_i n_{C,i}} = \chi_i \tag{18}$$

Note that in order to identify a specific compound, the retention time must be known. Over 90 percent of the compounds present in the vapor could be identified by their respective retention times and the remaining compounds were assumed to be C_6 hydrocarbons. Retention times were found by utilizing standards of known composition. Additionally, quantification of select hydrocarbons was verified by comparing results to those found by calibration curve. Appendix D shows detailed results of GC/TCD and GC/FID analyses.

Liquid Sample Analysis

Liquid samples were analyzed by both high performance liquid chromatography (HPLC) and gas chromatography-mass spectrometry (GC-MS). The Agilent model 1100 was utilized to perform the HPLC via American Society for Testing and Materials (ASTM) method D6379 to quantify one and two ring aromatic concentration in the stressed samples. The Agilent model 6890 gas chromatograph combined with Agilent model 5973 mass spectrometer was employed to quantify changes in individual component concentrations in select alkanes, alkenes and multi-ring (greater than two)

54

aromatics. In both the HPLC and GC-MS the samples were diluted in hexanes before

being injected into the column on either instrument. The columns installed in both the

HPLC and GC-MS work as described in the gaseous sample analysis section to separate

the different compounds in the fuel based on their respective volatility. They were then

eluted through the detector in either machine to produce a signal that was integrated.

Much like the GC/TCD, the signal responses were utilized for quantification by

comparing them with signal responses from calibration standards with known

concentrations. The sample injected into the GC-MS continued on to the mass

spectrometer (MS) for further analysis. As a compound entered the MS, it was

fragmented into its characteristic ions. The computer then compared the MS results to a

library of compounds for identification. Appendix D shows detailed results of GC-MS

and HPLC analyses.

Calculated Percentage of Liquid Converted to Gas

The percentage of liquid converted to gas is a metric that can be utilized as an

indicator of pyrolytic activity. As mentioned earlier, the sample mass flow rate was not

able to be determined by nozzle flow number. Therefore, the method of fuel sampling

that was used required a mass balance to be performed to determine the amount of liquid

that was converted to gas. The total mass of the fuel sample (m_{sam}) was the sum the mass

of the liquid portion of the sample (m_{liq}) and the mass of the vapor portion of the sample

(m_{vap}), shown in Eq. 19.

$$m_{sam} = m_{liq} + m_{vap} \tag{19}$$

The volume of the liquid portion of the sample (V_{liq}) was measured and the density (ρ_{liq}) was found by weighing a small portion of it. These two values allowed m_{liq} to be calculated using Eq. 20.

$$m_{liq} = \rho_{liq} V_{liq} \tag{20}$$

The volume of the vapor was also measured, but bag size made it impractical to find density by weighing the entire sample. Therefore, a different method had to be used to find the vapor mass. The GC gave data that enabled the knowledge of the mole fraction of each component (χ_i) that was present in the vapor (described in gaseous sample analysis section). The ideal gas law (Eq. 21a) allowed the identification of total number of moles in the vapor portion of the sample (n_{vap}). The number of moles for each individual component (n_i) was calculated in (Eq. 21b). Finally, the molecular weight (MW_i) for each component is a known value and allowed the total mass of the vapor (m_{vap}) to be calculated (Eq. 21c).

$$n_{vap} = \frac{PV}{RT} \tag{21a}$$

$$n_i = \chi_i n_{vap} \tag{21b}$$

$$m_{vap} = \sum n_i MW_i \tag{21c}$$

In Eq. 21a, T and P are the ambient temperature and pressure, respectively, in the test cell, n is the number of moles, V is the volume of the vapor sample collected, and R is the

universal gas constant (8.314 J/(mol*K) or 10.732 (ft^3*psi*lb)/mol*°R). The volumetric

liquid-to-gas conversion was computed as a percentage (% vol_{L-G}) defined as the volume

of liquid that was converted to gas (V_{L-G}) normalized by the sum of the volume of the

liquid sample (V_{liq}) and the volume of liquid that was converted to gas, given in Eq. 22.

$$\%vol_{L-G} = \left(\frac{V_{L-G}}{V_{liq} + V_{L-G}} \right) \cdot 100 \qquad (22)$$

The volume of liquid that was converted to gas (V_{L-G}) was found by taking the mass of

the vapor portion of the sample (m_{vap}) and normalizing it by the density of JP-8 (ρ_{JP-8}),

shown in Eq. 23.

$$V_{L-G} = \frac{m_{vap}}{\rho_{JP-8}} \qquad (23)$$

Volumetric liquid-to-gas conversion is an indicator that helps to gauge extent of

pyrolytic activity. From the discussion on pyrolytic reaction pathways given in Chapter

II, it is clear that the higher molecular weight hydrocarbons break down into lighter

compounds including some in gas phase at ambient conditions. More products in

gaseous phase are produced as free radical reactions persist further in cracking the fuel.

Volumetric liquid-to-gas conversion then serves as a means to indicate how much

cracking has occurred.

Calculation of Residence Time

One of the parameters that affect thermal decomposition is residence time. This

parameter can be described as the amount of lapsed time for a particle of fuel to transit

the heat exchanger from inlet to exit. As the fuel transited the heat exchanger through the annulus at a given pressure, the density decreased with increasing temperature. The changing density was accounted for in calculation of residence time by segmenting the flow path into individual lengths of 0.076 m (3 in.). The amount of time that lapsed for the fuel to travel in each segment was found by Eq. 24:

$$t_i = \frac{A_a L_i \rho_i}{\dot{m}_f} \tag{24}$$

where t_i is the incremental time lapse, ρ_i is the density in each segment, A_a is the area of the annulus, L_i is the length of each segment, and $\dot{m}_{fuel}$ is the fuel mass flow. The residence time (t_{res}) was found by summing all incremental time lapses, given in Eq. 25.

$$t_{res} = \sum t_i = \sum \frac{A_a L_i \rho_i}{\dot{m}_f} \tag{25}$$

The temperature for each incremental distance was found by creating a temperature profile from thermocouple measurements at various points along the length of the heat exchangers. The temperatures were used to estimate the density of the fuel in each segment from SUPERTRAPP density tables of a JP-8 surrogate produced by AFRL (Miser, 2005:99). See Appendix C for discussion on why SUPERTRAPP data was utilized to estimate density. Table 5 shows the chemical composition of the SUPERTRAPP JP-8 surrogate.

Table 5. Chemical composition of AFRL JP-8 surrogate used in SUPERTRAPP (Spadaccini, 1998)

Component	SUPERTRAPP Synonym	Mole Fraction	Mass Fraction
methylcyclohexane	MCC6	0.065	0.042
meta-xylene	MXYL	0.07	0.049
ethylcyclohexane	ECC6	0.067	0.050
n-decane	C10	0.157	0.147
butylbenzene	C4BNZ	0.056	0.050
isobutylbenzene	IC4BNZ	0.056	0.050
nampthalene	NAPH	0.058	0.049
n-dodecane	C12	0.175	0.207
1-methylnapthalene	1MNAPH	0.052	0.049
n-tetradecane	C14	0.113	0.156
n-hexadecane	C16	0.066	0.104
2,5-dimethylhexane	25DMH	0.065	0.049

Error Analysis

In any experiment it is desired to know how well the information presented correlates to true data that would be collected in a perfect environment. This section discusses the methods used to assess the errors encountered during experimentation. Both precision errors and bias errors are explored to further explain the data presented in this work.

The total experimental error can be examined by what is known as an uncertainty analysis, where uncertainty has components of both bias and precision errors. Equation 26 gives the method of combining the bias and precision errors by the root-sum-square method (Coleman, 1989:77).

$$U_X = \left[B_X{}^2 + P_X{}^2 \right]^{0.5} \qquad (26)$$

Equation 26 shows that the total root-sum-square uncertainty (U_X) is comprised of B_X, and P_X, the bias and precision limits, respectively.

The first type of analysis discussed involves precision error, which is sometimes referred to as repeatability or repeatability error (Coleman, 1989:7). Precision error is the random element of total error and can be examined on a statistical basis. If an infinite number of samples were taken, the expectation would be that they would all fall within a Gaussian or normal distribution (Coleman, 1989:19). In the following discussion, the infinite sample scenario will be referred to as the parent distribution. For obvious reasons, it is only possible to take a limited number of samples, which will be referred to as the sample distribution. The mean ($\bar{X}$) of the sample population is given by Eq. 27:

$$\bar{X} = \frac{1}{N} \sum_{i=1}^{N} X_i \tag{27}$$

where N is the number of individual readings, X_i (Coleman, 1989:26). The sample standard deviation, S_X, can be found by employing Eq. 28.

$$S_X = \left[\frac{1}{N-1} \sum_{i=1}^{N} (X_i - \bar{X})^2 \right]^{0.5} \tag{28}$$

During data reporting, the degree of confidence that the parent population mean falls within a certain interval can give an indication of data accuracy and reliability. The challenge faced in a finite sample population is that the true mean of the parent population is not known. Additionally, the sample population does not follow a Gaussian distribution. It is therefore necessary to define a confidence interval in terms of a t-

distribution (Coleman, 1989:28). The precision limit, P_X, is used to represent the

precision of the sample mean, given by Eq. 29:

$$P_X = tS_X / \sqrt{N} \tag{29}$$

where t is a t-function whose value is based on number of samples as well as confidence

required. For this work, the confidence interval of 95% was used. In other words, it was

expected (with 95% confidence) that the mean of the parent population would fall within

the interval $\overline{X} \pm P_X$.

Bias errors can be examined by considering elemental error sources that are

introduced through calibration, data acquisition, or data reduction (Coleman, 1989:78).

The contributions made by each elemental source are combined using the root-sum-

square method to find the bias limit (B_r), given by Eq. 30:

$$B_r = \sqrt{\sum_{k=1}^{m} (B_i)_k^2} \tag{30}$$

where B_r is the bias limit of each element for m number of elements (Coleman, 1989:79).

The elemental bias limits propagate throughout calculations and affect the end

experimental result. The bias limit of the experimental result (B_x) for a variable of

interest is given in Eq. 31.

$$B_x = \sqrt{\sum_{j=1}^{i} \left[\left(\frac{\partial r}{\partial X_j} \right)^2 B_j^2 \right]} \tag{31}$$

Equations 30 and 31 were used to perform an elemental bias limit analysis for the

volumetric liquid-to-gas conversion.

A detailed outline of bias limits found for the liquid-to-gas conversion is given in Appendix B. Sources of bias that contributed to the uncertainty during this work include: linear bag measurements (length and diameter), linear bag diameter irregularity, pressure transducer readings, thermocouple temperature measurements, GC accuracy, and graduated cylinder readings. Uncertainty is represented as error bars on the plots in Chapter V. Details of elemental bias limits and their propagation into experimental results are given in Appendix B.

V.   Results and Discussion

Overview

The overall objective of this research was to characterize decomposed JP-8 while studying its effect on performance of a pulse detonation engine. To accomplish this, the fuel was first reacted via zeolite coated thrust tube heat exchangers. Further insight was gained about chemical composition and reaction pathways by extracting samples of stressed fuel for off-line analysis. Vapor and liquid fuel samples that were taken at various heat exchanger exit temperatures were analyzed via gas chromatography to identify their chemical composition. In Chapter II, the theory was developed that fuel type changed the detonation structure via cell size, thereby affecting initiation energy. Furthermore, lower initiation energy fuels are desired to improve PDE performance by decreasing ignition time which allows higher operating frequency and increased thrust. PDE ignition time was used as the measured parameter to gauge what effect the cracked fuel had on engine performance. Testing was limited by coke deposition in the fuel filter and injection nozzles. For the majority of tests performed where heat exchanger exit temperatures were above 866 K (1100 $^{\circ}$F), the experiment was terminated by clogged nozzles and fuel filter.

Stressed gaseous and liquid fuel products were consistent with those produced by the free radical reaction mechanism discussed in Chapter II. As pyrolytic reactions persist, high molecular weight hydrocarbons are broken down into lighter species including some in gaseous form at ambient temperature and pressure. For this reason, volumetric liquid-to-gas conversion was determined to indicate the extent of pyrolysis.

63

Samples of reacted fuel were taken over heat exchanger exit temperatures ranging from 820 K (1016 $^{\circ}$F) to 940 K (1232 $^{\circ}$F). Analysis of the vapor samples indicated that principal gaseous components were C_1-C_3 alkanes and alkenes (>75% by volume). Gas chromatography performed on the liquid products showed that high molecular weight hydrocarbons were decomposed while shorter chain alkanes, aromatics and alkenes were formed, showing good agreement with expected thermal decomposition pathways that were discussed in Chapter II. Overall they are consistent with results that were observed from cracking long chain hydrocarbons at intermediate temperatures and high pressures for short reaction times (Edwards, 2006:4,5) (Fabuss, 1964:33-37). The engine data that was collected through the duration of testing was analyzed and showed that ignition time decreased as extent of fuel conversion increased.

Volumetric Liquid-to-gas Conversion

When the JP-8 was heated to a sufficient temperature that initiated pyrolytic reactions (approximately 811 K or 1000 $^{\circ}$F), higher molecular weight hydrocarbons began to break down into lighter species including some gaseous at ambient temperature and pressure. For this work, the percentage of liquid that was converted to gas was studied as a general indication of the extent of thermal decomposition realized during different test runs. Figure 24 shows a monatomic increase in vapor production as the heat exchanger exit temperature increases from 820 K (1016 $^{\circ}$F) to 940 K (1232 $^{\circ}$F). The extent of pyrolytic reactivity is dependent upon both temperature and residence time (discussed later). The residence time was calculated and is indicated on secondary x-axis

in Fig. 24. Details on how volumetric liquid-to-gas conversion and residence time were

calculated are given in Chapter IV.
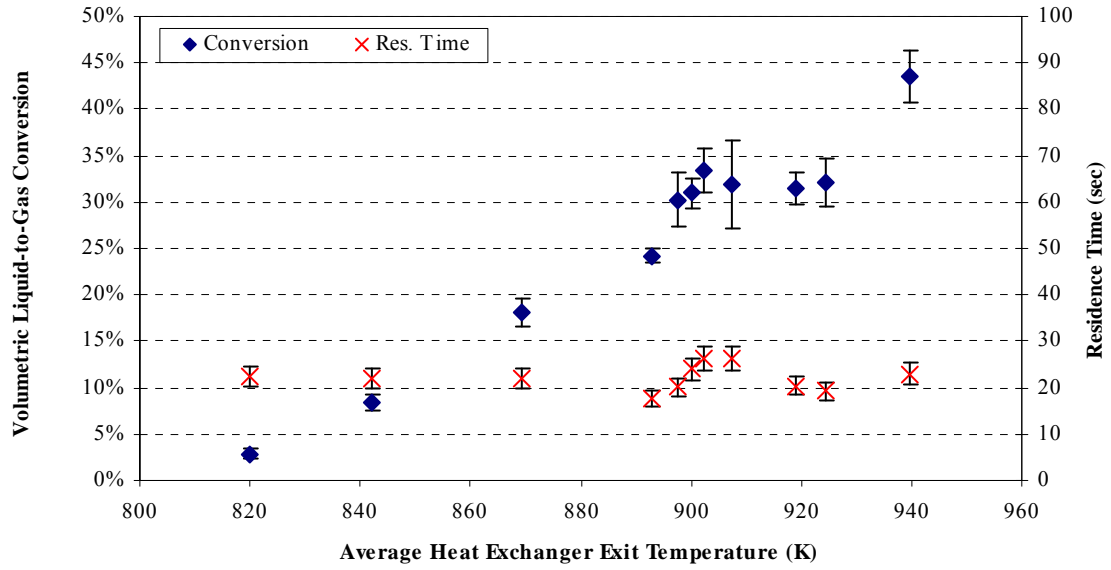
Figure 24. Volumetric liquid-to-gas conversion and calculated residence time as a function of average heat exchanger exit temperature

Residence Time Implications

The energy balance for a steady flow system with negligible kinetic and potential

energies and no work interaction is given in Eq. 32:

$$\dot{Q} = \dot{m}\Delta H = \dot{m}\overline{c}_p\Delta T \tag{32}$$

where $\dot{Q}$ is the rate of net heat transfer, $\dot{m}$ is the mass flow, $\overline{c}_p$ is the average specific

heat (constant pressure) for the process, and ΔT is the change in temperature (Cengel,

2006:13). Total amount of heat transfer (Q) is expressed in Eq. 33:

$$Q = \dot{Q}\Delta t = \Delta t \left(\dot{m} \overline{c}_p \Delta T \right) \tag{33}$$

where Δt is the change in time. This can be applied to the endothermic process to analyze the amount of heat that is imparted to the fuel (Q_{in}) and is expressed in Eq. 34:

$$Q_{in} = \dot{m}_f \Delta t (H_{ex} - H_{in}) = \dot{m}_f \Delta t \left[\overline{c}_p (T_{ex} - T_{in}) \right] \tag{34}$$

where $\dot{m}_{fuel}$ is the mass flow of the fuel and the enthalpies at the heat exchanger exit and inlet are H_{ex} and H_{in}, respectively (Huang, 2004:286). Of the total enthalpy change from the heat exchanger inlet to exit, some goes into raising the temperature of the fuel/products (sensible enthalpy) while the rest is absorbed in the endothermic reactions (Huang, 2004:286). Equation 34 shows that if the heat exchanger exit temperature is increased or if the amount of time is increased, more heat will be imparted to the fuel. Therefore an increase in either temperature or residence time will increase the amount of heat that is available to be absorbed by the endothermic reactions.

Figure 24 shows an increasing conversion as the temperature rises from 820 K (1016 °F) to 940 K (1232 °F). Around the temperatures ranging from 890 to 930 K there are deviations from the monatomic trend. The residence times remain relatively constant through all of the tests with the exception of those observed around the temperatures of 890 to 930 K. With the exception of these few deviations, volumetric liquid-to-gas conversion for this work can be compared almost solely as a function of temperature. Based on the discussion of residence time implications, an increase in time would correlate to increased reactivity and ultimately an increase in conversion. However, there is not currently enough data to compute the correlation between the residence time and

conversion deviations shown in Fig. 24. The results shown in Fig. 24 are in line with

what is expected of pyrolytic reaction pathways, which suggests that higher molecular

weight species are decomposed into lighter hydrocarbons. As more heat is imparted to

the fluid, the products from initial reactions of the parent fuel components should break

down in subsequent reactions that persist via free radical mechanisms (see Chapter II).

The result is an increased amount of lighter species that are in gaseous form at standard

temperature and pressure. The results presented in Fig. 24 compare well with other

research (Edwards, 2006:6) discussed in Chapter II. While the results are not

numerically identical, due to differing parent fuels and conditions, the results show

consistency in reaction pathways. The implications that liquid-to-gas conversion has on

ignition time are better understood with knowledge of vapor composition, discussed next.

Vapor Composition

Vapor analysis was completed on samples to identify products formed as a result

of pyrolysis and give further insight about cracked fuel composition affect on PDE

performance. The gaseous product analysis performed on all samples via GC/TCD and

GC/FID revealed predominant formation of C_1-C_3 alkanes and alkenes (>75% by

volume). Table 6 is a summary of primary vapor products that were formed. The most

abundant compounds present in the vapor were plotted in terms of both mole percent and

mass percent in Figs. 25 and 26, respectively. For clarity, uncertainty bars were omitted

from these plots. The errors are within ±5% of reported values in Table 6 as well as Fig.

25. Additional detailed results of the gaseous analysis can be found in Appendix D.

Table 6. Composition of vapor samples as analyzed by gas chromatography flame ionization and thermal conductivity detectors

Avg. Temp (K)	820	842	843	869	893	898	900	902	908	919	924	940
Avg. Temp (°F)	1016	1056	1057	1105	1148	1156	1161	1164	1174	1194	1204	1232
Products	**Mole Percent in Gaseous Sample (%)**											
Methane	29.2	25.9	31.3	27.9	27.3	29.0	28.3	29.6	30.6	29.3	30.8	34.2
Ethane	21.4	19.6	21.6	18.4	17.1	16.7	17.1	17.3	17.3	16.9	16.5	16.5
Ethylene	10.0	8.1	6.7	6.2	7.8	6.7	7.3	5.5	5.7	7.5	7.1	5.6
n-Propane	12.5	13.7	13.7	13.1	11.3	10.8	11.2	11.9	11.4	11.0	10.2	9.6
Propylene	12.5	13.2	11.5	11.7	12.5	11.6	12.1	10.6	10.6	12.0	11.4	9.6
iso-Butane	0.7	1.0	0.9	1.2	1.0	1.0	1.0	1.1	1.1	1.0	0.9	1.0
n-Butane	2.6	3.5	2.9	4.1	3.3	3.3	3.4	4.0	3.5	3.2	3.0	2.6
2-Butene (trans)	0.5	0.8	0.6	1.2	1.3	1.4	1.4	1.4	1.4	1.3	1.4	1.4
1-Butene	2.2	2.9	2.2	3.1	3.2	3.2	3.1	2.8	2.8	2.9	2.9	2.2
2-Butene (cis)	1.6	2.2	1.7	2.5	2.7	2.6	2.5	2.4	2.4	2.4	2.4	2.1
Hydrogen	4.3	3.8	4.0	3.8	4.2	3.8	4.1	4.1	4.1	4.1	4.3	4.8
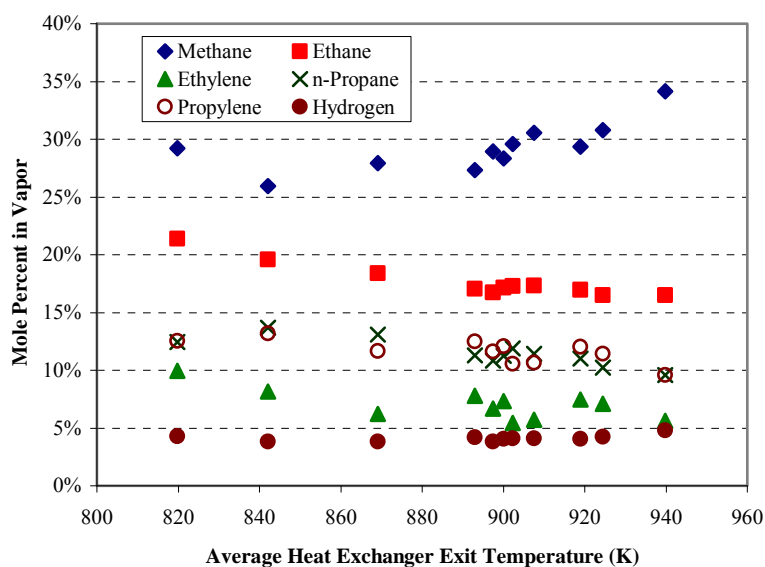
Figure 25. Mole percent of vapor compound as a function of average heat exchanger exit temperature, most abundant products shown (mole percentage of vapor only)

There is an overall trend that is seen in the mole fraction data for the vapor products. Figure 25 shows that methane mole percent increases at higher temperatures. At the same time, mole percent of the heavier alkanes and alkenes decreases. The reaction pathways that are followed during pyrolysis can explain why this is happening. Methane is a more stable species and not prone to participate in propagation reactions (Edwards, 2003:1104). The ethylene, ethane, propylene, and propane continue to react with other hydrocarbons in molecular addition propagation reactions (see Chapter II) to form aromatics and other species. As discussed next, this selective formation of methane coupled with decreases in strained hydrocarbons, like ethylene and propylene, is not desired for PDE performance enhancement.
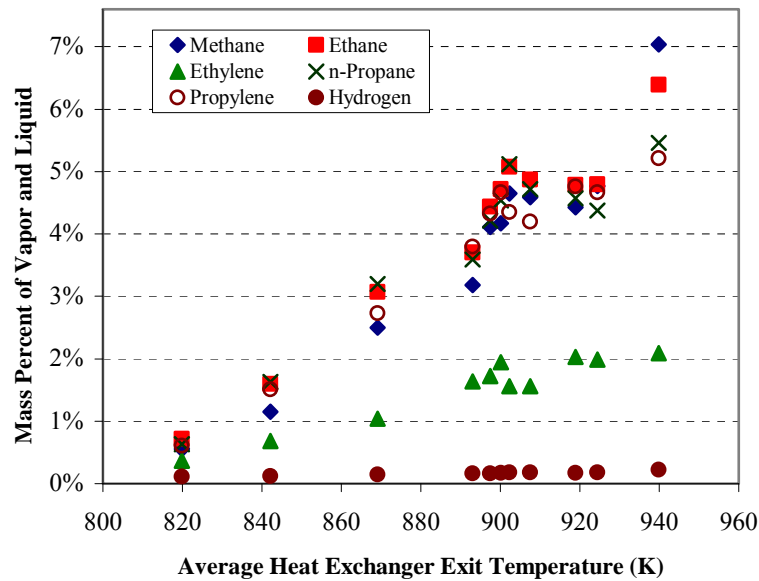
Figure 26. Percent mass of vapor compound as a function of average heat exchanger exit temperature, most abundant products shown (mass percentage of vapor and liquid)

In Chapter II, it was shown that choice of fuel has an impact on direct initiation energy, see Fig. 5 (Kaneshige, 1997), (Schauer, 2005:2). Figure 5 shows that acetylene (C_2H_2), hydrogen (H_2), and ethylene (C_2H_4) require a lower initiation energy than that required for unstrained hydrocarbons. Therefore, it is more desirable for these three species to be present in the gaseous products to improve ignition times. Figure 5 also shows that methane (CH_4) has an initiation energy much higher than that of practical hydrocarbons. Ethane (C_2H_6) and propane (C_3H_8) have initiation energies that are similar to practical hydrocarbons. The selective production of methane seen in this work acts against the end goal of improved PDE performance. At the same time the results presented in Table 6 , Figs. 25 and 26 show that hydrogen and ethylene were present in the gaseous product samples, but at lower amounts. The effect that each individual component in the vapor has on PDE performance is not known and requires further study, but the net effect proved to be positive in this work. It is not easy to gauge the overall initiation energy of the mixture. However, the improved PDE performance seen in this work and in previous experimentation (Helfrich, 2007:6,7) suggests that initiation energy of the cracked fuel is lower than that of JP-8.

Liquid Composition

Liquid sample analysis was performed via GC-MS to evaluate the liquid composition changes that occurred at different extents of reaction. Figure 27 shows that long straight-chain paraffins (C_9-C_{15}) are primary components in the JP-8 prior to heating with a molecular weight distribution spanning the C_7-C_{18} hydrocarbons. The GC-MS

spectra display a visual representation of the conversion of fuel components as the average heat exchanger exit temperature (extent of reaction) increases. Figure 27 shows that once sufficient temperatures are achieved to promote thermal decomposition, the abundance of C_7-C_{18} hydrocarbons was dramatically reduced.

The results presented in Fig. 27 give a lot of insight into the reaction pathways that were followed at different extents of cracking. The chromatogram showing the least amount of thermal decomposition (temperature of 820 K or 1016 ^{o}F) shows a small decrease in the long straight chain alkanes with a slight shift toward lower molecular weight species. This trend becomes much more pronounced as the extent of reaction increases. As the higher molecular weight alkanes are being consumed, alkenes and aromatics begin to form. The final composition at the greatest extent of reaction achieved in this work shows a preponderance of one and two ring aromatics. There are some of the original alkenes and alkanes present, but the composition barely resembles that of the parent fuel. Previous work (Huang, 2004:289), presented in Chapter II, shows a similar shift in overall composition for experiments involving JP-8 +100. This similarity was expected given that the controlling mechanisms are similar in both fuels.
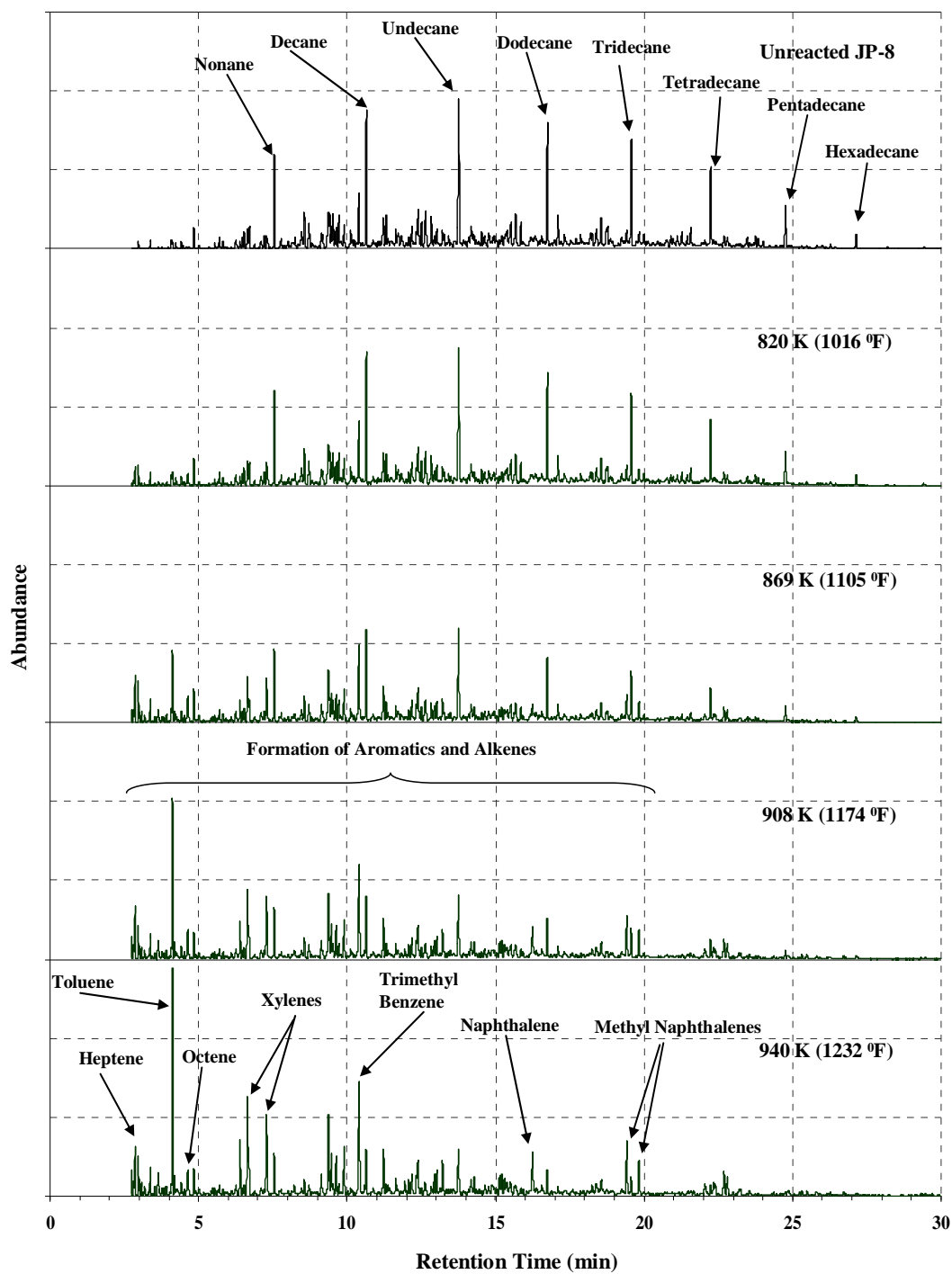
Figure 27. Comparison of GC-MS spectra of the unreacted JP-8 fuel and cracked JP-8 products at various temperatures

Chemical analyses of the liquid samples enabled quantification of compounds and further examination into controlling reaction pathways. Figure 28 shows mass percent (of liquid and vapor) as a function of average heat exchanger exit temperature. The mass percent of n-alkanes found in the liquid decreased dramatically from a total of 18.9% in the unreacted fuel to 1.9% in the fuel with the most conversion (calculated as percent mass of liquid and vapor samples). This trend shows that n-alkanes are being selectively decomposed to form other species. At the same time, Fig. 29 exhibits a sharp increase in concentration of lower molecular weight 1-2 ring aromatics. The observed increase in aromatics, mainly toluene, xylenes, and naphthalenes can be explained by secondary reactions that propagate via the free radical chain mechanism. These reactions that persisted at higher extents of pyrolysis involve some of the lighter gaseous species to form aromatics. This is consistent with what was seen in Fig. 25 where mole percentages of C_2-C_3 alkanes and alkenes dropped at higher extents of conversion. As mentioned earlier, some of the C_2 alkanes and alkenes are desired to support improved PDE performance. Therefore, it is not an appealing trend to see gaseous species being consumed in propagation reactions to form higher weight aromatics. Additionally the resulting multi-ring aromatics are precursors to coke deposition, which is also not desired. The effect that is seen in PDE performance from each of the species found in the liquid samples is not known and should be the focus of future studies. But the lowered ignition time seen in this work shows that a net positive result is realized from the overall shift in fuel composition. Detailed results from GC-MS and HPLC analysis are given in Appendix D.
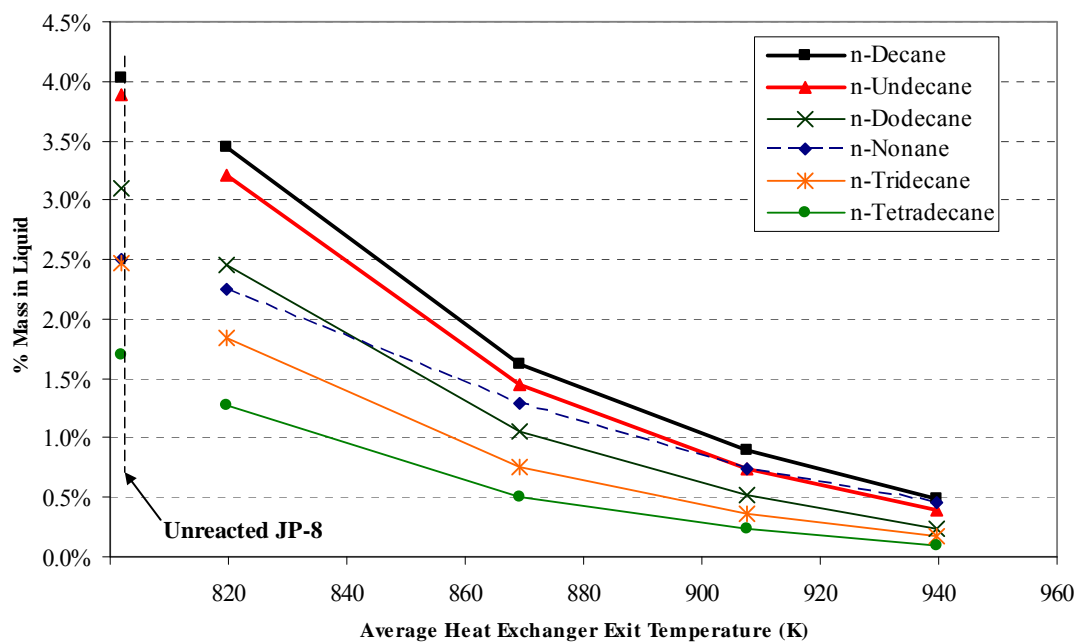
Figure 28. n-alkanes present in the liquid samples on a mass basis as a function of average heat exchanger exit temperature
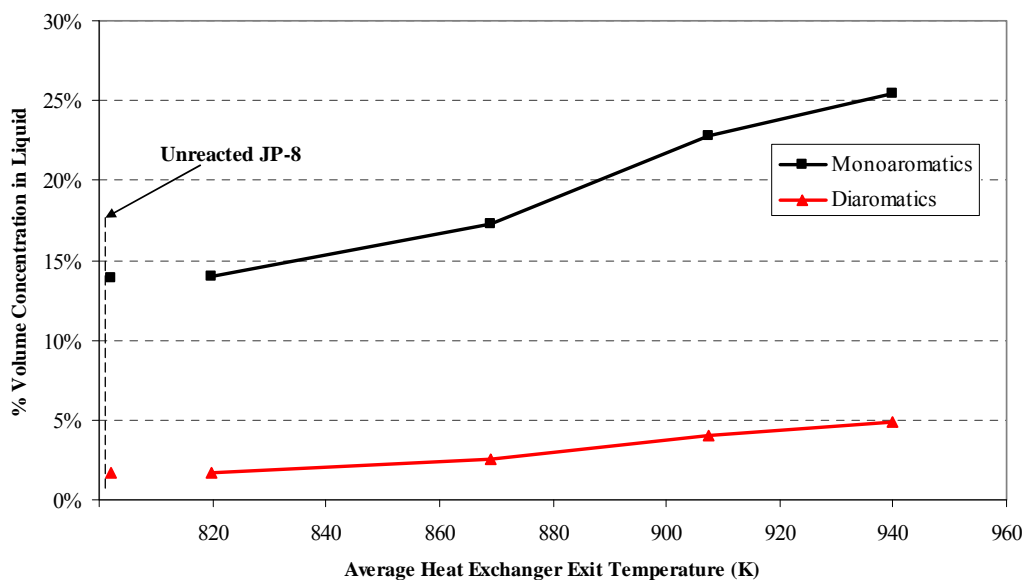
Figure 29. One and two ring aromatics present in the liquid on a volume concentration basis as a function of average heat exchanger exit temperature

74

Coking

Coke formation proved to be a major limiting factor during experimentation. For runs where the heat exchanger exit temperature exceeded 866 K (1100 $^{\circ}$F), the test was almost inevitably terminated by a clogged fuel filter. Figure 30 shows a filter that has been used during experimentation next to a filter without coke deposits. As mentioned in Chapter II, coking occurs as in the latter part of the reaction pathways that are followed during pyrolysis. This explains why tests that involved further extents of reaction were more prone to clog the fuel filter. Carbon deposition was not the focus of this work and was not quantified.
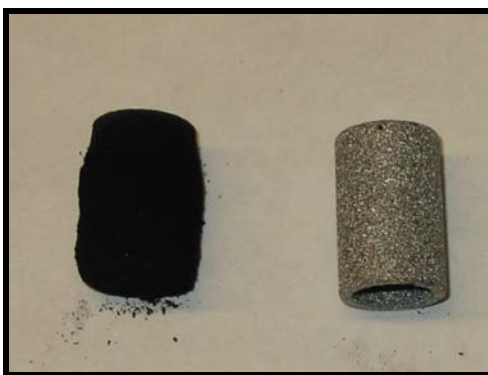
Figure 30. Photograph of coke covered filter after testing next to a filter without coking

Ignition Times

The end goal in altering the JP-8 by pyrolysis was to produce a fuel that supported improved PDE performance through decreasing ignition times. Previous work (Helfrich, 2007:7,8) showed that thermally reacted fuel yielded a nearly 20% decrease in ignition

time. This work sought to correlate the decrease in ignition time to the chemical composition at different extents of reaction. To accomplish this, engine data was recorded through the duration of experimentation and analyzed.

It was difficult to independently study temperature or equivalence ratio effects on ignition time. Control of the equivalence ratio was limited by the fact that heat exchanger temperature had to remain relatively steady during the collection of a fuel sample. Any deviation in equivalence ratio that affected engine operation, also affected heat transfer to the fuel through the heat exchangers. Therefore, data was not always taken at the same equivalence ratio at different temperatures, limiting the amount of comparison that can be made between ignition times at varying temperatures.

The first set of data analyzed was for equivalence ratios around unity (±5%). Figure 31 shows ignition time as a function of average heat exchanger exit temperature. The variation in uncertainty represented by the error bars is explained by the number of samples taken coupled with varying standard deviations for each data point. The same amount of data readings was not collected for each run yielding larger uncertainty for data points with fewer readings. Also included are data points from previous work (Helfrich, 2007:6,8). The point corresponding to ignition time that was seen with flash vaporized JP-8 represents fuel that had not yet been thermally decomposed. The other data points were taken during endothermic fuel testing with similar operating conditions. The data from previous work shows that slightly lower ignition times were reached consistently for all temperatures. As mentioned before, temperature as well as residence time affect the change in fuel composition achieved via pyrolysis. It is unknown what

residence times were previously used. Direct comparison of ignition times seen in this work to those seen in previous work is not possible if fuel composition is not known. However, the data points from previous work presented in Fig. 31give a basis to compare overall trends.
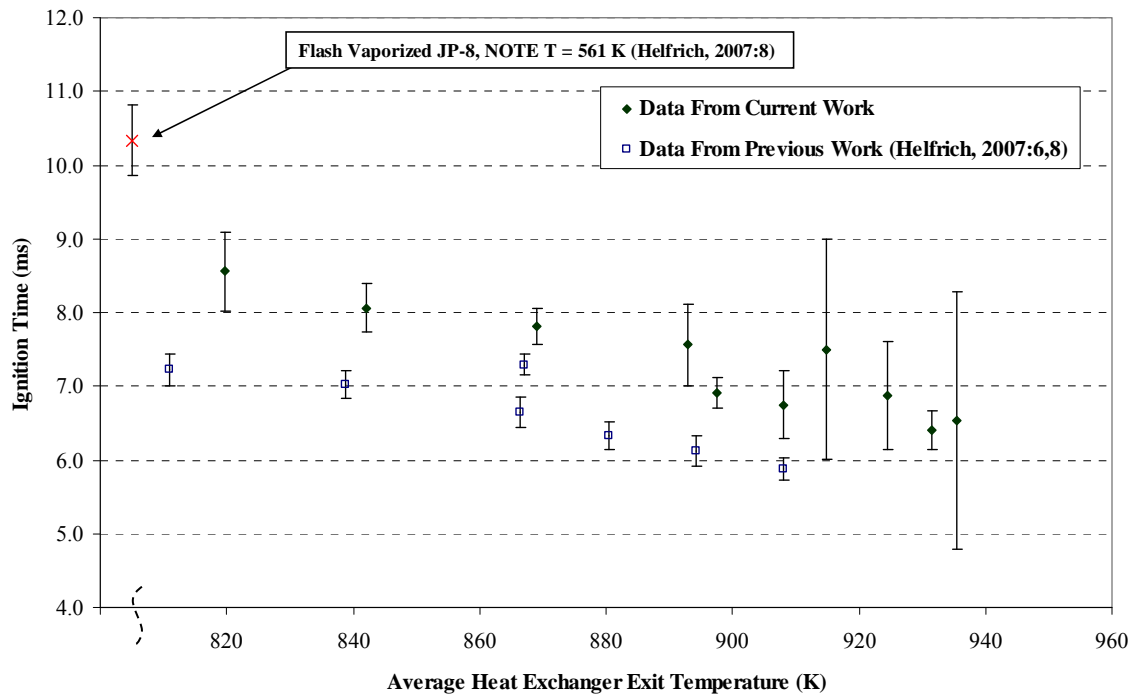
Figure 31. Ignition times as a function of average heat exchanger exit temperature for $\varphi \approx 1$

Figure 31 shows that as temperature increased from 820 K (1016 ^{o}F) to 935 K (1224 ^{o}F), ignition time decreased by over 20% and by more than 30% when compared to unreacted (flash vaporized) JP-8. This same trend was realized in previous work (Helfrich, 2007:6,8) which achieved maximum JP-8 temperatures just above 900K (1160 ^{o}F). Helfrich et al. showed that ignition time remained relatively constant until fuel temperature reached 800 K (980 ^{o}F). As shown in Fig. 31, data from Helfrich et al.

showed that ignition time decreased by 19 % as temperature increased from 800 K (980 ^{o}F) to 900 K (1160 ^{o}F). This is consistent with the temperature that thermal decomposition occurs; suggesting that the decrease in ignition time is due to the shift in chemical composition. A proposed hypothesis suggested that a further increase in temperature (above 900 K or 1160 ^{o}F) would yield a continued decrease in ignition time (Helfrich, 2007:6). Data collected during this work neither supports nor denies the suggestion. Furthermore, with the current configuration, the deleterious effects of coking would make prolonged engine runs at higher extents of reaction improbable.

The ignition time data was further categorized by temperature, and ignition times were looked at as a function of equivalence ratio. The majority of fuel samples and engine data was taken in the temperature range that spanned 894 K (1150 ^{o}F) to 922 K (1200 ^{o}F). Figure 32 shows ignition times as a function of equivalence ratio for this temperature range. The same plot also displays data that was taken in previous work (Helfrich, 2007:8) for flash vaporized JP-8 at a temperature of 561 K (550 ^{o}F) and data from an endothermic fuel studies with a similar configuration. A more than 30 percent decrease is seen in ignition time across all equivalence ratios when comparing cracked fuel to flash vaporized JP-8. The data from Helfrich et al. shows that similar ignition times were reached at lower temperatures, 866K (1000°F). This can be partly explained by the grouping of the temperatures for sake of comparison in this study. The temperatures represented in Fig. 32 span an averaged temperature range of 28 K (50 ^{o}F). The data from previous work does not. As mentioned earlier, heat transfer to the fuel is a function of equivalence ratio, among other parameters. Therefore, control of equivalence

ratio was limited by the necessity to keep heat exchanger temperature steady during sample collection. This illustrates the dependence that the pyrolysis has on engine operation with the current configuration. The conditions at time of cracking and the composition are again unknown for the data from Helfrich et al. Because of this, interpretation of the previous data is limited. The data contributed from this effort adds knowledge of fuel composition coupled with engine performance. This information is vital to exploring why ignition times are dropping and expands the potential for future research.
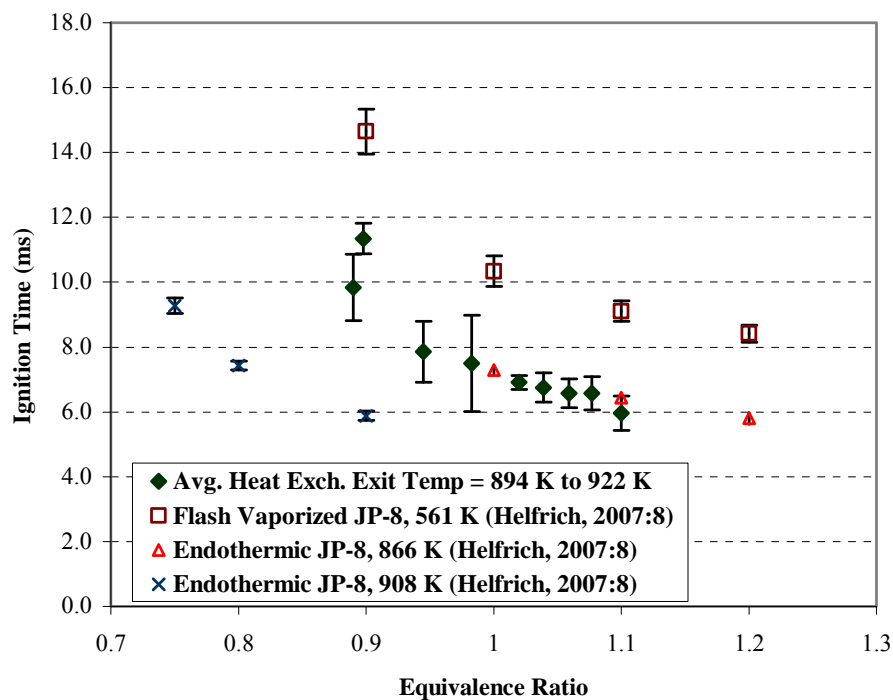
Figure 32. Ignition times as a function of equivalence ratio for average heat exchanger temperatures of 894 K (1150 ^{o}F) to 922 K (1200 ^{o}F)

Overall the reduced ignition times presented in Figs. 31 and 32 show that altering JP-8 by thermal decomposition results in improved PDE performance. Even though

some of the species that are formed require a higher initiation energy than the parent fuel, the net effect of conversion is a decreased ignition time. While this research does not suggest an operating window that optimizes performance at a certain level of reactivity, it does help to close the gap in knowing why performance is changed at different extents of reaction. The ability to know composition concurrently with PDE performance extends boundaries for future work.

VI.   Conclusions and Recommendations

Conclusions

This work is the first known to use waste heat from a steady state operating engine to react JP-8 while simultaneously extracting cracked fuel for analysis. It examined the vital link between extents of pyrolytic reaction and PDE performance. Understanding how JP-8 fuel decomposes and what types of product yields are seen is important if an operational PDE using cracked fuel is to become a reality. This study explored the thermal and catalytic cracking of JP-8 for use in a PDE by employing thrust tube waste heat to thermally decompose fuel via concentric counter flow heat exchangers with a zeolite catalyst coating. A fuel sampling method was developed that allowed sample extraction of cracked fuel during steady state PDE operation. Fuel samples were taken at different extents of reaction with temperature being the primary controlled parameter. During sample collection, the heat exchanger exit temperature ranged from 820 K (1016 ^{o}F) to 940 K (1232 ^{o}F). The samples were analyzed by gas chromatography to explore chemical composition and reaction pathways. Engine data was collected through the duration of testing to evaluate how chemical composition affected ignition time. The overall results showed that ignition time decreased by over 20% as temperature increased from 820 K (1016 ^{o}F) to 940 K (1232 ^{o}F) and by more than 30% when compared to unreacted (flash vaporized) JP-8. Thermal decomposition of the JP-8 yielded a volumetric liquid-to-gas conversion that increased from 3% to 44% while spanning the same temperatures. Furthermore, chemical analysis showed a dramatic shift in the liquid composition from primarily C_9-C_{15} alkanes in the unreacted fuel to lower

molecular weight aromatics, alkenes and smaller alkanes at higher extents of pyrolysis. Analysis showed that the primary vapor composition at all temperatures was C_1-C_3 alkanes and alkenes (>75% by volume) with moderate amounts of hydrogen and C_4-C_6 alkanes and alkenes.

Recommendations for Future Work

It is well known from this study as well as previous work (Helfrich, 2007) that thrust tube waste heat can be used to thermally decompose fuel. Because of the complexity of PDE operation, independent evaluation of a selected parameter is limited. The ability to react the fuel independent of PDE operation would separate reactivity from engine performance. Fuel could be reacted at a fixed temperature and residence time and then injected into the PDE. This would allow parameters such as equivalence ratio or ignition delay to be adjusted for further evaluation without inadvertently changing heat input to the fuel. If PDE performance is to be thoroughly evaluated at various extents of reaction, a reactor independent of PDE operation should be considered.

Limitations in run time due to filter coking made it difficult to reach a higher extent of conversion. The coke deposits are inherent to the thermal decomposition of any hydrocarbon. However, the amount of coking that is produced will change with parent fuel composition. Fuels other than JP-8 may produce less carbon deposition while yielding species that are desired to support lower ignition times. It would be beneficial to explore use of other practical hydrocarbons that may reduce coke deposition.

Hydrogen as well as strained hydrocarbons such as acetylene and ethylene are species that are desired to support improved PDE performance. Pyrolysis of JP-8 proves to successfully produce hydrogen and ethylene. It would be beneficial to explore other fuels that selectively form more of the desired species when reacted. It is also known that catalysts may improve the selective formation of desired species (see Chapter II). Use of other catalysts than are in the current configuration should also be explored.

It was shown in the results that some of the individual compounds that were produced from reacting the fuel were beneficial to PDE performance while others were not. Furthermore the effect that many of the individual species have on PDE performance is unknown. It would be beneficial to study how some of the prevalent species from JP-8 pyrolysis, particularly some of the aromatics, affect overall PDE performance. This would allow knowledge of the species that need to be selectively formed for improved performance. A fuel or catalyst could then be chosen that would promote formation of these species.

A substantial amount of coking was seen in the tube immediately following the heat exchanger exit. The temperature of the tube wall was lower than the temperature of the heat exchanger. This decrease in temperature caused carbon in the bulk fuel to condense and attach to the tube wall. It is recommended that the tubing be heated as well as insulated to help prevent carbon deposition.

Appendix A: Heat Exchanger Selection for Fuel Cooling System

Overview

The experiments performed for this research involved working with fuels that had been exposed to temperatures well above 800K (1000 ^{o}F). In the interest of safety and material the fuel was cooled before samples were collected. One of the challenges confronted multiple times in the design process was the lack of fluid property data for JP-8 at the experimental temperatures expected. The position of conservatism was taken whenever an assumption had to be made. When calculations were finalized, a safety factor of four was applied to alleviate hazards introduced by numerous unknowns. The objective was to develop an approximation for an initial design and reform the plans as necessary if sufficient fuel cooling was not provided. When the heat exchanger was tested, it supplied the heat transfer necessary to cool the fuel to ambient temperature and reconfiguration was not necessary. Appendix A will explain the calculations that were required to select the proper length, diameter, and orientation of stainless steel tubing required for the heat exchanger.

Heat Transfer Calculations

Several approaches were explored to transfer heat away from the fuel. After initial calculations were performed, length requirements ruled out the practical use of a concentric counter-flow tube-in-tube design. The basic plan of a coiled tube submersed in water was found to be a practical and viable solution. It was known that some of the post-cracked hydrocarbon products would be in the vapor form. However, the portion of

vapor products was not known. Knowing that heat transfers more readily through liquid than gas, a conservative approximation was made by utilizing property values for methane (instead of JP-8) at atmospheric pressure with a temperature of 811K (1000 °F) throughout fluid flow calculations. Potable water was employed as the cooling fluid. Water flowed into the bucket through a ¾ in hose and was expelled through two exit ports at the bottom of the bucket. A standing water tube was attached to one exit port to enable the water height to remain constant (at same height as standing water tube, above heat exchanger). Natural convection was the assumed method of heat transfer for the immersed tubing because the volumetric flow rate was small relative to the size of cooling vessel (galvanized steel trash can).

Rate of Heat Transfer from the Fuel

The rate of heat transfer required from the heated fuel was determined by applying conservation of energy to the heat exchanger tube. For steady flow and no work interactions, the rate of heat transfer ($\dot{Q}_{required}$) is determined by Eq. A.1:

$$\dot{Q}_{required} = \dot{m} c_p (T_e - T_i) \tag{A.1}$$

where $\dot{m}$ is the mass flow and c_p is the constant pressure specific heat (Cengel, 2006:458). The mean temperatures at the heat exchanger inlet and exit are T_i and T_e, respectively.

Rate of Heat Transfer to the Water

The required rate of heat transfer from the fuel ($\dot{Q}_{required}$) was set equal to the rate heat transferred to the surrounding water through natural convection ($\dot{Q}_{conv}$), Eq. A.2.

$$\dot{Q}_{required} = \dot{Q}_{conv} \tag{A.2}$$

Natural convection from a uniform temperature solid surface to a surrounding fluid can be expressed by Newton's law of cooling, Eq. A.1:

$$\dot{Q}_{conv} = hA_s(T_s - T_\infty)$$ (A.3)

where h is the convection heat transfer coefficient, A_s is the area exposed to the fluid, T_s is the surface temperature, and T_∞ is the free-stream temperature (Cengel, 2006:510). The convection heat transfer coefficient (h) was found by Eq. A.2:

$$h = \frac{k}{D}Nu$$ (A.4)

where k is the thermal conductivity of the fluid, D is the diameter of the tube, and Nu is the Nusselt number (Cengel, 2006:388). The dimensionless convection heat transfer coefficient, Nusselt number, is found by an empirical correlation that varies by physical orientation and shape. The tubing that was used in the design concept was approximately horizontal. To give a first approximation, the empirical correlation employed was for a horizontal cylinder and is given by Eq. A.3:

$$Nu = \left\{ 0.6 + \frac{0.387 Ra_D^{1/6}}{\left[1 + (0.469/\text{Pr})^{9/16} \right]^{4/9}} \right\}$$ (A.5)

where Ra and Pr are the Rayleigh and Prandtl numbers, respectively (Cengel, 2006:511). The Rayleigh number is the product of the Grashof and Prandtl numbers given by Eq. A.4:

$$Ra_D = \frac{g\left(1/T_f \right)(T_s - T_\infty)D^3}{v^2}\text{Pr}$$ (A.6)

where g is acceleration due to gravity, D is the diameter of the tubing, ν is the kinematic

viscosity, and T_f is the film temperature ($0.5(T_s - T_\infty)$).

Solve

Find: What length of type 316-stainless steel 3/8" tubing is required to cool heated and

cracked JP-8 from 811 K (1000 °F) to 300 K (80 °F)?

Assumptions:

1) Internal forced convection, no work interactions, and steady flow for heat

transfer from the fuel.

2) Natural convection from a uniform solid surface to surrounding fluid for heat

transfer from the tube to the water. Tubing is approximately horizontal.

3) Use property values of methane for heated and cracked JP-8.

4) Potable water is at the uniform temperature of 303 K (86 °F).

5) Must support $\dot{m} = 0.00756 \dfrac{kg}{s}$

Tools:

$$\dot{Q}_{required} = \dot{Q}_{conv}$$

$$\dot{Q}_{required} = \dot{m}c_p(T_e - T_i)$$

$$\dot{Q}_{conv} = hA_s(T_s - T_\infty)$$

$$h = \frac{k}{D}Nu$$

$$Nu = \left\{0.6 + \frac{0.387Ra_D^{\frac{1}{6}}}{\left[1+(0.559/Pr)^{\frac{9}{16}}\right]^{\frac{8}{27}}}\right\}^2$$

$$Ra_D = \frac{g\left(\frac{1}{T_f}\right)(T_s - T_\infty)D^3}{\nu^2}Pr$$

$$\nu = \frac{\mu}{\rho}$$

87

Properties of water @ 303.15 K (Cengel, 2006:854)

$$\mu = 0.798e-3 \ \frac{kg}{m \cdot s}$$

$$\rho = 996 \ \frac{kg}{m^3}$$

$$\text{Pr} = 5.42$$

$$k = 0.615 \frac{W}{m \cdot K}$$

Constant pressure specific heat, use average value between T_i and T_e (Cengel, 2006:861)

$$\overline{c_{p_{CH_4}}} = 3200.7 \ \frac{J}{kg \cdot K}$$

Solution:

$$\dot{Q}_{required} = \dot{m}c_p (T_e - T_i)$$

$$\dot{Q}_{required} = (0.00756)(3200.7)(811-300) = 12,364.8 \ W$$

$$Ra_D = \frac{g\left(\frac{1}{T_f}\right)(T_s - T_\infty)D^3}{\nu^2}\text{Pr}$$

$$Ra_D = \frac{9.81\left(\frac{1}{555.5}\right)(811-300)(0.0078125)^3}{(8.012e-7)^2}(5.42)$$

$$Ra_D = 3.633 \ e7$$

$$Nu = \left\{0.6 + \frac{0.387Ra_D^{\frac{1}{6}}}{\left[1+(0.559/\text{Pr})^{\frac{9}{16}}\right]^{\frac{8}{27}}}\right\}^2$$

$$Nu = \left\{0.6 + \frac{(0.387)(3.633e7)^{\frac{1}{6}}}{\left[1+(0.559/5.42)^{\frac{9}{16}}\right]^{\frac{8}{27}}}\right\}^2$$

$$Nu = 51.099$$

$$h = \frac{k}{D}Nu$$

$$h = \frac{0.615}{0.0078125}51.099$$

$$h = 4022.5 \ \frac{W}{m \cdot K}$$

$$\dot{Q}_{required} = 12,364.8 \ W = \dot{Q}_{conv}$$
$$\dot{Q}_{conv} = hA_s(T_s - T_\infty)$$
$$12,364.8 = (4022.5)(811 - 300)A_s$$
$$A_s = 0.00602 \ m^2$$

$$L = \frac{A_s}{\pi D}$$
$$L = \frac{0.00602}{\pi(0.0078125)} = 0.245 \ m$$

Multiplied by 4 (factor of safety)
$$L = (0.245 \ m)(4) = 0.98 \ m$$

The final calculated length of type 316-stainless steel 3/8" tubing was > 0.98m. Figure A.1 shows the tubing after it was coiled with a tubing bender, using 60^0 bends. The heat exchanger used was actually 3.66 m (12 ft). After final calculations, a longer tube length was chosen to facilitate possible larger mass flow rates in future experimentation.

Figure A.1. Coiled type 316 stainless steel 3/8 in. tubing used in fuel cooling system

Appendix B: Elemental Bias Limits and Their Propagation into Experimental Results

Elemental bias limits and their propagation into experimental results were analyzed for the volumetric liquid-to-gas conversion. The following text outlines the steps taken to find the final bias limit. For clarity of text, only S.I. units will be reported in Appendix B.

Bias Limits in Bag Volume

The predominant bias uncertainties introduced by the calculation of bag volume can be categorized into two areas: calibration and data acquisition. The volume of gas that was collected during experimentation was found by measuring the bag diameter and length. Bag length could be measured within ± 0.0508 m, while diameter could be measured within ± 1.588 e-3 m. There was also a slight amount of irregularity in the bag diameter, which was within ± 1.588 e-3 m. The bias was also a function of how much gas was collected. Table B.1 gives a summary of the elemental bias limit for each sample that was taken.

Table B.1. Elemental bias limits for bag volume

Sample #	Volume Collected (L)	Bias Limit (L)	Bias as % of collected volume
2_1	11.35	1.04	9.2%
2_2	20.95	1.40	6.7%
2_3	16.98	1.26	7.5%
2_4	18.63	1.32	7.1%
3_1	4.27	0.66	15.4%
3_2	13.97	1.15	8.2%
3_3	10.28	0.99	9.6%
3_4	6.31	0.79	12.5%
4_1	14.94	1.19	8.0%
4_3	26.50	1.44	5.4%
4_4	22.82	1.34	5.9%

Bias Limits in Moles of Vapor

The bias limits introduced in finding the total number of moles present in the vapor are due to the measured pressure and temperature. The bias limits in bag volume also propagate through to total number of moles found in the vapor. The ideal gas relation was used to find total number of moles. Temperature and pressure could be measured within $\pm$ 2.28 K and $\pm$ 1.021 e-3 atm, respectively (Helfrich, 2006:75). Table B.2 gives the bias limits for the moles of vapor collected in each fuel sample.

Table B.2. Elemental bias limits for moles of vapor collected

Sample	Moles of Vapor	Bias Limit	Bias as % of moles
2_1	0.45	0.041	9.2%
2_2	0.82	0.055	6.7%
2_3	0.67	0.050	7.5%
2_4	0.73	0.052	7.1%
3_1	0.17	0.026	15.4%
3_2	0.55	0.046	8.2%
3_3	0.41	0.039	9.6%
3_4	0.25	0.031	12.5%
4_1	0.60	0.048	8.0%
4_3	1.04	0.057	5.4%
4_4	0.90	0.053	5.9%

Bias Limits in Mass of Vapor

In finding the mass of the vapor there are two contributors to the bias uncertainty, the bias limit for moles of vapor and the uncertainty introduced by the gas chromatograph. The gas chromatograph is a highly sensitive instrument. Some uncertainty is introduced because of the multiple species that are found in the sample collected. If the sample analyzed was a single component fuel, much less uncertainty would be introduced. The chemical composition reported by the GC was within $\pm$5% of the absolute value. Table B.3 is a summary of the bias limits in the mass of vapor.

Table B.3. Elemental bias limits for mass of vapor collected

Sample	Vapor Mass (g)	Bias Limit (g)	Bias as % of mass
2_1	15.77	1.65	10.4%
2_2	28.62	2.39	8.4%
2_3	23.10	2.07	9.0%
2_4	25.58	2.22	8.7%
3_1	5.22	0.84	16.2%
3_2	19.00	1.83	9.6%
3_3	13.75	1.49	10.9%
3_4	8.58	1.15	13.4%
4_1	20.39	1.92	9.4%
4_3	35.62	2.63	7.4%
4_4	30.19	2.33	7.7%

Bias Limits in Volumetric Liquid-to-gas Conversion

The volumetric liquid-to-gas conversion bias limit includes uncertainties that are introduced by the measurement of the liquid sample as well as the bias limits in the vapor portion of the sample. The liquid sample could be measured within ± 4 ml. This uncertainty includes the amount of liquid that may remain in the fuel lines and measurement sensitivity. The values of bias limit for volumetric liquid-to-gas conversion are given in Table B.4. They are also included in the amount of uncertainty that is reported in Chapter V plots as error bars.

Table B.4. Elemental bias limits for liquid-to-gas conversion

Sample	Volumetric Liquid-to-gas Conversion	Bias Limit	Bias as % of vol. L - G conv.
2_1	0.30	0.029	9.5%
2_2	0.24	0.017	6.9%
2_3	0.31	0.023	7.5%
2_4	0.33	0.024	7.1%
3_1	0.03	0.005	15.8%
3_2	0.18	0.015	8.5%
3_3	0.08	0.009	10.1%
3_4	0.32	0.048	15.0%
4_1	0.32	0.026	8.1%
4_3	0.31	0.018	5.8%
4_4	0.44	0.028	6.3%

Appendix C: Calculated Density and Coking Effects on Flow Number

Calculated Density

An examination of the experimental fuel density based on nozzle flow number was conducted at elevated fuel injection temperatures. The relationship for flow number (*FN*) was introduced in Chapter III and is expressed in Eq. C.1 (Bartok, 1991:552-553).

$$FN = \frac{\dot{m}_{fuel}}{\sqrt{\Delta p_{fuel}}} \sqrt{\frac{\rho_{cal}}{\rho_{fuel}}}$$

(C.1)

From this relationship, fuel mass flow ($\dot{m}_{fuel}$) is a function of nozzle flow number, square root of pressure drop (Δp_{fuel}) across the nozzle, and square root of fuel density (ρ_{fuel}). Density of the fluid used to calibrate the nozzle (ρ_{cal}) must also be included. During this work, instrumentation enabled fuel mass flow and the pressure drop across the nozzle to be known. The calibration density was that of JP-8 at atmospheric temperature and pressure. As mentioned in Chapter III, coking effects changed nozzle flow number, making it impossible to control mass flow by nozzle selection.

After experimentation was complete, Eq. C.1 was used to determine what the nozzle flow number was during selected test runs. It was found that the calculated flow number was in some cases reduced by a much as 50 percent when compared to the installed flow number. Based on the discussion on coke formation in Chapter II, deposition due to pyrolysis is expected to occur around the temperature that cracking begins. The expectation would then be that coking would not affect nozzle flow number until fuel temperatures reach somewhere between 750 K and 800 K (890 ^{o}F and 980 ^{o}F), see Fig. C.1 (Edwards, 2003:1099).
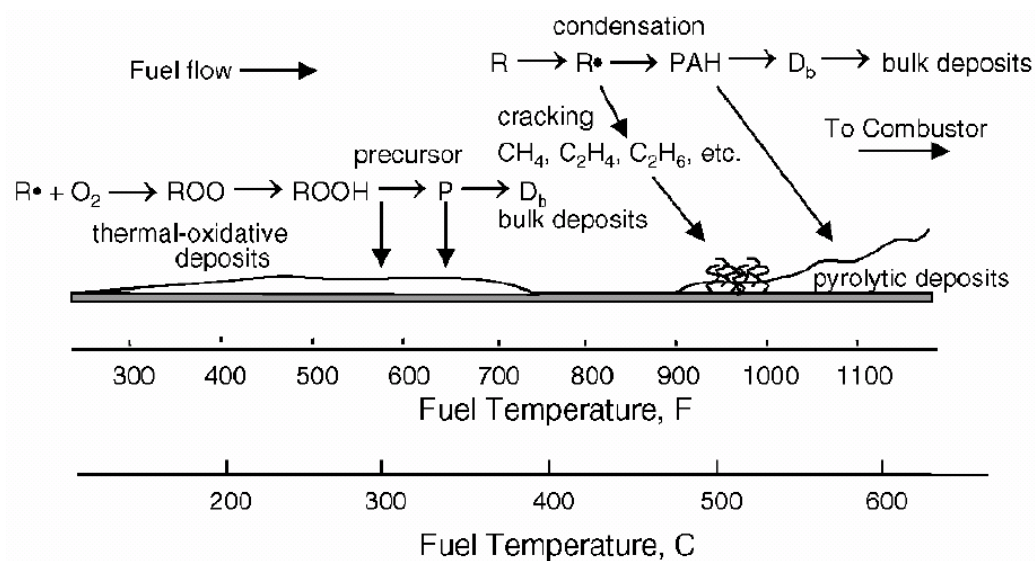
Figure C.1. Fuel carbon deposition temperature regimes (Edwards, 2003:1099)

In Appendix A, the lack of thermodynamic data for JP-8 at elevated temperatures made it necessary to estimate density for the cracked fuel at supercritical conditions. One density estimate that can be employed is produced from employing a JP-8 surrogate in the SUPERTRAPP program (Miser, 2005:99). A limiting factor in use of this data is the assumption that chemical composition does not change. Based on the discussion in Chapter II, it is known that fuel composition changes if sufficient heat is imparted to the fuel to induce thermal cracking; therefore a better estimation of density was desired.

Calculation of density was explored based on Eq. C.1 and data collected during experimentation. An initial nozzle flow number was found at the beginning of a test run and assumed to remain constant through the duration of the test (as discussed earlier, this is a reasonable assumption until coke deposition starts affecting nozzle flow number). The flow number relation was rearranged to solve for density, given in Equation C.2.

$$\rho_{fuel} = \frac{\dot{m}_{fuel}^2 \rho_{cal}}{FN^2 \Delta p_{fuel}}$$
(C.2)

Equation C.2 allowed for density of the fuel to be solved for, and the results are shown in

Fig. C.2. The calculated density and SUPERTRAPP estimated density are shown as a

function of heat exchanger exit temperature. SUPERTRAPP data points were found by

utilizing pressure and temperature data to look up tabulated SUPERTRAPP density

values.
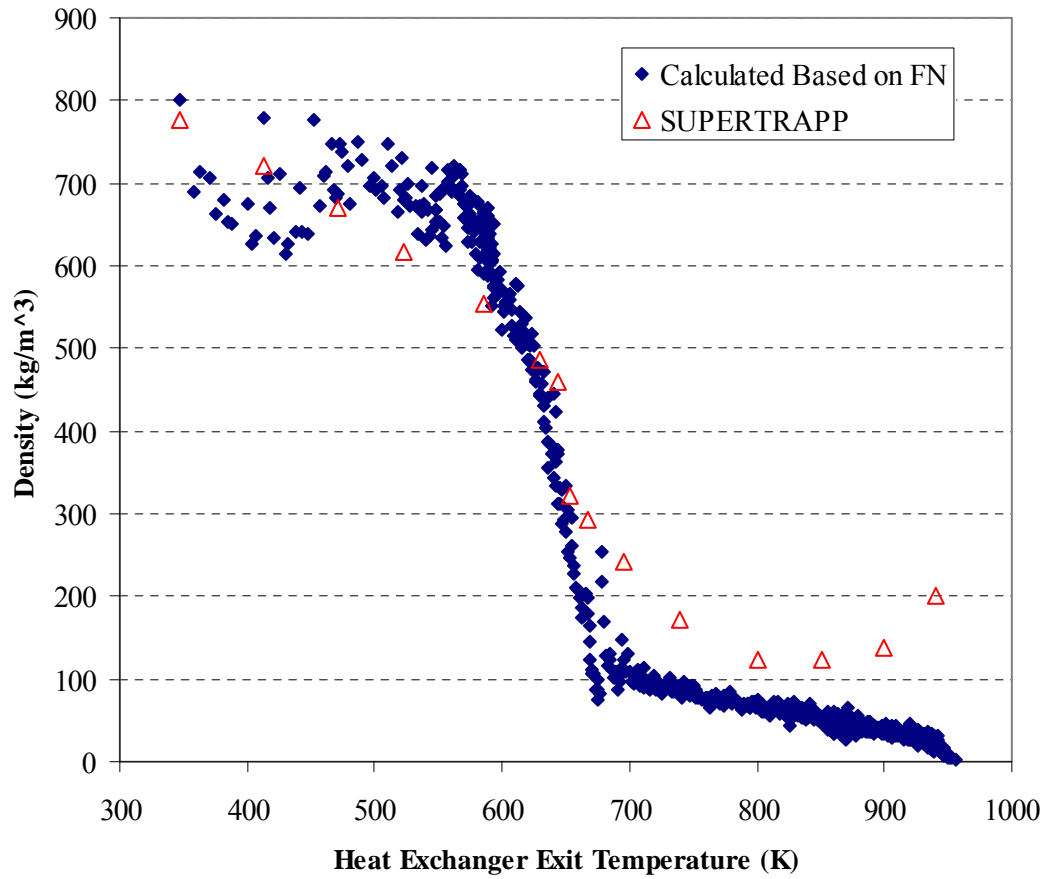
Figure C.2. Calculated and SUPERTRAPP density as a function of heat exchanger exit temperature (calculated based on nozzle FN)

In Fig. C.2, the variation in density seen from 360 K to 550 K (188 ^{o}F to 530 ^{o}F) is explained by unsteady PDE operation. Pressure was manually adjusted to control the fuel mass flow to produce a desired equivalence ratio. The time lag between the rise in pressure and the change in mass flow led to a varying calculated density during unsteady operation. The calculated values started to diverge from SUPERTRAPP data between 700 K and 750 K (800 ^{o}F and 890 ^{o}F) and even greater divergence was seen above 800 K (980 ^{o}F). It was around 800 K (980 ^{o}F) that thermal decomposition became prominent. As mentioned earlier, coke deposition is a product of the pyrolytic process and can be seen as a factor affecting calculated density in Fig. C.2. During a typical test run, the decreasing flow number yielded a decreasing fuel mass flow. At the same time, pressure was increased greatly to keep fuel flowing to the PDE in attempt to overcome the blockage due to coking. In Eq. C.2, a large pressure increase coupled with a drop in fuel mass flow yields a decreasing density. Unless the changing nozzle flow number is accounted for, the density that is calculated will be less than the actual value. This is shown in Fig. C.2 as the density shows a steady decrease 700 K to 950 K. The sharp rise in SUPERTRAPP density from 800 K to 950 K is explained by the increase in injection pressure due to coking. It is hypothesized that the actual density at the temperatures from 700 K to 900 K is somewhere between the calculated density and the SUPERTRAPP density. This leads to the conclusion that an assumed constant flow number after thermal decomposition occurs is not reasonable and that density calculations based on a fixed flow number is inaccurate. For this reason SUPERTRAPP data was used to estimate density in residence time calculations (see Chapter IV).

Appendix D: Liquid and Vapor Analysis Results

Liquid Results

Liquid analysis was performed via HPLC and GC-MS. Tables D.1a – c show the products that were formed in the liquid samples. The products here are defined as compounds that occurred in larger amounts than found in the neat (unreacted) fuel. Table D.2 shows the reactants that were present in the liquid samples. The reactants are defined as compounds that occurred in smaller amounts than found in the neat sample. All values are given as weight percentage of the liquid only. Quantitation of one and two ring aromatics was performed via HPLC by ASTM method D6379. The GC-MS was employed to perform quantitative and semi-quantitative analysis by two different methods. The first method utilized selective ion monitoring. This is where the mass spectrometer is set to detect characteristic ions of multi-ring (higher than two) aromatics. The second method used a conventional scanning mode to detect all other components. This is where the mass spectrometer is set to detect all ions in a specified range. A single asterisk is placed in the second column of Tables D1a – c and D.2 to annotate the compounds that were detected and quantified using standards. The other compounds were tentatively quantified using calibration curves for compounds that had a similar characteristic ion signature.

Table D.1a. Products found in the liquid sample by gas chromatography

Sample #			Neat	2-1	2-2	2-3	2-4	3-1	3-2	3-3	3-4	4-1	4-3	4-4
Average Heat Exch. Exit Temp (K)			298	898	893	900	902	820	869	842	908	924	919	940
Average Heat Exch. Exit Temp (°F)			77	1156	1148	1161	1164	1016	1105	1056	1174	1204	1194	1232
% L – G conversion				30.2	24.2	30.9	33.5	2.9	18.0	8.4	31.8	32.1	31.5	43.5
Products		Ret. Time					Weight Percent of Liquid Sample (%)							
Methyl-cyclopentene		2.44	<0.05	0.54	0.81	1.07	1.06	0.14	0.61	0.38	1.00	0.95	0.98	1.10
Methyl-hexene		2.50	<0.05	0.13	0.17	0.18	0.14	0.05	0.13	0.10	0.16	0.18	0.16	0.13
Benzene	*	2.54	<0.05	0.50	0.85	1.27	1.49	0.04	0.48	0.13	1.53	1.40	1.25	2.05
Methyl-hexane		2.68	<0.05	0.07	0.09	0.12	0.14	0.06	0.12	0.09	0.09	0.09	0.11	0.10
Cyclohexene		2.75	<0.05	0.28	0.39	0.51	0.48	0.06	0.29	0.16	0.49	0.50	0.49	0.55
Dimethyl-cyclopentane		2.80	<0.05	0.08	0.10	0.13	0.13	0.03	0.10	0.06	0.11	0.10	0.11	0.11
Methyl-hexene		2.82	<0.05	0.38	0.42	0.55	0.42	0.17	0.45	0.37	0.50	0.46	0.57	0.48
1-Heptene	*	2.86	<0.05	0.82	1.05	1.21	1.03	0.41	0.99	0.69	1.08	1.08	1.13	0.92
n-Heptane	*	2.97	0.11	0.34	0.44	0.57	0.59	0.28	0.57	0.45	0.43	0.39	0.51	0.46
Dimethyl-cyclopentene		3.00	<0.05	0.39	0.53	0.74	0.72	0.12	0.48	0.31	0.65	0.61	0.67	0.68
Heptene		3.08	<0.05	0.16	0.20	0.25	0.23	0.05	0.20	0.13	0.21	0.22	0.24	0.22
Heptene		3.19	<0.05	0.09	0.13	0.15	0.14	0.03	0.11	0.07	0.12	0.13	0.14	0.14
Methyl-cyclohexane	*	3.38	0.13	0.25	0.30	0.37	0.38	0.18	0.31	0.26	0.31	0.28	0.32	0.33
Ethyl-cyclopentane		3.53	<0.05	0.05	0.07	0.09	0.11	0.03	0.07	0.05	0.07	0.07	0.08	0.10
Methyl-cyclohexene		3.65	<0.05	0.34	0.45	0.60	0.58	0.09	0.36	0.23	0.56	0.55	0.59	0.62
Ethyl-cyclopentene		3.90	<0.05	0.13	0.18	0.21	0.24	0.04	0.15	0.10	0.20	0.19	0.21	0.23
Octene		3.92	<0.05	0.13	0.14	0.15	0.12	0.06	0.15	0.14	0.14	0.15	0.17	0.11
Methyl-heptane		4.08	0.08	0.16	0.16	0.17	0.16	0.12	0.18	0.15	0.17	0.16	0.17	0.14
Toluene	*	4.12	0.10	0.98	1.64	2.54	3.11	0.18	1.08	0.42	2.79	2.29	2.39	4.49
Methyl-cyclohexene		4.19	<0.05	0.33	0.44	0.58	0.58	0.09	0.37	0.23	0.54	0.51	0.56	0.61
Dimethyl-cyclohexane		4.42	0.23	0.25	0.24	0.27	0.26	0.24	0.28	0.27	0.24	0.22	0.25	0.22
1-Octene	*	4.64	<0.05	0.48	0.52	0.61	0.44	0.24	0.53	0.43	0.55	0.58	0.58	0.45
Dimethyl-cyclohexene		4.92	<0.05	0.11	0.14	0.17	0.16	0.05	0.14	0.09	0.16	0.15	0.16	0.15
n-Octane	*	4.84	0.41	0.43	0.43	0.49	0.45	0.51	0.56	0.54	0.40	0.39	0.44	0.37
Octene		4.99	<0.05	0.07	0.08	0.11	0.10	0.03	0.10	0.07	0.09	0.09	0.10	0.09
Dimethyl-cyclohexene		5.48	<0.05	0.38	0.46	0.62	0.60	0.13	0.41	0.30	0.55	0.48	0.59	0.55
Ethyl-cyclohexene		6.14	<0.05	0.16	0.23	0.26	0.25	0.05	0.18	0.13	0.23	0.22	0.25	0.26
Ethylbenzene (C2)	*	6.40	0.11	0.30	0.41	0.59	0.67	0.15	0.35	0.19	0.60	0.51	0.56	0.85
p-Xylene (C2)	*	6.65	0.32	0.70	0.90	1.28	1.38	0.39	0.76	0.47	1.23	1.05	1.19	1.74
m-Xylene (C2)	*	6.69	0.10	0.26	0.35	0.43	0.53	0.14	0.26	0.18	0.44	0.41	0.41	0.60
o-Xylene (C2)	*	7.29	0.26	0.53	0.67	0.91	0.99	0.31	0.57	0.38	0.90	0.79	0.87	1.21

*Compounds that were positively identified and directly quantified using standards.

Table D.1b. Products found in the liquid sample by gas chromatography (continued)

Sample #			Neat	2-1	2-2	2-3	2-4	3-1	3-2	3-3	3-4	4-1	4-3	4-4
Average Heat Exch. Exit Temp (K)			298	898	893	900	902	820	869	842	908	924	919	940
Average Heat Exch. Exit Temp (^{o}F)			77	1156	1148	1161	1164	1016	1105	1056	1174	1204	1194	1232
% L – G conversion				30.2	24.2	30.9	33.5	2.9	18.0	8.4	31.8	32.1	31.5	43.5
Products		Ret. Time					Weight Percent of Liquid Sample (%)							
1-Nonene	*	7.29	<0.05	0.59	0.56	0.58	0.41	0.31	0.52	0.46	0.53	0.55	0.53	0.41
Nonene		7.72	<0.05	0.17	0.19	0.20	0.17	0.12	0.21	0.18	0.18	0.17	0.19	0.14
C3- Alkylbenzenes 8.0-10.2 min		9.37	1.91	2.61	2.87	3.64	3.63	2.06	2.62	2.19	3.45	3.07	3.38	4.45
1-Decene	*	10.37	<0.05	0.30	0.29	0.30	0.20	0.18	0.29	0.27	0.27	0.30	0.29	0.20
1,2,4-Trimethyl-benzene (C3)	*	10.40	1.26	1.64	1.73	2.09	1.99	1.37	1.60	1.40	1.99	1.83	1.95	2.30
C3 -Alkylbenzenes 11.1-11.7 min		11.23	0.43	0.54	0.55	0.66	0.62	0.46	0.52	0.48	0.62	0.58	0.60	0.70
Indane	*	11.64	0.05	0.10	0.12	0.15	0.17	0.06	0.10	0.07	0.16	0.13	0.15	0.20
C4-Alkylbenzenes 12-12.3 min		12.18	0.45	0.49	0.48	0.56	0.52	0.46	0.48	0.45	0.51	0.48	0.51	0.57
Butylbenzene (C4)	*	12.34	0.30	0.31	0.30	0.32	0.31	0.34	0.30	0.28	0.32	0.28	0.33	0.32
C4-Alkylbenzenes 12.4-13.2 min		12.38	1.23	1.41	1.45	1.63	1.56	1.27	1.40	1.28	1.66	1.43	1.52	1.67
C4-Alkylbenzenes 13.2-14.4 min		14.28	1.07	1.28	1.32	1.56	1.47	1.13	1.24	1.14	1.51	1.37	1.46	1.65
1-Undecene**	*	13.48	< 0.1	0.28	0.25	0.24	0.17	0.20	0.26	0.27	0.24	0.23	0.24	0.14
C5-Alkylbenzenes 14-15.4 min		15.30	0.80	0.76	0.73	0.81	0.77	0.80	0.76	0.75	0.76	0.72	0.75	0.78
Pentylbenzene (C5)	*	15.43	0.06	0.04	0.03	0.04	0.03	0.05	0.04	0.05	0.04	0.04	0.03	0.04
C5 Alkylbenzenes - 15.5-17 min		15.49	0.98	0.92	0.88	0.97	0.92	0.95	0.91	0.89	0.92	0.87	0.88	0.96
Tetralin	*	15.53	0.13	0.12	0.11	0.13	0.11	0.13	0.12	0.12	0.12	0.11	0.12	0.12
Naphthalene	*	16.24	0.12	0.27	0.35	0.50	0.58	0.14	0.27	0.17	0.54	0.46	0.48	0.71
1-Dodecene**	*	16.47	< 0.1	0.17	0.15	0.13	0.10	0.14	0.14	0.15	0.13	0.12	0.12	0.07
2-Methyl-naphthalene		19.42	0.31	0.49	0.60	0.79	0.84	0.33	0.50	0.37	0.83	0.71	0.73	1.00
1-Methyl-naphthalene	*	19.83	0.21	0.33	0.40	0.52	0.55	0.21	0.34	0.25	0.54	0.47	0.48	0.67
Dimethyl-naphthalenes 22-22.6 min		22.34	0.27	0.36	0.41	0.52	0.53	0.27	0.36	0.29	0.53	0.46	0.48	0.63
1,3-Dimethyl-naphthalene	*	22.69	0.20	0.27	0.31	0.39	0.39	0.20	0.31	0.21	0.40	0.35	0.35	0.46
Dimethyl-naphthalenes 22.8-23.8 min		22.80	0.29	0.39	0.45	0.57	0.58	0.29	0.40	0.31	0.58	0.51	0.53	0.70
Acenaphthylene	*	23.49	<0.001	0.005	0.010	0.012	0.014	<0.001	0.004	0.001	0.017	0.015	0.013	0.025
Acenaphthene	*	24.33	<0.001	0.009	0.015	0.021	0.028	0.002	0.011	0.004	0.026	0.021	0.020	0.035
Fluorene	*	26.75	0.005	0.020	0.033	0.046	0.061	0.005	0.024	0.009	0.058	0.047	0.046	0.077
Phenanthrene	*	31.14	<0.001	0.013	0.026	0.048	0.077	0.001	0.016	0.004	0.067	0.056	0.053	0.094
Anthracene	*	31.38	<0.001	0.004	0.008	0.014	0.019	<0.001	0.005	0.001	0.018	0.014	0.013	0.022
Fluoranthene	*	36.69	<0.001	0.003	0.005	0.009	0.015	<0.001	0.003	0.001	0.012	0.011	0.011	0.019
Pyrene	*	37.67	<0.001	0.014	0.025	0.041	0.056	0.001	0.017	0.004	0.047	0.039	0.038	0.059
Benz(a)anthracene	*	43.38	<0.001	0.002	0.003	0.006	0.010	<0.001	0.002	<0.001	0.007	0.006	0.007	0.010

*Compounds that were positively identified and directly quantified using standards.
** Interfering compound in neat fuel,different from compound in stressed fuel resulting in higher reporting limit.

Table D.1c. Products found in the liquid sample by gas chromatography (continued)

Sample #			Neat	2-1	2-2	2-3	2-4	3-1	3-2	3-3	3-4	4-1	4-3	4-4
Average Heat Exch. Exit Temp (K)			298	898	893	900	902	820	869	842	908	924	919	940
Average Heat Exch. Exit Temp (^{o}F)			77	1156	1148	1161	1164	1016	1105	1056	1174	1204	1194	1232
% L – G conversion				30.2	24.2	30.9	33.5	2.9	18.0	8.4	31.8	32.1	31.5	43.5
Products		Ret. Time					Weight Percent of Liquid Sample (%)							
Chrysene	*	43.52	<0.001	0.001	0.003	0.005	0.009	<0.001	0.001	<0.001	0.006	0.005	0.006	0.009
Benzo(b)fluoranthene	*	48.08	<0.001	0.001	0.002	0.005	0.009	<0.001	0.001	<0.001	0.005	0.005	0.007	0.011
Benzo(k)fluoranthene	*	48.17	<0.001	<0.001	<0.001	0.001	0.001	<0.001	<0.001	<0.001	0.001	0.001	0.001	0.001
Benzo(a)pyrene	*	49.31	<0.001	0.002	0.003	0.007	0.011	<0.001	0.002	<0.001	0.007	0.006	0.007	0.011
Indeno(1,2,3-cd)pyrene	*	53.52	<0.001	0.002	0.004	0.006	0.011	<0.001	0.003	<0.001	0.008	0.006	0.008	0.013
Dibenz(a,h)anthracene	*	53.72	<0.001	<0.001	<0.001	0.001	0.002	<0.001	<0.001	<0.001	0.001	0.001	0.001	0.002
Benzo(g,h,i)perylene	*	54.55	<0.001	0.001	0.003	0.006	0.010	<0.001	0.002	<0.001	0.005	0.004	0.006	0.010

*Compounds that were positively identified and directly quantified using standards.

Table D.2. Reactants found in the liquid sample by gas chromatography

Sample #			Neat	2-1	2-2	2-3	2-4	3-1	3-2	3-3	3-4	4-1	4-3	4-4
Average Heat Exch. Exit Temp (K)			298	898	893	900	902	820	869	842	908	924	919	940
Average Heat Exch. Exit Temp (^{o}F)			77	1156	1148	1161	1164	1016	1105	1056	1174	1204	1194	1232
% L – G conversion				30.2	24.2	30.9	33.5	2.9	18.0	8.4	31.8	32.1	31.5	43.5
Reactants		Ret. Time					Weight Percent of Liquid Sample (%)							
3-Methyl-octane	*	6.71	0.43	0.30	0.24	0.24	0.18	0.41	0.29	0.35	0.21	0.22	0.22	0.16
n-Nonane	*	7.55	2.51	1.62	1.30	1.22	0.90	2.33	1.58	1.98	1.07	1.12	1.10	0.78
Dimethyl-octane		8.56	2.10	1.36	1.07	0.99	0.69	1.94	1.23	1.55	0.92	0.97	0.92	0.65
2-Methyl-nonane	*	9.53	0.78	0.49	0.36	0.32	0.23	0.71	0.45	0.55	0.30	0.31	0.30	0.21
n-Decane	*	10.64	4.02	2.25	1.68	1.44	0.98	3.55	2.00	2.69	1.31	1.37	1.29	0.85
Butyl-cyclohexane	*	11.64	0.33	0.18	0.14	0.13	0.08	0.29	0.17	0.23	0.12	0.12	0.12	0.08
trans-Decalin	*	12.43	0.23	0.18	0.14	0.14	0.12	0.23	0.18	0.20	0.12	0.12	0.13	0.09
2-Methyl-decane	*	12.65	0.90	0.51	0.37	0.32	0.22	0.78	0.45	0.61	0.30	0.31	0.28	0.20
3-Methyl-decane	*	12.83	0.68	0.40	0.29	0.25	0.17	0.61	0.35	0.48	0.23	0.25	0.23	0.15
n-Undecane	*	13.76	3.89	1.97	1.43	1.18	0.77	3.31	1.77	2.46	1.09	1.16	1.07	0.67
n-Dodecane	*	16.74	3.10	1.50	1.03	0.83	0.52	2.52	1.30	1.83	0.76	0.80	0.72	0.42
n-Tridecane	*	19.57	2.46	1.09	0.72	0.58	0.34	1.90	0.92	1.37	0.52	0.54	0.50	0.29
Methyl-tridecane		21.27	0.22	0.12	0.08	0.06	0.04	0.21	0.11	0.14	0.06	0.07	0.06	0.04
n-Tetradecane	*	22.23	1.70	0.72	0.46	0.34	0.19	1.31	0.62	0.91	0.34	0.34	0.32	0.17
Methyl-tetradecane		23.85	0.15	0.07	0.43	0.04	0.02	0.11	0.06	0.08	0.03	0.03	0.03	0.02
n-Pentadecane	*	24.75	0.87	0.34	0.24	0.15	0.10	0.68	0.32	0.46	0.15	0.17	0.14	0.07
n-Hexadecane	*	27.14	0.28	0.09	0.06	0.04	0.02	0.18	0.08	0.12	0.04	0.04	0.04	0.02
n-Heptadecane	*	29.41	0.06	0.02	0.015	0.011	0.008	0.04	0.02	0.03	0.01	0.01	0.01	0.01

*Compounds that were positively identified and directly quantified using standards.

Vapor Results

Analysis was performed on the vapor samples via GC/TCD and GC/FID. Tables D.3a – d summarize the results that were obtained from analysis. The tables include the data that was needed to compute percent volumetric liquid-to-gas conversion. For details on calculation, see Chapter IV.

Table D.3a. Vapor analysis performed on gaseous samples

Sample	2-1				2-2				2-3			
Heat Exch. Exit Temp (K)	898				893				900			
Heat Exch. Exit Temp (^{o}F)	1156				1148				1161			
Volume Liquid Collected (ml)	45.5				112.0				64.5			
Density Liquid Collected (g/ml)	0.791				0.788				0.793			
Mass Liguid (g)	35.97				88.24				51.16			
Volume Vapor Collected (ml)	11350.3				20954.5				16977.0			
Mole Vapor Collected (mol)	0.448				0.823				0.667			
Mass Vapor Collected (g)	15.77				28.62				23.10			
Vol. Liquid-to-gas (ml)	19.72				35.78				28.88			
Products	χ_i	mol_i	Y_i	$mass_i$ (g)	χ_i	mol_i	Y_i	$mass_i$ (g)	χ_i	mol_i	Y_i	$mass_i$ (g)
Methane	0.290	0.130	0.131	2.074	0.273	0.225	0.126	3.599	0.283	0.189	0.131	3.024
Ethane	0.167	0.075	0.142	2.245	0.171	0.140	0.147	4.210	0.171	0.114	0.149	3.431
Ethylene	0.067	0.030	0.053	0.838	0.078	0.064	0.063	1.797	0.073	0.049	0.059	1.369
n-propane	0.108	0.048	0.135	2.129	0.113	0.093	0.143	4.085	0.112	0.075	0.143	3.294
Propylene	0.116	0.052	0.139	2.185	0.125	0.103	0.151	4.323	0.121	0.081	0.147	3.388
iso-Butane	0.010	0.004	0.016	0.252	0.010	0.008	0.016	0.456	0.010	0.007	0.017	0.381
n-Butane	0.033	0.015	0.054	0.853	0.033	0.027	0.056	1.591	0.034	0.022	0.056	1.301
2-Butene (trans)	0.014	0.006	0.023	0.361	0.013	0.011	0.022	0.620	0.014	0.009	0.022	0.515
1-Butene	0.032	0.014	0.051	0.803	0.032	0.027	0.052	1.496	0.031	0.021	0.050	1.155
iso-Butylene	0.001	0.001	0.002	0.033	0.002	0.002	0.003	0.090	0.001	0.001	0.002	0.047
2-Butene (cis)	0.026	0.011	0.041	0.644	0.027	0.022	0.043	1.225	0.025	0.017	0.041	0.936
iso-C5	0.013	0.006	0.026	0.407	0.012	0.010	0.025	0.722	0.012	0.008	0.026	0.594
n-Pentane	0.010	0.004	0.019	0.307	0.009	0.007	0.018	0.509	0.009	0.006	0.019	0.447
Butadiene	0.003	0.002	0.005	0.081	0.003	0.003	0.005	0.153	0.003	0.002	0.005	0.116
Methyl alkenes	0.018	0.008	0.035	0.552	0.012	0.010	0.025	0.702	0.013	0.009	0.027	0.619
1-Pentene	0.012	0.006	0.025	0.390	0.011	0.009	0.021	0.611	0.010	0.007	0.021	0.482
Unidentified Compounds	0.042	0.019	0.101	1.586	0.034	0.028	0.083	2.366	0.035	0.023	0.084	1.950
Hydrogen	0.038	0.017	0.002	0.034	0.042	0.035	0.002	0.069	0.041	0.027	0.002	0.054

Table D.3b. Vapor analysis performed on gaseous samples (continued)

Sample	2-4				3-1				3-2			
Heat Exch. Exit Temp (K)	902				820				869			
Heat Exch. Exit Temp (^{o}F)	1164				1016				1105			
Volume Liquid Collected (ml)	63.5				219.0				108.0			
Density Liquid Collected (g/ml)	0.798				0.776				0.776			
Mass Liguid (g)	50.67				170.01				83.84			
Volume Vapor Collected (ml)	18626.2				4268.5				13969.6			
Mole Vapor Collected (mol)	0.732				0.169				0.553			
Mass Vapor Collected (g)	25.58				5.22				19.00			
Vol. Liquid-to-gas (ml)	31.97				6.53				23.75			
Products	χ_i	mol_i	Y_i	$mass_i$ (g)	χ_i	mol_i	Y_i	$mass_i$ (g)	χ_i	mol_i	Y_i	$mass_i$ (g)
Methane	0.296	0.217	0.135	3.465	0.292	0.049	0.151	0.790	0.279	0.154	0.130	2.469
Ethane	0.173	0.126	0.148	3.793	0.214	0.036	0.207	1.083	0.184	0.102	0.161	3.051
Ethylene	0.055	0.040	0.044	1.117	0.100	0.017	0.090	0.471	0.062	0.034	0.051	0.964
n-propane	0.119	0.087	0.150	3.827	0.125	0.021	0.177	0.925	0.131	0.072	0.168	3.187
Propylene	0.106	0.077	0.127	3.243	0.125	0.021	0.170	0.889	0.117	0.064	0.143	2.708
iso-Butane	0.011	0.008	0.019	0.486	0.007	0.001	0.012	0.065	0.012	0.006	0.019	0.370
n-Butane	0.040	0.029	0.066	1.694	0.026	0.004	0.048	0.252	0.041	0.023	0.070	1.328
2-Butene (trans)	0.014	0.010	0.022	0.565	0.005	0.001	0.009	0.046	0.012	0.007	0.020	0.376
1-Butene	0.028	0.021	0.045	1.158	0.022	0.004	0.040	0.211	0.031	0.017	0.050	0.953
iso-Butylene	0.002	0.001	0.002	0.064	0.000	0.000	0.000	0.002	0.001	0.000	0.001	0.026
2-Butene (cis)	0.024	0.018	0.038	0.981	0.016	0.003	0.029	0.153	0.025	0.014	0.040	0.764
iso-C5	0.014	0.010	0.028	0.721	0.005	0.001	0.011	0.058	0.012	0.007	0.025	0.473
n-Pentane	0.012	0.009	0.024	0.625	0.004	0.001	0.010	0.051	0.010	0.006	0.021	0.401
Butadiene	0.002	0.002	0.003	0.084	0.001	0.000	0.002	0.008	0.002	0.001	0.003	0.057
Methyl alkenes	0.018	0.013	0.035	0.900	0.003	0.001	0.008	0.041	0.011	0.006	0.022	0.414
1-Pentene	0.010	0.007	0.019	0.495	0.005	0.001	0.011	0.059	0.010	0.005	0.019	0.370
Unidentified Compounds	0.037	0.027	0.090	2.296	0.007	0.001	0.020	0.105	0.023	0.012	0.055	1.049
Hydrogen	0.041	0.030	0.002	0.060	0.043	0.007	0.003	0.014	0.038	0.021	0.002	0.042

Table D.3c. Vapor analysis performed on gaseous samples (continued)

Sample	3-3				3-4				4-1			
Heat Exch. Exit Temp (K)	842				908				924			
Heat Exch. Exit Temp (^{o}F)	1056				1174				1204			
Volume Liquid Collected (ml)	188.0				23.0				54.0			
Density Liquid Collected (g/ml)	0.778				0.806				0.788			
Mass Liguid (g)	146.23				18.54				42.57			
Volume Vapor Collected (ml)	10283.2				6305.7				14939.8			
Mole Vapor Collected (mol)	0.407				0.249				0.597			
Mass Vapor Collected (g)	13.75				8.59				20.39			
Vol. Liquid-to-gas (ml)	17.19				10.73				25.49			
Products	χ_i	mol_i	Y_i	$mass_i$ (g)	χ_i	mol_i	Y_i	$mass_i$ (g)	χ_i	mol_i	Y_i	$mass_i$ (g)
Methane	0.259	0.105	0.123	1.688	0.306	0.076	0.142	1.218	0.308	0.184	0.144	2.942
Ethane	0.196	0.080	0.174	2.391	0.173	0.043	0.151	1.293	0.165	0.099	0.145	2.957
Ethylene	0.081	0.033	0.067	0.928	0.057	0.014	0.046	0.397	0.071	0.042	0.058	1.186
n-propane	0.137	0.056	0.178	2.447	0.114	0.028	0.146	1.253	0.102	0.061	0.132	2.690
Propylene	0.132	0.054	0.164	2.254	0.106	0.026	0.129	1.111	0.114	0.068	0.141	2.873
iso-Butane	0.010	0.004	0.016	0.225	0.011	0.003	0.018	0.154	0.009	0.005	0.016	0.318
n-Butane	0.035	0.014	0.061	0.837	0.035	0.009	0.059	0.507	0.030	0.018	0.050	1.029
2-Butene (trans)	0.008	0.003	0.014	0.189	0.014	0.003	0.022	0.191	0.014	0.008	0.023	0.474
1-Butene	0.029	0.012	0.048	0.657	0.028	0.007	0.046	0.392	0.029	0.018	0.048	0.985
iso-Butylene	0.001	0.000	0.001	0.011	0.002	0.000	0.003	0.022	0.001	0.001	0.002	0.045
2-Butene (cis)	0.022	0.009	0.036	0.497	0.024	0.006	0.039	0.331	0.024	0.014	0.040	0.811
iso-C5	0.008	0.003	0.017	0.236	0.013	0.003	0.027	0.230	0.012	0.007	0.026	0.534
n-Pentane	0.007	0.003	0.015	0.209	0.010	0.002	0.021	0.177	0.008	0.005	0.018	0.361
Butadiene	0.001	0.001	0.002	0.033	0.003	0.001	0.005	0.039	0.004	0.002	0.006	0.113
Methyl alkenes	0.008	0.003	0.016	0.218	0.015	0.004	0.031	0.265	0.014	0.009	0.030	0.606
1-Pentene	0.008	0.003	0.016	0.218	0.010	0.003	0.021	0.182	0.012	0.007	0.025	0.508
Unidentified Compounds	0.020	0.008	0.050	0.685	0.038	0.010	0.094	0.803	0.038	0.023	0.094	1.912
Hydrogen	0.038	0.015	0.002	0.031	0.041	0.010	0.002	0.020	0.043	0.025	0.002	0.051

Table D.3d. Vapor analysis performed on gaseous samples (continued)

Sample	4-3				4-4			
Heat Exch. Exit Temp (K)	919				940			
Heat Exch. Exit Temp (^{o}F)	1194				1232			
Volume Liquid Collected (ml)	97.0				49.0			
Density Liquid Collected (g/ml)	0.801				0.829			
Mass Liguid (g)	77.71				40.64			
Volume Vapor Collected (ml)	26498.5				22818.2			
Mole Vapor Collected (mol)	1.044				0.899			
Mass Vapor Collected (g)	35.62				30.19			
Vol. Liquid-to-gas (ml)	44.53				37.74			
Products	χ_i	mol_i	Y_i	$mass_i$ (g)	χ_i	mol_i	Y_i	$mass_i$ (g)
Methane	0.293	0.306	0.138	4.900	0.342	0.307	0.163	4.912
Ethane	0.169	0.177	0.149	5.308	0.165	0.148	0.147	4.452
Ethylene	0.075	0.078	0.061	2.185	0.056	0.050	0.047	1.409
n-propane	0.110	0.115	0.142	5.067	0.096	0.086	0.126	3.797
Propylene	0.120	0.126	0.148	5.282	0.096	0.086	0.120	3.622
iso-Butane	0.010	0.010	0.016	0.578	0.010	0.009	0.017	0.498
n-Butane	0.032	0.033	0.054	1.940	0.026	0.023	0.045	1.351
2-Butene (trans)	0.013	0.014	0.022	0.768	0.014	0.012	0.023	0.692
1-Butene	0.029	0.031	0.048	1.724	0.022	0.019	0.036	1.083
iso-Butylene	0.001	0.001	0.002	0.069	0.002	0.002	0.003	0.092
2-Butene (cis)	0.024	0.026	0.040	1.429	0.021	0.019	0.035	1.043
iso-C5	0.008	0.008	0.017	0.610	0.008	0.007	0.018	0.529
n-Pentane	0.004	0.005	0.009	0.329	0.004	0.004	0.009	0.283
Butadiene	0.011	0.012	0.018	0.627	0.011	0.010	0.018	0.539
Methyl alkenes	0.013	0.013	0.026	0.937	0.013	0.011	0.027	0.805
1-Pentene	0.010	0.010	0.020	0.711	0.010	0.009	0.020	0.611
Unidentified Compounds	0.035	0.037	0.086	3.076	0.058	0.052	0.145	4.383
Hydrogen	0.041	0.042	0.002	0.085	0.048	0.043	0.003	0.086

Bibliography

Bartok, W. and Sarofim, A. F. *Fossil Fuel Combustion: A Source Book*. New York. John Wiley & Sons, Inc., 1991.

Cengel, Yunus. *Heat and Mass Transfer: A Practical Approach*, 3rd ed. New Delhi. Tata McGraw-Hill Publishing Co. Ltd., 2006.

Coleman, Hugh W. and Steele, W. Glenn. *Experimentation and Uncertainty Analysis for Engineers*. New York. JohnWiley & Sons, 1989.

Cooper, M and Shepherd, J.E. "Experiments Studying Thermal Cracking, Catalytic Cracking, and Pre-Mixed Partial Oxidation of JP-10," *39th AIAA/ASME/SAE/ASEE Joint Propulsion Conference and Exhibit*. Hunstville, AL. AIAA 2003-4687, 20-23 July 2003.

DeWitt, Matthew J. "Overview of Pyrolysis." PowerPoint Presentation. University of Dayton Research Institute, Dayton, OH, 16 July 2007.

Edwards, Tim. "Liquid Fuels and Propellants for Aerospace Propulsion: 1903-2003," *Journal of Propulsion and Power*, Vol. 19, No. 6: 1089-1107 (Nov-Dec 2003).

Edwards, Tim, DeWitt, Matthew J., Shafer, Linda M., Brooks, David, Huang, He, Bagley, Sean P., Ona, Jorge O., Wornat, Mary J. "Fuel Composition Influence on Deposition in Endothermic Fuels," *14th AIAA/AHI Space Planes and Hypersonic Systems and Technologies Conference.* Canberra, Australia. AIAA 2006-7973, 6-9 November 2006.

Fabuss, B.M., Smith, J.O., Lait, R.I., Fabuss, M.A., and Satterfield, C.N. "Kinetics of Thermal Cracking of Paraffinic and Naphthenic Fuels at Elevated Pressures," *Journal of Industrial &Engineering Chemistry Process Design and Development*, Vol. 3, No. 1. 33-37 (Jan 1964).

Fickett, W. and Davis, W. C. *Detonation: Theory and Experiment*. New York. Dover Publications Inc., 1979.

Ford, Thomas J. "Liquid-Phase Thermal Decomposition of Hexadecane: Reaction Mechanisms," *Journal of Industrial & Engineering Chemistry Fundamentals*, Vol. 25, No. 2. 240-243 (May 1986)

Galligan, Carrie. *Catalytic Cracking of Jet Propellant-10 for Pulse Detonation Engine Applications*, MS thesis, Université Laval, Quebec City, Quebec. March 2005.

Helfrich, Tim M. *Cycle performance of a Pulse Detonation Engine with Supercritical Fuel Injection,* MS thesis, AFIT/GAE/ENY/06-M14. Graduate School of Engineering and Management, Air Force Institute of Technology, Wright-Patterson AFB, OH. March 2006.

Helfrich, Tim M., Schauer, Frederick, R., Bradley, Royce P., and Hoke, John L. "Evaluation of Catalytic and Thermal Cracking in a JP-8 Fueled Pulsed Detonation Engine," *45th AIAA Aerospace Sciences Meeting and Exhibit*. Reno, NV. AIAA 2007-235, 8-11 January 2007.

Heneghan, S.P., Zabarnick, S., Ballal, D.R., and Harrison, W.E. "JP-8 + 100: Development of a Thermally Stable Jet Fuel," *ASME Journal of Energy Resources Technology*, Vol. 119: 170-179 (1996).

Huang, He, Spadaccini, Louis J., Sobel, David R. "Fuel-Cooled Thermal Management for Advanced Aeroengines," *Journal of Engineering for Gas Turbines and Power*, Vol. 126. 284-293 (Apr 2004).

Huang, He, Sobel, David R.., and Spadaccini, Louis J. "Endothermic Heat-Sink of Hydrocarbon Fuels for Scramjet Cooling," *38th AIAA/AMSE/SAE/ASEE Joint Propulsion Conference and Exhibit*. Indianapolis, IN. AIAA 2002-3871, 7-10 July 2002.

Kaneshige, M. and Shepherd, J. E. *Detonation Database*. Technical Report FM97-8, GALCIT, July 1997.

Knystautas, R., Guirao, C., Lee, J. H., and Sulmistras, A. "Measurement of Cell Size in Hydrocarbon-Air Mixtures and Predictions of Critical Tube Diameter, Critical Initiation Energy, and Detonability Limits." *Progress in Aeronautics and Astronautics*, *AIAA*, Vol. 94. 23-37 (1984).

Kossiakoff, A. and Rice, F.O. Journal of American Chemical Society, Vol. 65. 590-595 (1943).

Kuo, Kenneth K. *Principles of Combustion*, 2nd ed. Hoboken. John Wiley and Sons Inc., 2005.

Littlewood, A. *Gas Chromatography*, 2nd ed. New York, Academic Press, 1970.

Miser, Christen L. *Pulse Detonation Engine Thrust Tube Heat Exchanger for Flash Vaporization and Supercritical Heating of JP-8*, MS thesis, AFIT/GAE/ENY/05-M11. Graduate School of Engineering and Management, Air Force Institute of Technology, Wright-Patterson AFB, OH. March 2005.

Panzenhagen, Kristin L. *Detonation Branching in a PDE with Liquid Hydrocarbon Fuel*. MS thesis, AFIT/GAE/ENY/04-M14. Graduate School of Engineering and Management, Air Force Institute of Technology, Wright-Patterson AFB,OH. March 2004.

Parker, Jason and Schauer, Frederick R. "Data Analysis and Compression Techniques for Megabyte-Data PDE Experiments,' *41st AIAA Aerospace Sciences Meeting*. Reno, NV. AIAA 2003-0892, 6-9 January 2003.

Rice, F.O. *Journal of the American Chemical Society*, Vol. 55. 3035-3040 (1933).

Schauer, Frederick R., Stutrud, Jeffery, and Bradley, Royce P. "Detonation Initiation Studies and Performance Results for Pulse Detonation Engine Applications," *39th AIAA Aerospace Sciences Meeting and Exhibit*. Reno, NV: AIAA 2001-129, 8-11 January 2001.

Schauer, Frederick R., Miser, Christen. L., Tucker, K. Colin., Bradley, Royce. P., and Hoke, John. L. "Detonation Initiation Hydrocarbon-Air Mixtures in a Pulsed Detonation Engine," *43rd AIAA Aerospace Sciences Meeting and Exhibit*. Reno, NV. AIAA 2005-1343, 10-13 January 2005.

Shchelkin, K. L. *Soviet Journal of Technical Physics,* Vol. 10. 823-827 (1940).

Slack, J. David. *Branch Detonation of a Pulse Detonation Engine with Flash Vaporized JP-8,* MS thesis, AFIT/GAE/ENY/07-D04. Graduate School of Engineering and Management, Air Force Institute of Technology, Wright-Patterson AFB, OH. Dec 2006.

Song, C., Lai, W.C., and Schobert, H.H. "Hydrogen-Transferring Pyrolysis of Long-Chain Alkanes and Thermal Stability Improvement of Jet Fuels by Hydrogen Donors," *ACS Industrial & Engineering Chemistry Research*, Vol. 33. 548-557 (1994).

Spadaccini, L.J., Sobel, D.R., Huang, H., and Dardas, Z. "Coke Depostion/Mitigation in Endothermic Fuels: Advanced Fuel Development and Fuel Combustion," *AFRL-PR-WP-TR-1998-2098*. June 1998.

Turns, Stephen R. *An Introduction to Combustion: Concepts and Applications*, 2nd ed. Boston. McGraw Hill, 2000.

Vita

Lieutenant Eric Allen Nagley was born in Lancaster, PA. He graduated from Blue Mountain Academy in Hamburg, PA in June of 1998. He attended Andrews University in Berrien Springs, MI where he graduated with a Bachelor of Science in Engineering Technology in Mechanical Engineering in May 2002. He attended Naval Officer Candidate School in Pensacola, FL where he received his commission in December 2002.

Lieutenant Nagley was first assigned to the USS JOHN C. STENNIS (CVN 74) homeported in San Diego, CA. As Aircraft Intermediate Maintenance Department Quality Assurance Officer, he maintained the programs and training that governed intermediate level maintenance on airframes, avionics, support equipment, and powerplants to support the 75+ aircraft embarked airwing. His next assignment as Support Equipment Officer required the maintenance management of the aircraft support equipment for the embarked airwing as well as leadership of the maintenance personnel. In September 2006, he entered the Air Force Institute of Technology Graduate School of Engineering and Management to pursue a Masters of Science in Aeronautical Engineering. His emphasis was in air breathing propulsion and digital avionics. After graduating in June 2008, he will be assigned to Helicopter Anti-Submarine Squadron Five at Naval Air Station Jacksonville, FL as Assistant Maintenance Officer.

REPORT DOCUMENTATION PAGE	Form Approved OMB No. 074-0188

The public reporting burden for this collection of information is estimated to average 1 hour per response, including the time for reviewing instructions, searching existing data sources, gathering and maintaining the data needed, and completing and reviewing the collection of information. Send comments regarding this burden estimate or any other aspect of the collection of information, including suggestions for reducing this burden to Department of Defense, Washington Headquarters Services, Directorate for Information Operations and Reports (0704-0188), 1215 Jefferson Davis Highway, Suite 1204, Arlington, VA 22202-4302. Respondents should be aware that notwithstanding any other provision of law, no person shall be subject to an penalty for failing to comply with a collection of information if it does not display a currently valid OMB control number. **PLEASE DO NOT RETURN YOUR FORM TO THE ABOVE ADDRESS.**

1. REPORT DATE (DD-MM-YYYY) 19-06-2008	2. REPORT TYPE Master's Thesis	3. DATES COVERED (From – To) Sep 2006 – Jun 2008

4. TITLE AND SUBTITLE	5a. CONTRACT NUMBER
Fuel Composition Analysis of Endothermically Heated JP-8 Fuel for Use in a Pulse Detonation Engine	5b. GRANT NUMBER
	5c. PROGRAM ELEMENT NUMBER

6. AUTHOR(S)	5d. PROJECT NUMBER
Nagley, Eric A., Lieutenant, USN	5e. TASK NUMBER
	5f. WORK UNIT NUMBER

7. PERFORMING ORGANIZATION NAMES(S) AND ADDRESS(S)	8. PERFORMING ORGANIZATION REPORT NUMBER
Air Force Institute of Technology Graduate School of Engineering and Management (AFIT/ENY) 2950 Hobson Way, Building 640 WPAFB OH 45433-8865	AFIT/GAE/ENY/08-J08

9. SPONSORING/MONITORING AGENCY NAME(S) AND ADDRESS(ES)	10. SPONSOR/MONITOR'S ACRONYM(S)
AFRL/RZTC ATTN: Dr. Frederick R. Schauer Building 71A, D-Bay, 7th Street Wright Patterson AFB, OH 45433 DSN: 785-6462	11. SPONSOR/MONITOR'S REPORT NUMBER(S)

12. DISTRIBUTION/AVAILABILITY STATEMENT

APPROVED FOR PUBLIC RELEASE; DISTRIBUTION UNLIMITED.

13. SUPPLEMENTARY NOTES

14. ABSTRACT

Waste heat from a pulse detonation engine (PDE) was extracted via zeolite catalyst coated concentric tube-counter flow heat exchangers to produce supercritical pyrolytic conditions for JP-8 fuel. A sampling system and method were developed that enabled samples of reacted fuel to be extracted during steady state operation. Samples were taken over a range of heat exchanger exit temperatures from 820 K (1016 ^{o}F) to 940 K (1232 ^{o}F). Offline analysis of liquid and vapor fuel samples indicated fuel decomposition via typical pyrolytic reaction pathways. The liquid analysis showed conversion of parent fuel components with formation of unsaturates (aromatics and alkenes) and smaller alkanes. The gaseous products consisted of predominantly C_1-C_3 alkanes and alkenes (> 75% of total vapor yield) with moderate amounts of hydrogen and C_4-C_6 alkanes and alkenes. The components that were present in the stressed fuel samples were more detonable and could be linked to improved PDE performance. The ignition time decreased by over 20% as temperature increased from 820 K (1016 ^{o}F) to 935 K (1224 ^{o}F) and by more than 30% when compared to unreacted (flash vaporized) JP-8.

15. SUBJECT TERMS
Pulse detonation engine, pyrolysis, catalytic cracking, pyrolytic, JP-8

16. SECURITY CLASSIFICATION OF:			17. LIMITATION OF ABSTRACT	18. NUMBER OF PAGES	19a. NAME OF RESPONSIBLE PERSON Dr. Paul I. King
a. REPORT U	b. ABSTRACT U	c. THIS PAGE U	UU	124	19b. TELEPHONE NUMBER (Include area code) (937) 255-3636, ext 4628 (paul.king@afit.edu)

Standard Form 298 (Rev. 8-98)
Prescribed by ANSI Std. Z39-18